République Algérienne Démocratique et Populaire
Ministère de l'Enseignement Supérieur et de la Recherche Scientifique
Ecole Normale Supérieure d'Enseignement Technologique de Skikda

Département de Physique et Chimie

Thèse

Par: Melle. Hayet Bouabbaci

Pour l'obtention du diplôme de Doctorat en Chimie

Spécialité: Chimie Théorique et Computationnelle

Thème:

Simulation et caractérisation des propriétés physico-chimiques des matériaux organiques

Jury :

Mr. Youcef Saihi	Président	MCA	ENSET de Skikda
Mr. Abdelmalek Khorief Nacereddine	Directeur de thèse	Professeur	ENSET de Skikda
Mme. Chafia Sobhi	Examinatrice	Professeur	Université de Skikda
Mr. Hacene Bendjeffal	Examinateur	Professeur	ENSET de Skikda
Mr. Fouad Chafaa	Examinateur	MCA	Université de Batna-2
Mr. Khaireddine Kraim	Examinateur	MCA	ENSET de Skikda

Acknowledgments

This work was carried out at the Laboratory of Physical Chemistry and Biology of Materials at the Higher Normal School of Technological Education of Skikda.

I express my deepest gratitude to Dr. Abdelmalek Khorief Nacereddine, Professor at the Higher Normal School of Technological Education of Skikda, who agreed to supervise me during the four years of this thesis and who introduced me to a new field of theoretical and computational chemistry, that is optical properties of organic materials. I would especially like to thank him for his patience, support and invaluable help, in which I feel incredibly lucky and grateful for the opportunity to be his doctoral student and a member of his research group.

I extend my heartfelt thanks to Dr. Youcef Saihi, Lecturer "A" at the Higher Normal School of Technological Education of Skikda , who honored me by chairing the jury of this thesis.

I would like also to thanks Dr. Chafia Sobhi, Professor at University of Skikda for accepting to be a member of this jury and for reviewing this manuscript.

My deep appreciation goes also to Dr. Hacene Bendjeffal, Professor at the Higher Normal School of Technological Education of Skikda, for taking the time to evaluate my work.

I am deeply grateful to Dr. Fouad Chafaa, Lecturer "A" at the University of Batna 2, for the time he devoted to review this manuscript, and I'm very honored to count him among the members of this jury.

My thanks are also addressed to Dr. Khaireddine Kraim, Lecturer "A" for their unwavering support and encouragement and for accepting to be member in the jury of this thesis.

Finally, I thanks all persons who help, support and advice me for performing this work during my stay at LPCBM laboratory

Dedications

I dedicate this work to:

- *My parents*

- *My brothers and sisters*

- *All my friends*

- *All my colleagues*

Abbreviations

BCP	Bond Critical Point
BSSE	Basis Set Superposition Error
B3LYP	Becke, 3-parameter, Lee-Yang-Parr
CAM-B3LYP	Counterpoise Corrected for Adsorption Model
CCP	Cage Critical Point
CI	Configuration Interaction
CIS	Common wealth of Independent States
COSMO	Conductor-like Screening Model
CPHF	Coupled Perturbation Hartree-Fock
DFT	Density Functional Theory
DMSO	Dimethy Sulfoxide
ELF	Electron Localization Function
EL	Electroluminescence
FMO	Frontier Molecular Orbitals
FP	Finite Perturbation
GCRD	Global Chemical Reactivity Descriptors
HB	Hydrogen Bond
HOMO	Highest Occupied Molecular Orbital
HF	Hartree-Fock
ICT	Intramolecular Charge Transfer
LCAO	Linear Combination of Atomic Orbitals
LO	Linear Optical
LUMO	Lowest Unoccupied Molecular Orbital
MEP	Molecular Electrostatic Potential
MPn	Moller-Plesset
NBO	Natural Bond Orbitals

NCP	Nuclear Critical Point
NLO	Non Linear Optical
OM	Organic Materials
OFETs	Organic field-effect transistors
OLEDs	Organic light-emitting diodes
OPV	Organic photovoltaic
OSCs	Organic conjugated systems
PBE	Perdew-Burke-Ernzerhof
QTAIM	Quantum Theory of Atomic In Molecules
LCDs	Liquid crystal displays
SC	Solar Cell
THz	Terahertz
TFA	Trifluoroacetic acid

Symbols

μ	Dipole moment
α	Mean polarizability
$\Delta\alpha$	Anisotropy of polarizability
β	First hyperpolarizability
γ	Second hyperpolarizability
η	Global hardness
χ	Electronegativity
μ	Electronic potential
s	Chemical Softness
ω	Electrophilicty
ρ	Electron densitry
$\nabla^2\rho(r)$	Electron densitry Laplacian
V(r)	Potential density
G(r)	Local gradient kinetic energy density

ملخص

يعد تطوير مواد عضوية جديدة من اجل استخدامها في العديد من التطبيقات الصناعية كمواد بديلة غير مكلفة وصديقة للبيئة تحديًا كبيرًا في السنوات الأخيرة. إن التنبؤ بالخصائص الفيزيائية والكيميائية للجزيئات أمر ممكن باستخدام النماذج النظرية و مختلف النظريات الرياضية من خلال الموارد الحاسوبية. في هذا العمل، درسنا نظريًا الخصائص البصرية الخطية و اللاخطية ، الفيزيائية والكيميائية لبعض مشتقات الكينولين ضمن طريقة DFT من خلال المستوى النظري PBE/6-311G++(d, p). تم وصف الخصائص البصرية الخطية من حيث الاستقطاب α وتباين الاستقطاب Δα ، بينما بالنسبة للخصائص البصرية اللاخطية فتم من حيث فرط الاستقطاب الأول βtot حيث تم حسابها باستخدام نموذج COSMO في مذيب DMSO. تم تحليل الخصائص الفيزيائية والكيميائية من خلال طاقة الفجوة و مؤشرات الفعالية العامة التي تم حسابها انطلاقا من طاقات المحطات الجزيئية الحدودية. تم أيضًا تقييم خصائص هيكلية أخرى، مثل التوزيع الإلكتروني باستخدام تحليل QTAIM وتحليل الكمون الإلكتروني الجزيئي. بينت النتائج المتحصل عليها أن مشتقات الكينولين هذه يمكن اعتبارها مواد عضوية شبه موصلة، مما يجعل مشتق 6-أمينو-2-فورميل-كينولين مادة عضوية واعدة لاستخدامها كمواد عضوية بديلة للطاقة الكهروضوئية في الخلايا الشمسية وغيرها من التطبيقات البصرية اللاخطية.

Abstract

The development of new organic materials for possible use in several industrial applications as alternative non expensive and green material is a great challenge in recent years. The prediction of the physical and chemical properties of molecules is plausible using different theoretical models and theories through computational resources. In this work, we have studied theoretically the linear and non-linear optical, physical and chemical properties of some quinoline derivatives within DFT method through PBE/6-311G++(d, p) theoretical level. The description of linear optical properties has been performed in terms of the polarizability $< \alpha >$ and the polarizability anisotropy $< \Delta\alpha >$, while for the non-linear optical properties in terms the first hyperpolarizability β_{tot}, in which they were calculated using COSMO model in DMSO solvent. The physical and

chemical properties have been analysed in terms of gap energy and global reactivity descriptors which were calculated from the frontier molecular orbitals energies. Other structural properties were also evaluated such as electronic distribution using QTAIM and molecular electron potential analyses. The obtained results indicate that these quinoline derivatives may be considered as a semiconductor organic materials, making the 6-amino-2-formyl–quinoline derivative as a promising green energy organic material for possible future using as alternative organic photovoltaic material in solar cells and other nonlinear optical applications.

Résumé

Le développement de nouveaux matériaux organiques, potentiellement utilisables dans diverses applications industrielles comme matériaux alternatifs, économiques et écologiques, constitue un défi majeur ces dernières années. La prédiction des propriétés physiques et chimiques des molécules est plausible grâce à différents modèles et théories théoriques et à des ressources informatiques. Dans ce travail, nous avons étudié théoriquement les propriétés optiques, physiques et chimiques linéaires et non linéaires de certains dérivés de la quinoléine par la méthode DFT au niveau théorique PBE/6-311G++(d, p). La description des propriétés optiques linéaires a été réalisée en termes de polarisabilité $< \alpha >$ et d'anisotropie de polarisabilité $< \Delta\alpha >$, tandis que pour les propriétés optiques non linéaires en termes de première hyperpolarisabilité β_{tot}, dans lesquelles elles ont été calculées en utilisant le modèle COSMO dans le solvant DMSO. Les propriétés physiques et chimiques ont été analysées en termes d'énergie de gap et de descripteurs de réactivité globale, calculés à partir des énergies des orbitales moléculaires frontières. D'autres propriétés structurales ont également été évaluées, telles que la distribution électronique par QTAIM et les analyses du potentiel électronique moléculaire. Les résultats obtenus

indiquent que ces dérivés de quinoléine peuvent être considérés comme des matériaux organiques semi-conducteurs, faisant du dérivé 6-amino-2-formyl-quinoléine un matériau organique prometteur pour l'énergie verte, susceptible d'être utilisé comme matériau photovoltaïque organique alternatif dans les cellules solaires et d'autres applications optiques non linéaires.

Contents

I Bibliographic Study **1**

1 Quinoline and its derivatives **2**

1.1 Introduction 2

1.2 Chemical and physical properties of quinoline 3

1.3 Chemical structures of quinoline and its analogs 4

1.4 Important synthetic methods of quinoline derivatives 4

1.4.1 The Skraup reaction 5

1.4.2 Friedlander method 5

1.4.3 Conrad–Limpach reaction 6

1.4.4 Doebner–Miller method 6

1.4.5 The Vilsmeier-Haack reaction 7

1.4.6 Pfitzinger method 8

1.4.7 The Povarov reaction 8

1.5 Biological activity of some quinoline derivatives 9

1.5.1 Antibacterial activity 9

1.5.2 Anti-malarial activities 10

1.5.3 Antiviral activities of quinoline derivatives 10

1.5.4 Anti-inflammatory activities of quinoline derivatives 10

1.5.5 Anti-cancer activities of quinoline derivatives 11

1.6 Industrial applications of some quinoline derivatives 13
1.6.1 In Dye and chemical industries 13
1.6.2 In electronics industry 14
1.6.3 In corrosion inhibition 22

2 Quantum computation methods 25

2.1 Introduction 25
2.2 The Schrödinger equation 26
2.3 Approximation of Born-Oppenheimer 27
2.4 *ab-initio* methods 27
2.4.1 Hartree method 28
2.4.2 Hartree-Fock method 28
2.4.3 The Hartree-Fock-Roothaan method 30
2.4.4 Configuration interaction method (CI) 31
2.4.5 Møller–Plesset perturbation theory 32
2.5 Density functional theory (DFT) 34
2.5.1 The B3LYP functional 36
2.5.2 The PBE functional 37
2.5.3 The B3PW91 functional 37
2.5.4 The CAM-B3LYP functional 38
2.6 The atomic orbital basis set 38
2.6.1 The inner orbitals 40
2.6.2 The valence zone 41
2.6.3 The diffuse zone 41
2.6.4 Common nomenclature of basis set 41

3 Quantum models and descriptors for chemical reactivity 43

3.1 Introduction 43

3.2 Frontier molecular orbital method 43
3.3 Global reactivity indices 44
3.3.1 The electronegativity χ 45
3.3.2 The chemical potential μ 45
3.3.3 The hardness η 46
3.3.4 The softness S 46
3.3.5 The electrophilicity ω 46
3.4 Quantum theory of atoms in molecules 47
3.5 The molecular electrostatic potential (MEP) 48

4 General aspects and theoretical estimation of molecular optics 50
4.1 Optical field 50
4.1.1 Linear optical OL 51
4.1.2 Non-linear optical NLO 53
4.2 Quantum mechanical estimation of μ, α, β tensors 54
4.3 Matter polarization 54
4.4 Calculation methods of μ, α, β tensor elements 55
4.4.1 The Hellmann-Feyman theorem 55
4.4.2 The Hartree-Fock coupled perturbation theorem (CPHF) 55
4.4.3 Finite perturbation theory FF 57
4.4.4 Practical application of nonlinear optics 58
4.4.5 The optical properties of organic materials 58
4.5 UV-Vis spectroscopy 59
4.5.1 Generalities 59
4.5.2 Types of electronic transitions 61
4.5.3 Gap energy 63

II Results and discussion **65**

5 Results and discussion **66**

5.1 Introduction 66

5.2 Computational methods 67

5.2.1 Optical Properties 68

5.2.2 Frontier Molecular Orbitals (FMO) 70

5.2.3 Global Chemical Reactivity Descriptors (GCRD) 71

5.2.4 MEP maps analysis 72

5.2.5 QTAIM analysis 73

5.3 Optimized geometries and choice of the computational level 75

5.3.1 Choice of the best DFT functional and basis set 77

5.3.2 Global Chemical Reactivity Descriptors (GCRD) 84

5.3.3 MEP analysis 85

5.3.4 QTAIM analysis 86

5.3.5 UV-Vis Spectral analysis 89

List of Figures

1.1 Structure of quinoline 2

1.2 Chemical structures of quinoline and isoquinoline heterocycles 4

1.3 Skraup synthetic method to form unsubstituted quinoline 5

1.4 Synthesis of substituted quinolines using Friedlander synthetic method . . 6

1.5 Synthesis of 4-hydroxyquinoline through Conrad–Limpach reaction 6

1.6 Synthesis of substituted quinolines through Doebner-Miller method . . . 7

1.7 Vilsmeier-Haack reaction for the preparation of quinoline derivative . . . 7

1.8 Synthesis of tricyclic quinolines via Pfitzinger method 8

1.9 Synthesis of 2-aryl-substituted quinolines using Povarov reaction 9

1.10 Some commercialized drugs based on quinoline motif with antibacterial activity 10

1.11 Some selected quinoline derivatives with anti-malarial activity 11

1.12 Some quinoline derivatives with anti-viral activity 12

1.13 Selected quinoline derivatives with anti-inflammatory activity 13

1.14 Some quinoline derivatives with anti-cancer activity 14

1.15 Chemical structure of the dye quinoline yellow 15

1.16 Schematisation of organic solar cell 15

1.17 Structure of some OSCs quinoline derivatives synthesised by Arslan and co-workers 16

1.18 Schematisation of basic structure of an OLED 17
1.19 Molecular structure of two 4H-pyrano[3,2-c]quinoline derivatives studied by Zeyada and co-workers 19
1.20 Synthesis of 2-(8-(benzyloxy)quinolin-2-yl)-1-phenyl-1H-phenanthro[9,10-d]imidazole 19
1.21 Structure of quinoline based Schiff bases studied by Priyadarshini and co-workers 21
1.22 Structure of disubstituted quinoline with carbazole studied by Ali et al . . 23
1.23 Synthesis of 2-(8-(benzyloxy)quinolin-2-yl)-1-phenyl-1H-phenanthro[9,10-d]imidazole 24

2.1 Comparison between STO and GTO 40

3.1 Electron density in HFC=O molecule 47
3.2 Types pf bond critical points 48
3.3 Map of molecular electrostatic potential of 3-bromopyridin-2-ol molecule . 49

4.1 The possible electron transition in Uv-vis spectroscopy 61
4.2 Classification of materials according to their band gap 63
4.3 Determination of optical gap energy schematically 64

5.1 Structure of studied quinoline derivatives 67
5.2 Structure of quinoline together with atoms labels 75
5.3 Structure of 7-amino-quinoline (a) and 2-formyl-quinoline (b) 79
5.4 8-amino-quinoline 91
5.5 7-amino-quinoline 91
5.6 6-amino-quinoline 91
5.7 5-amino-quinoline 91
5.8 4-amino-quinoline 91

5.9 3-amino-quinoline 91
5.10 2-amino-quinoline 91
5.11 amino-quinoline position isomers 91
5.12 2-formyl-quinoline 92
5.13 3-formyl-quinoline 92
5.14 4-formyl-quinoline 92
5.15 5-formyl-quinoline 92
5.16 6-formyl-quinoline 92
5.17 7-formyl-quinoline 92
5.18 8-formyl-quinoline 92
5.19 formyl-quinoline position isomers 92
5.20 Molecular electrostatic potential map of formyl-quinoline molecule 93
5.21 Molecular graphs of quinoline 93
5.22 Analysis of electron density with (3,-1) critical point of quinoline 93
5.23 QTAIM molecular graphs of quinoline and analysis of electron density with (3,-1) critical points 93
5.24 Molecular graphs of 7-amino-quinoline 94
5.25 analysis of electron density with (3,-1) critical point of 7-amino-quinoline 94
5.26 QTAIM molecular graph of 7-amino-quinoline together with analysis of electron density with (3,-1) critical points 94
5.27 B3LYP-6-311G++(d,p) optimized structure of 2-formyl-quinoline dimer together with the distances of the pertinent intramolecular interactions . . 94
5.28 Molecular graphs of 7-amino-quinoline 95
5.29 analysis of electron density with (3,-1) critical point of 7-amino-quinoline 95
5.30 QTAIM molecular graph of 2-formyl-quinoline dimer together with analysis of electron density with (3,-1) critical points 95

5.31 Theoretical Uv-vis spectrum of quinoline, 7-amino-quinoline, 2-formyl-quinoline, 6-amino-2-formyl-quinoline and 2-formyl-quinoline dimer 96

List of Tables

5.1 Some selected theoretical and experimental values of geometrical parameters associated with quinoline structure 76

5.2 Calculated values (in a.u) of μ, α, $\Delta\alpha$, β, $\beta_{//}$ of quinoline using B3LYP, CAM-B3LYP, PBE and B3PW91 functionals 77

5.3 Calculated μ, α, $\Delta\alpha$, β, $\beta_{//}$ (in a.u) of quinoline using B3LYP, CAM-B3LYP, PBE and B3PW91 functionals of quinoline using COSMO model with DMSO solvent at DFT/6-311++G(d, p) 77

5.4 PBE values of polarizability α (in a.u) for quinoline with different basis set in gas phase 78

5.5 Values of μ, α, $\Delta\alpha$, β and β_{tot} (in a.u) of quinoline with the COSMO model and in the DMSO solvent at PBE/6-311++G(d, p) theoretical level. 79

5.6 Values of μ, α, $\Delta\alpha$, β and $\beta_{//}$ in (a.u.) of quinoline with the COSMO model and in the DMSO solvent at the PBE/6-311++G(d, p) theoretical level 79

5.7 PBE/6-311++G(d, p) in DMSO solvent LO and NLO properties (in a.u) of amino-quinoline position isomers 80

5.8 PBE/6-311++G(d, p) in DMSO solvent LO and NLO properties (in a.u) of formyl-quinoline 81

5.9 PBE/6-311++G(d, p) in DMSO solvent LO and NLO properties (in a.u) of n-amino-6-formylquinoline derivatives 81

5.10 PBE/6-311++G(d, p) in DMSO solvent LO and NLO optical properties of quinoline, 6-amino-quinoline, formyl-quinoline, 6-amino-1-formyl-quinoline and formyl-quinoline dimer 82

5.11 B3LYP/6-311G++(d, p) values (in a.u) of optical properties and electronic gap energy (in eV) of quinoline, 7-amino-quinoline, 2-formyl-quinoline, 6-amino-2-formyl-quinoline and 2-formyl-quinoline dimer 84

5.12 GCRD values (in eV) for quinoline and some its derivatives at B3LYP/6-311++G(d, p) theoretical level 85

5.13 QTAIM (3,-1) bond critical point parameters in (a.u.) of quinoline 87

5.14 QTAIM (3,-1) bond critical point parameters in (a.u.) of 7-amino-quinoline 88

5.15 QTAIM (3,-1) bond critical point parameters in (in a.u) of 2-formyl-quinoline dimer. 89

5.16 Values of electronic gap (in eV), optical gap (in nm and eV) and optical properties (in a.u) for quinoline and its derivatives 90

Part I

Bibliographic Study

Chapter 1

Quinoline and its derivatives

1.1 Introduction

Quinoline is a nitrogen aromatic heterocyclic organic compound and belonging to the alkaloid family. It also named as 1-azanaphthalene, leucoline, 1-benzazine and benzopyridine. Its structure considered as an organic base which composed of benzene ortho-fused with a pyridine ring (Figure 1.1).

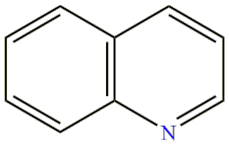

Figure 1.1: Structure of quinoline

In 1834, Ferdinand Rung discovered the quinoline, where he obtained from the distillation of natural coal tar [1], which also contains isoquinoline as well as several alkyl quinolines and alkyl isoquinolines, that are difficult to separate, and it was some years before pure quinoline was available in quality for investigation of its properties. In 1842, Gerhardt [2] obtained it from the degradation of quinine and cinchonine.

The quinoline structure exist also in various natural products, namely in alkaloids, which have been isolated in the Common wealth of Independent States (CIS) countries from different plants and are found in 13 plant families, particularly, the genus Haplophyllum which has quinoline alkaloids with various structures and different pharmacological activities [3].

1.2 Chemical and physical properties of quinoline

Pure quinoline is a colorless oily hygroscopic liquid with a strong odour, and it has an acidic pKa of 4.85 in aqueous solution at 293 K. The molecular formula of quinoline C_9H_7N and thus its molecular weight is 129.16g.mol^{-1}. When it exposure to light it become has a dark colour, and it considered a very stable molecule. From a chemical point of view, quinoline structure is a weak tertiary base, thereby; it can form a quaternary salt with acids. Because its structure composed of benzene ortho-fused with a pyridine rring, quinoline displays reactions similar to those later, such as electrophilic and nucleophilic substitution reactions. Quinoline compound is non-toxic to humans on oral absorption and inhalation. Tetrahydroquinoline is particularly important that may be prepared by a reduction reaction of the corresponding quinoline, using a simple reduction by tin and hydrochloric acid [4].

Quinoline is sparingly miscible with cold water, but completely miscible with hot water. With a logP value of 2.04, it is readily soluble in many organic solvents at ambient temperature. It possesses the ability to absorb water molecules from the environment [5]. From a physical point of view, quinoline exhibits a density of 1.093 g mol-1, melting point of -15 °C and boiling point of 238 °C [6].

1.3 Chemical structures of quinoline and its analogs

The structure of quinoline is characterized by the presence of double ring, that are a pyridine and benzene rings fused together by two adjacent carbon atoms. The chemical formula of the benzene is C_6H_6, while the pyridine is C_5H_5N, where a methine group is replaced with a nitrogen atom in compared to the benzene structure [6]
It exists an other molecule isomer to quinoline that is isoquinoline, in which the position of nitrogen atom is different, that is situated at position 2 in the structure of isoquinoline, whereas the heteroatomic nitrogen in quinoline is at position 1 of the heterocyclic ring portion (Figure 1.2) [5].

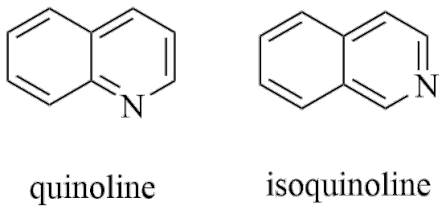

Figure 1.2: Chemical structures of quinoline and isoquinoline heterocycles

1.4 Important synthetic methods of quinoline derivatives

The literature tells us that quinoline derivatives extracted from natural compounds have several biological activities [7], which have attracted both synthetic chemist and biologists because of its diverse chemical and pharmacological properties. Among the reliable methods for their synthesis, we can cite the Skraup reaction, Doebner-von Miller, Friedländer, Pfitzinger, Conrad-Limpach and Combes syntheses [8]

1.4.1 The Skraup reaction

The reaction of Skraup has been used for synthesising non-substituted quinoline. It consists of heating aniline on acrolein in the presence of concentrated sulphuric acid in a mild oxidizing agent and glycerol at refluxing temperature to give unsubstituted quinoline (Figure 1.3). The acid used therein serves a double role because it acts as both as a catalyst and dehydrating agent simultaneously [6]. The Skraup synthesis enabled the laboratory-scale synthesis of quinoline for the first time, and subsequently other methods were developed for the preparation of diverse substituted quinolines with several medicinal activities.

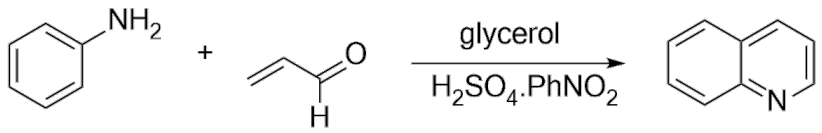

Figure 1.3: Skraup synthetic method to form unsubstituted quinoline

1.4.2 Friedlander method

In 1882 Friedlander discovered a new synthetic approach for the synthesis of quinoline, which is considered as one of the most important methods for the preparation of quinoline derivatives. This approach consists of the condensation between 2-aminobenzaldehydes and ketones to yields the corresponding quinoline derivatives. The Friedlander synthetic approach is catalyzed by trifluoroacetic acid (TFA) or Lewis acids, iodine and p-toluene sulfonic acid [9]. Thus, Wang *et al* have prepared 2,3,7-trisubstituted quinoline derivatives using the Friedlander method from 1-amino-4-bromo benzaldehyde with ethyl acetoacetate using HCl as the catalyst and H_2O as the solvent (Figure 1.4).

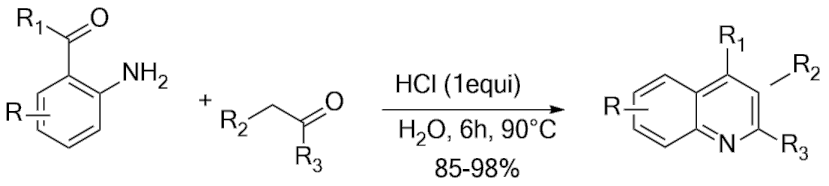

Figure 1.4: Synthesis of substituted quinolines using Friedlander synthetic method

1.4.3 Conrad–Limpach reaction

In the method of Conrad-Limpach, we use aniline that condensed with b-ketoesters under appropriate reaction conditions to yields 4-hydroxyquinolines passing by an intermediate that is a Schiff base [10]. The reaction mechanism consists of an addition reaction followed by a condensation reaction.

The rate-determining step is that associated with the thermal cyclization through molecular ring closure, in which the Schiff base intermediate was heated to 250 °C (Figure 1.5) [11].

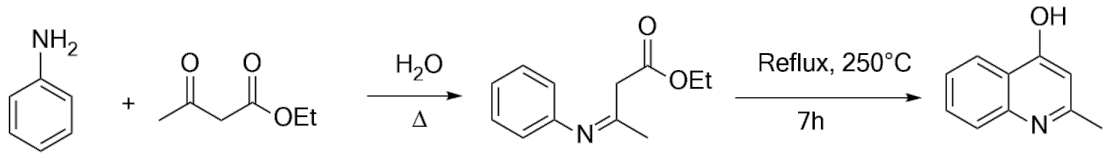

Figure 1.5: Synthesis of 4-hydroxyquinoline through Conrad–Limpach reaction

1.4.4 Doebner–Miller method

In this method, Doebner and Miller used an a,b-unsaturated aldehyde or ketone with aniline [12] This synthetic method consists of a the condensation between aromatic amines and chalcones to afford the corresponding quinolines. Wu *et al* have showed that the reaction of aniline or its derivatives with chalcones under refluxing solvent trifluoroacetic

acid solvent [13] gave an intermediate which after cyclisation followed by oxidation leading to the formation of trisubstituted quinoline derivatives (Figure 1.6).

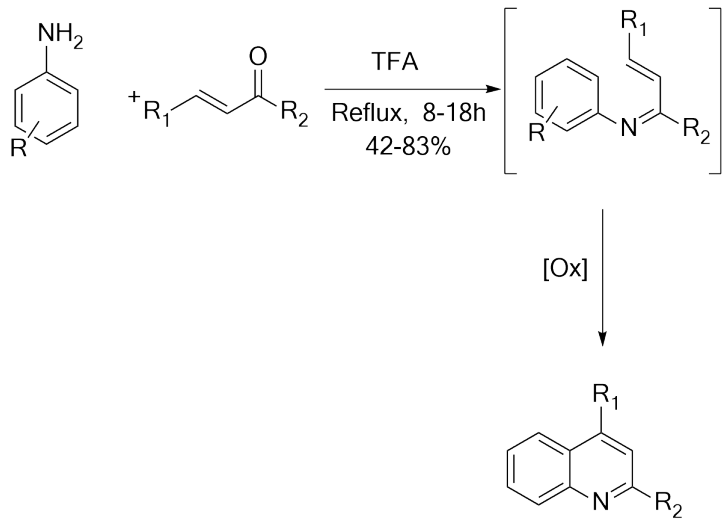

Figure 1.6: Synthesis of substituted quinolines through Doebner-Miller method

1.4.5 The Vilsmeier-Haack reaction

The treatment of acetanilide by phosphorus oxychloride in dimethylformamide at 80–90 °C for 5h leading to the formation 2-chloroquinoline-3-carboaldehydes through an intramolecular cyclization (Figure 1.7) [14].

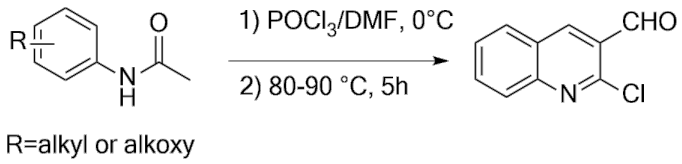

Figure 1.7: Vilsmeier-Haack reaction for the preparation of quinoline derivative

1.4.6 Pfitzinger method

The reaction begin by an hydrolysis of isatin in a aqueous solution of potassium hydroxide, then the pH adjusted between 2 and 3, affording an intermediate anilino-based acid. This last condensed in situ with cyclic 1,3-diketone giving the tricyclic quinoline (Figure 1.8) [15].

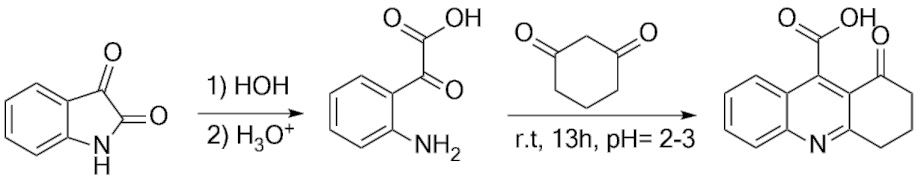

Figure 1.8: Synthesis of tricyclic quinolines via Pfitzinger method

1.4.7 The Povarov reaction

The Povarov route is an aza-Diels–Alder reaction, which was reported originally as a one-pot reaction of aryl aldimines derived from the reaction of benzaldehyde with aniline having an electron-rich substituent, namely, ethyl vinyl ether or ethyl vinyl sulfide in BF_3/OEt_2 catalyst, affording the tetrahydro-quinoline derivatives, which may be oxidized to the corresponding quinolines (Figure 1.9) [16].

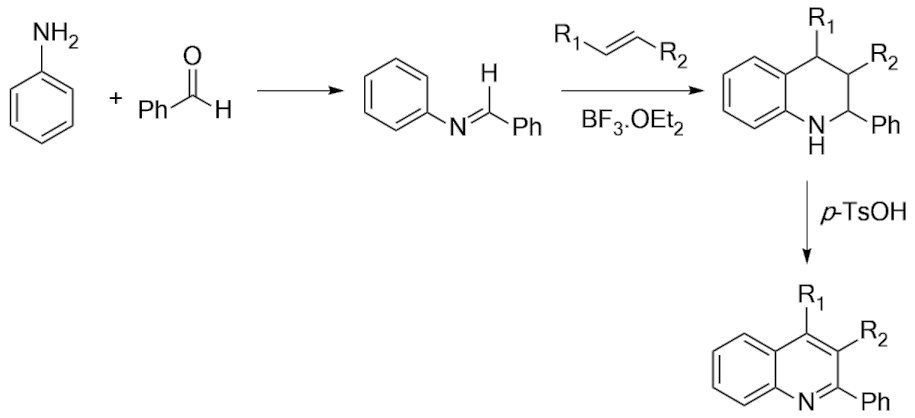

Figure 1.9: Synthesis of 2-aryl-substituted quinolines using Povarov reaction

1.5 Biological activity of some quinoline derivatives

Quinoline and its derivatives have shown several biological activities constitute an important class of compounds for new drug development. Therefore, this class of compounds have been the main research axis of tremendous researchers which synthesised those compounds and evaluated their biological activities.

1.5.1 Antibacterial activity

The literature reported that several quinoline-based compounds were designed with that bearing a carbothioamide-based quinoline motif, exhibiting the most significant antibacterial activity with a zone of inhibition of 20 mm against P. aeruginosa [17]. The commercially available quinoline based antimicrobial drugs include ciprofloxacin [18] and Ofloxacin [19](Figure 1.10).

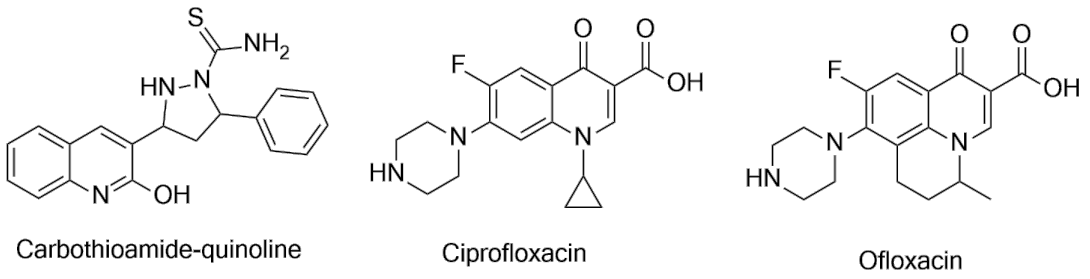

Figure 1.10: Some commercialized drugs based on quinoline motif with antibacterial activity

1.5.2 Anti-malarial activities

Quinoline derivatives are considered to be the dominant class of heterocyclic compounds used as anti-malarial agents. In the pharmaceutical field, two quinoline derivatives are used, namely, the 4-amino quinolines (chloroquine, amodiaquine, and piperaquine) and aminoalcohols (quinine and mefloquine) (Figure 1.11) [20].

1.5.3 Antiviral activities of quinoline derivatives

Quinoline and its derivatives have been used as antiviral agents, thus, Zhuang and co-workers reported that emerged as the most promising anti-HCV motif with an EC_{50} of 3.1 mM against the entire tested HCV virus(Figure 1.12) [21].

1.5.4 Anti-inflammatory activities of quinoline derivatives

Several quinoline derivatives with anti-inflammatory activity can be found in the literature (Figure 1.13). The 7-chloro-4-phenylsulfonyl-quinoline which bearing a chlorine substituent on the 7-position that has been screened against inflammation in mice with

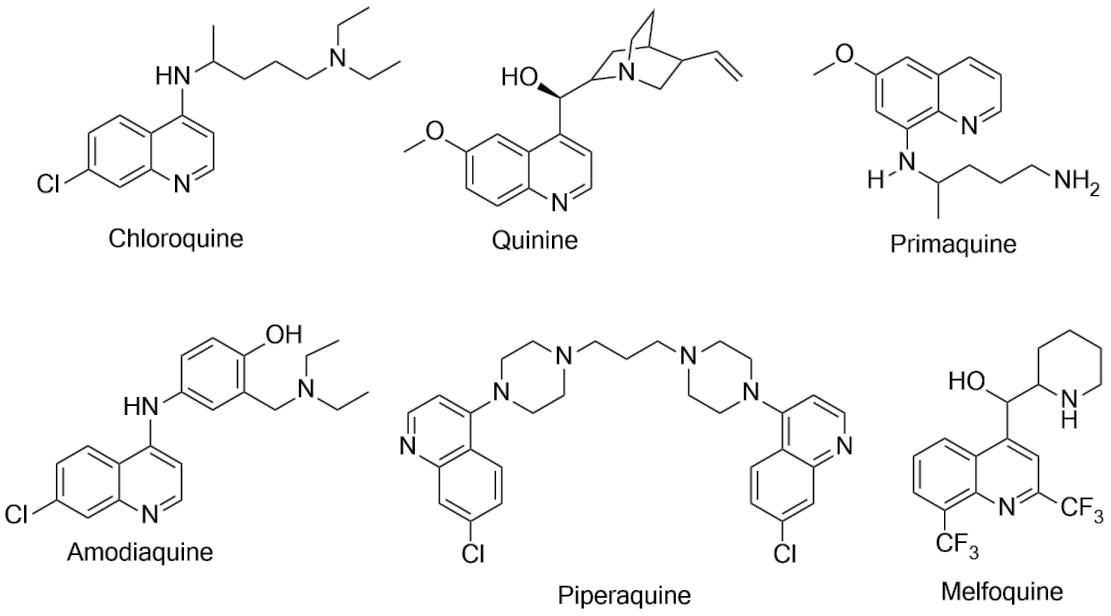

Figure 1.11: Some selected quinoline derivatives with anti-malarial activity

use of croton oil and was found to exhibit good anti-inflammatory potential. Among the studied quinoline derivative, the 2-phenylquinoline which being a nucleoside-linked analogue possessed remarkable anti-inflammatory properties comparable to the standard drug (diclofenac sodium).

Also, amodiaquine was reported by Mandewale and co-workers to be an anti-inflammatory agent with high efficacy (Figure 1.13). [22]

1.5.5 Anti-cancer activities of quinoline derivatives

Several quinoline derivatives were reported to be a potent anti-cancer agent against breast, lung and CNS tumors, such as quinoline structures possess 2,4-disubstitution, namely, the N-2-diphenylquinol-4-carboxamide. On the other hand, the naturally occurring quinoline-based alkaloids such as dictamine and berberine have been reported to

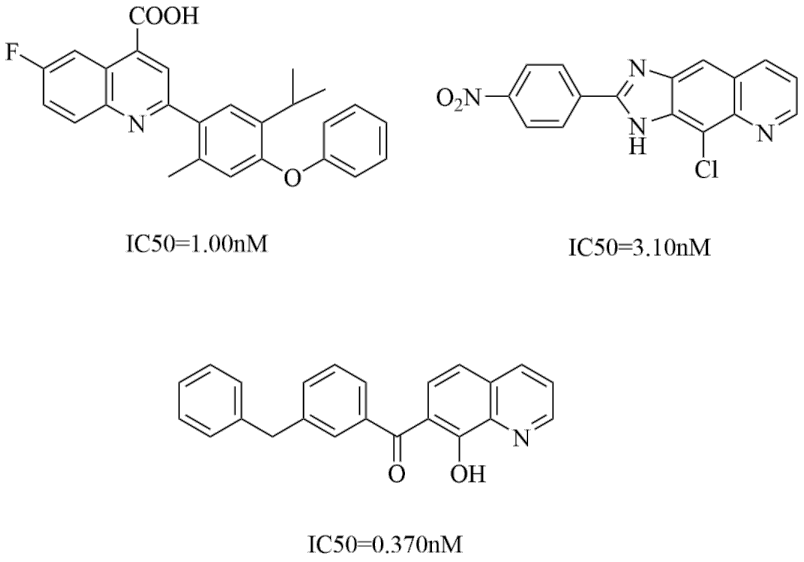

Figure 1.12: Some quinoline derivatives with anti-viral activity

play a vital function as new anti-cancer agents [5].

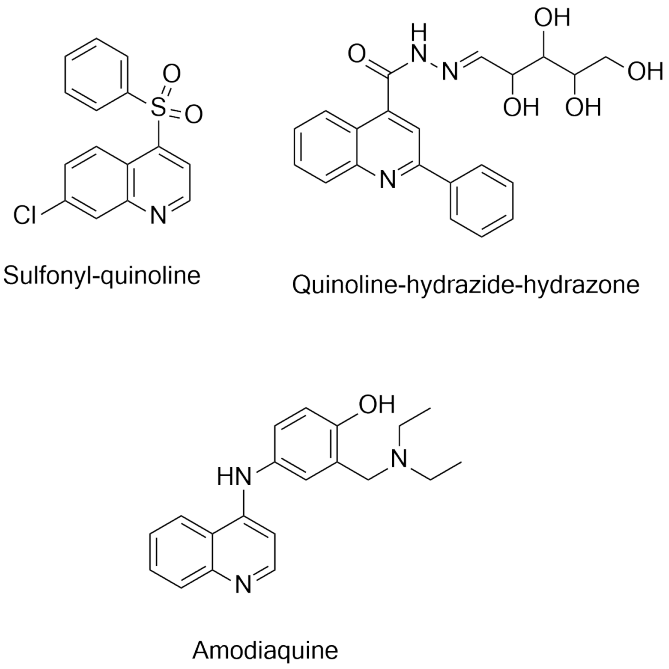

Figure 1.13: Selected quinoline derivatives with anti-inflammatory activity

1.6 Industrial applications of some quinoline derivatives

Quinoline derivatives are widely used in several industrial applications due to their unique chemical properties.

Due to their distinctive structural and chemical properties, quinoline derivatives find extensive use across industrial applications.

1.6.1 In Dye and chemical industries

Synthetic dyes are widely used across various industries, such as the cosmetics, textiles, pharmaceuticals, food, wood, plastics, photography and paper industries [23]. Among synthetic dyes, the dye quinoline yellow which is derived from chinophthalon, is commonly used in cosmetic fomulations for application on the skin, lips and body surface (Figure 1.15) [24].

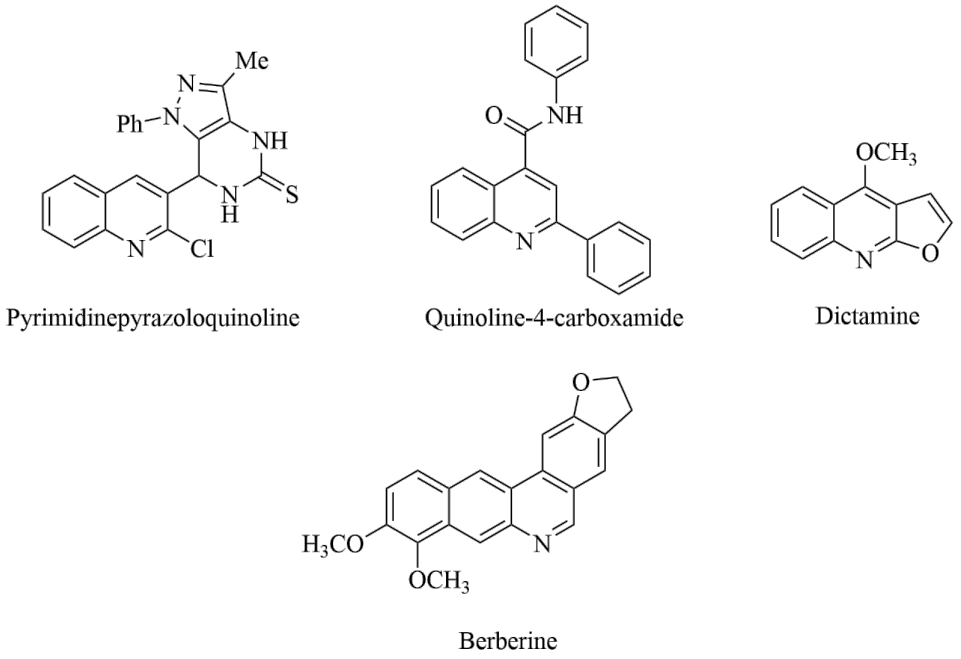

Figure 1.14: Some quinoline derivatives with anti-cancer activity

1.6.2 In electronics industry

In Solar cells

Carbon-based organic semiconductor materials have gained recognition as a promising class of materials for electronic and optoelectronic applications. Unlike inorganic semiconductors, organic ones provide advantages like low-cost processing, flexibility, and the potential for large area devices. The special properties of these compounds originate from the delocalization of π electron in their conjugated systems; make possible of their employment in development of organic field-effect transistors (OFETs), organic light-emitting diodes (OLEDs), and organic photovoltaic (OPV) cells. Heterocyclic semiconductors have attracted significant interest for their ability to fine-tune optoelectronic properties via structural modifications. These compounds have been utilized in several

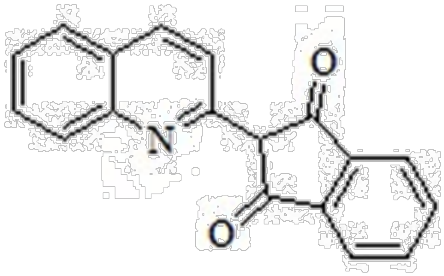

Figure 1.15: Chemical structure of the dye quinoline yellow

fields, namely, organic electronics, photonics, and sensing [25] Organic solar cells (OSCs) are characterized by economical cost, manufacturing simplicity, sustainable, adaptable power conversion efficiency. Due to these benefits, it has gained attention as key methods of converting solar radiation to electrical energy serving as an alternative to silicon solar cells (Figure 1.16).

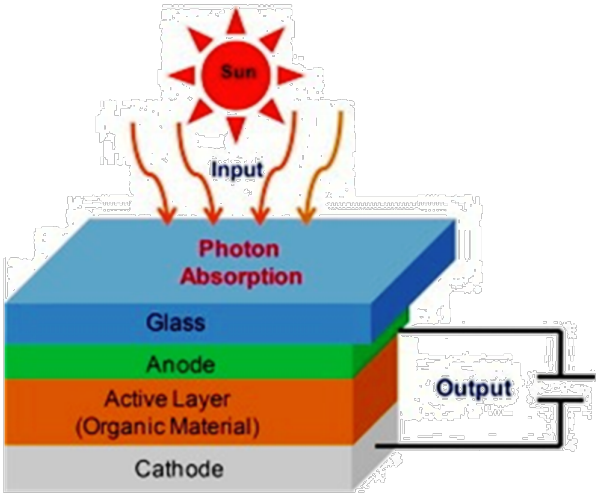

Figure 1.16: Schematisation of organic solar cell

The active organic layer enclosed a donor-π-bridge-acceptor (D-Π-A), in which the induced electron is transported from the donor to the acceptor through intramolecular charge transfer (ICT) [26]. It has been found that the conjugated systems increase photovoltaic performance by wide absorption in the visible radiation region. Thus, several organic conjugated systems have been used in OSCs, namely, phenothiazine [27] anthracene [28] N-annulated perylene [29], phenanthrocarbazole [30], phenylene [31], furan [32], thiophene derivatives [33] and quinoline [34].

Many studies show that quinoline and its derivatives can be utilized in electronics [35]. In this regards, Arslan and co-workers have synthesised three new quinoline derivatives for possible use as OSCs (Figure 1.17) [36], in which their results indicate that the insertion of benzothiadiazole into quinoline structure can effectively improve its photovoltaic performance.

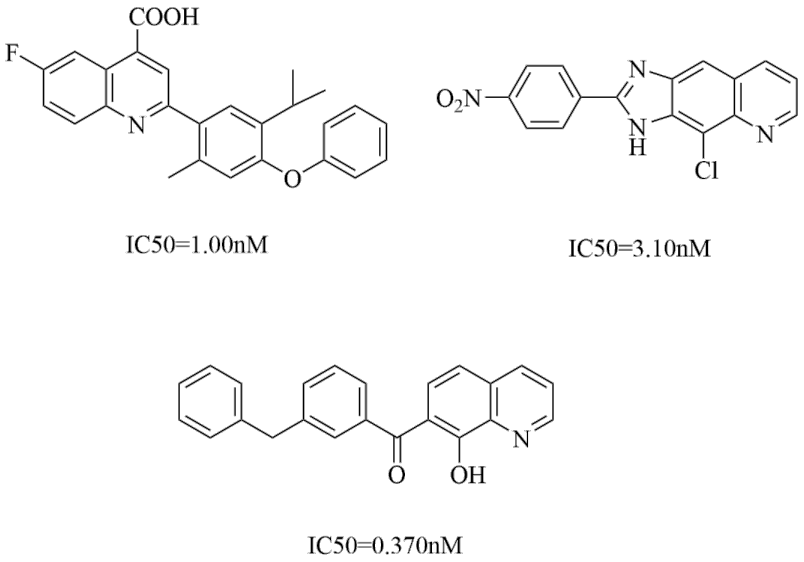

Figure 1.17: Structure of some OSCs quinoline derivatives synthesised by Arslan and co-workers

In OLEDS industries

Over the past two decades, organic light-emitting diodes (OLEDs) have garnered significant attention due to their potential applications in flat screen through the replacement of cathode ray tubes or liquid crystal displays (LCDs).

Electroluminescence is a phenomenon in which the materials might a light under an electric field. This phenomenon has been discovered in an experience of single crystals of anthracene In 1960s [37]. The first discovery has been obtained by Tang and Van Slyke in 1987 in which they recorded sufficient low voltage OLEDs devices based on p-n heterostructure of thin films organic materials. After that, in 1990, at the University of Cambridge, Burroughes et al discover an important new technology of electroluminescence that is come from from polymers [38]. The fundamental structure of an OLED comprised of a thin organic film positioned between two electrodes (Figure 1.18).

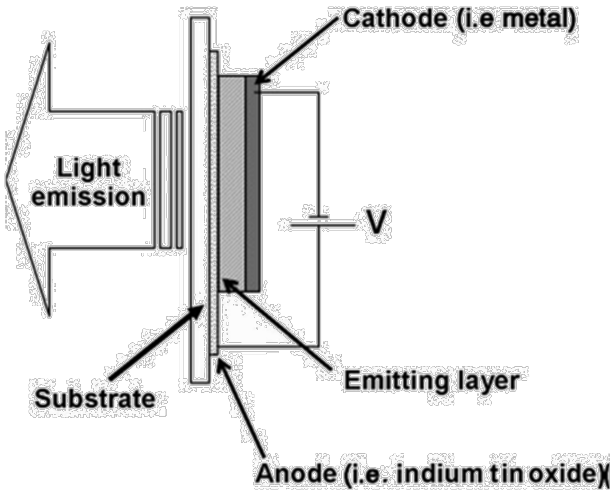

Figure 1.18: Schematisation of basic structure of an OLED

Organic electroluminescent materials based on π-conjugated molecules are nearly insulating, with light generation occurring through the recombination of holes and electrons must injected at the electrodes. The anode is uncoloured and is generally fabricated from indium tin oxide, while the cathode is reflective and fabricated from metal, and the organic layer is very thin, in which its thickness lengths are between 100 and 150 nm. When a voltage is applied across the electrodes, organic material receives injected charges from the anode and electrons from the cathode. Then, from electron hopping phenomenon, the charges flow within the material, follow by recombination in the diode into excitons. After diffusion, the exciton recombines and a photon is emitted.

The energy difference between the highest occupied molecular orbital (HOMO) and the lowest unoccupied molecular orbital (LUMO) levels of the electroluminescent molecule is the origin of the emitted photon colour. Thereby, we can control the frequency of the light emission by the degree of the conjugation in the molecule or the polymer constituted the organic layer of the diode. In order to obtain high performance in the injection from the anode, a low barrier is required regarding the HOMO level of the organic material (typically 5–6 eV).

Quinoline derivatives are heterocyclic compounds which have electroluminescence (EL) properties [39]. Thus, quinoline derivatives ligands or complexes are used to fabricate organic light emitting diodes (OLEDs) [40]. In this regards, Zeyada and co-workers have been developed new 4H-pyrano[3,2-c]quinoline derivatives (Figure 1.19) and investigated their applications in organic photodiode fabrication, in which they found that the new two devices satisfy the conditions to be used as photodiodes. Also, the presence of the chlorophenyl as a substitution group improved the diode parameters.

Recently, Shao *et al* synthesised a novel quinoline derivative containing a phenanthroimidazole moiety that is 2-(8-(benzyloxy)quinolin-2-yl)-1-phenyl-1H-phenanthro[9,10-

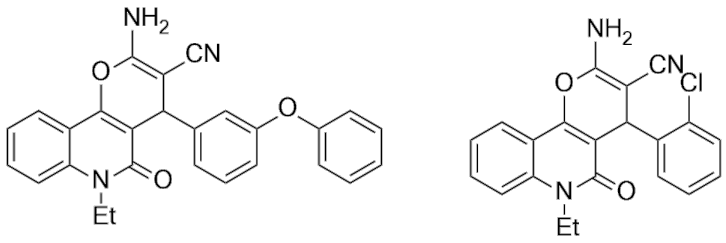

Figure 1.19: Molecular structure of two 4H-pyrano[3,2-c]quinoline derivatives studied by Zeyada and co-workers

d]imidazole (QL-PPI) (Figure 1.20), and studied their physical properties and light-emitting diodes application, in which they found that the QL-PPI shows sky-blue emission, and high thermal stability, in which was employed as emitter to fabricate non-doped OLED.

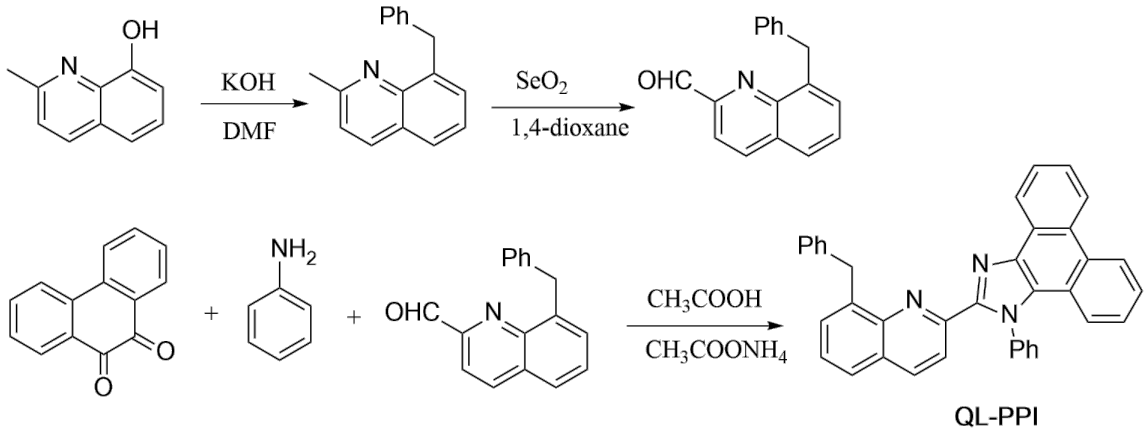

Figure 1.20: Synthesis of 2-(8-(benzyloxy)quinolin-2-yl)-1-phenyl-1H-phenanthro[9,10-d]imidazole

In Optical communications

Optical communications serve as the foundation of information technology infrastructure in today's society, with global Internet traffic increasing 60 percent annually. There is extensive evidence that organic nonlinear optical (NLO) materials are essential for advancing photonic platforms [41].

In recent years, the need for more highly efficient optoelectronic materials has surged dramatically. Thus, numerous theoretical and experimental research groups placed their researches on the development of nonlinear optical (NLO) materials [42]. Organic NLO materials have garnered significant research interest due to their vast potential across various applications such as microlasers, on-chip optical communication, lighting, displaying and Terahertz (THz) generation [43]

Quinoline-based compounds exhibit key properties desired in optoelectronic applications, such as high thermal and chemical stability, efficient electron transport capabilities and structural modification easy. Thanks to these properties, quinoline and its derivatives have applications in various fields, such as organic light-emitting diode (OLED) [44] and solar cell (SC) technologies [45].

Generally, non-symmetric organic compounds are characterized by a second-order nonlinear polarizability behaviour [46]. Especially, the molecules having a π-conjugated bridge and an electron donor and electron acceptor groups which led to a significant increase in the ICT process [47]. Consequently, the transfer of electron density from electron donor to electron acceptor fragment occurs through the π-bridge which lead to NLO properties for electron-donor-π-electron-acceptor organic compounds [48]. In this context, several research groups have concentrated their research to the development of novel quinoline derivatives with optoelectronic properties. Thus, Priyadarshini and coworkers [49] have investigated the non linear optical properties of quinoline derivatives with Schiff bases, in which they synthesised four series of substituted hydrazinoquinoline Schiff bases, that are 4-methyl-2-salicylidenehydrazinoquinoline (1), 4,6-dimethyl-2-

salicylidene hydrazine quinoline (2), 6-chloro-4-methyl 2 salicylidenehydrazinoquinoline (3) and 4-methyl-6-methoxy-2-salicylidene hydrazine quinoline (4) (Figure 1.21). Their computational study suggests that these compounds are characterized by good non-linear properties, which have prospective used in technological related applications.

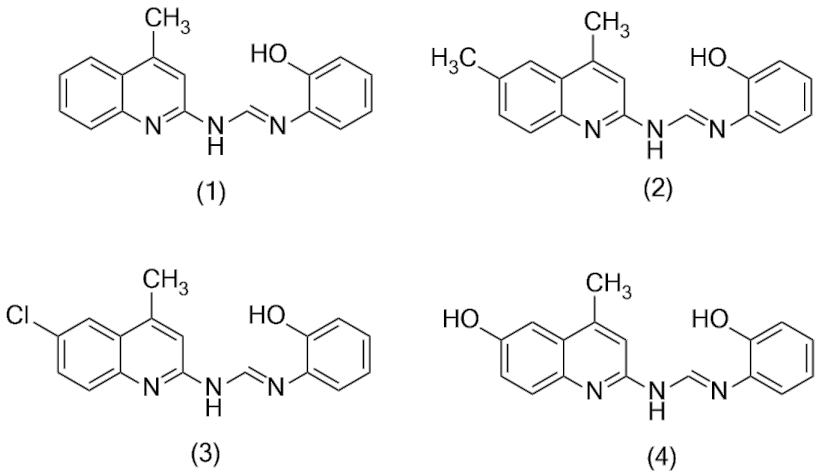

Figure 1.21: Structure of quinoline based Schiff bases studied by Priyadarshini and co-workers

Ali *et al* [50] have reported a computational study included electronic, linear and nonlinear optical properties of di-substituted quinoline derivatives with carbazole moiety (Figure 1.22). They have found that the dipole polarizabilities and hyperpolarizability values of the studied compounds exceed that of the molecules taken as references, which lead to suggest that these NLO active compounds, may find their place in future hi-tech optical devices.

1.6.3 In corrosion inhibition

Corrosion represents a significant global challenge, posing a treat not only to critical industries as petrochemicals but also to infrastructures, including bridges and public buildings [51], which can result in catastrophic failures and significant repair costs [52]. The financial burden of corrosion is substantial. Several researches have been dedicated to finding new effective organic compounds with anti-corrosion properties in highly acidic media [51]. The organic compounds that may have corrosion inhibition activity generally possess in their structure electron-donating atoms such as nitrogen, oxygen, sulphur and phosphorus, which make their adsorption onto metal surfaces easy, thereby, protecting them from acidic solutions [51]. The action mechanism of these compounds may be chemisorption, physisorption, complexation, or precipitation [53].

Many studies have analysed several compounds, such as imidazole derivatives, benzimidazole derivatives and quinoline derivatives as substantial corrosion inhibitors [51]. Thus, quinoline derivatives have become a highly promising class of corrosion inhibitors, especially in acidic media, owing to their distinctive properties and minimal environmental toxicity. In this regards, recently, Belkheiri et al [51] investigates the corrosion inhibition of two synthesized compounds based on quinoline structures, namely, 2-methyl-5-(propoxymethyl) quinolin-8-ol and 2- aminoethyl)amino)methyl)-2-methylquinolin-8-ol (Figure 1.23), in protecting metal alloy in acidic conditions, especially hydrochloric acid, in which they have found that the inhibitors exhibited significant corrosion inhibition efficiencies of 92.37 % for 2-methyl-5-(propoxymethyl) quinolin-8-ol and 84.13 % for 2-aminoethyl)amino)methyl)-2-methylquinolin-8-ol.

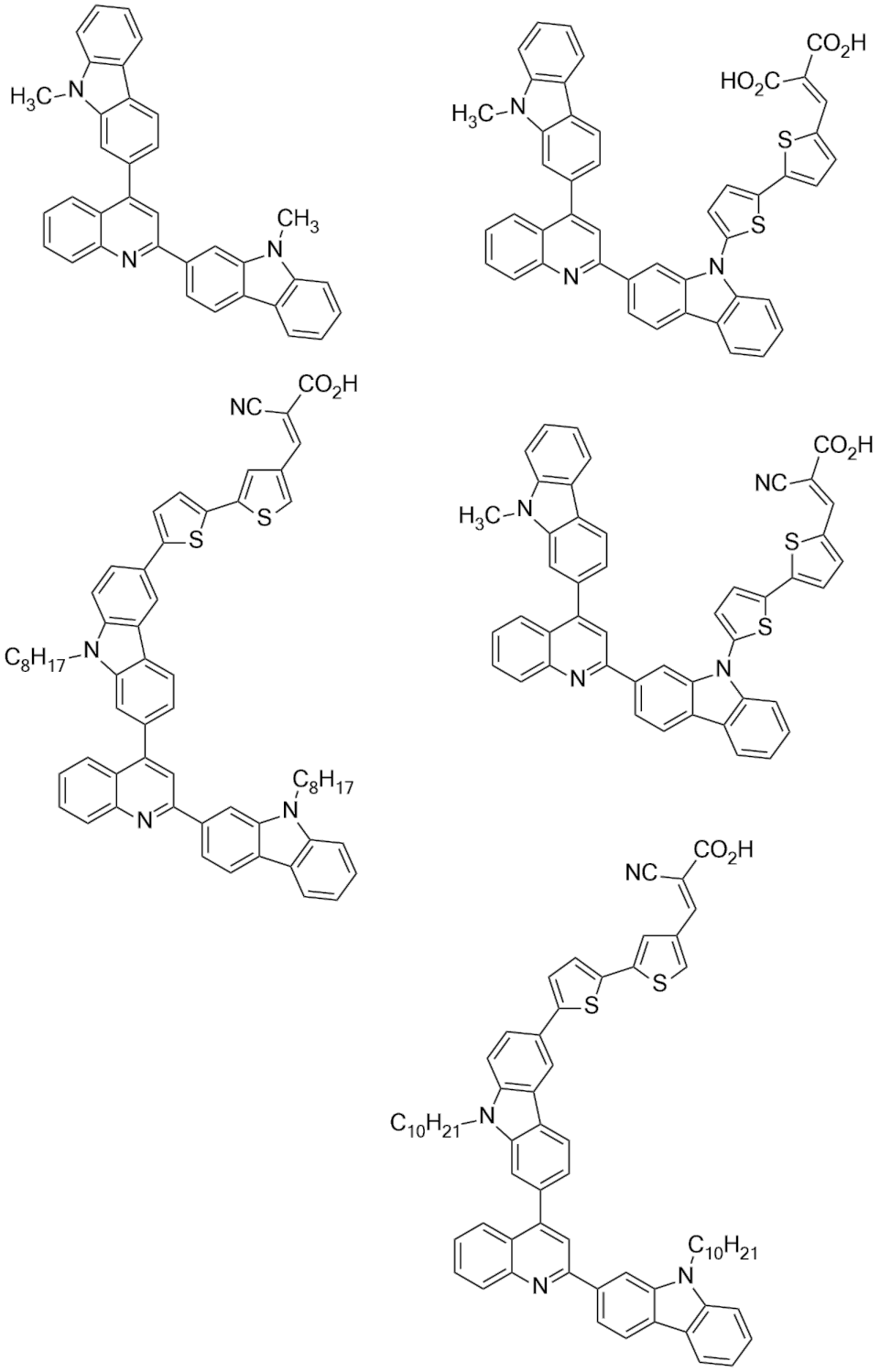

Figure 1.22: Structure of disubstituted quinoline with carbazole studied by Ali et al

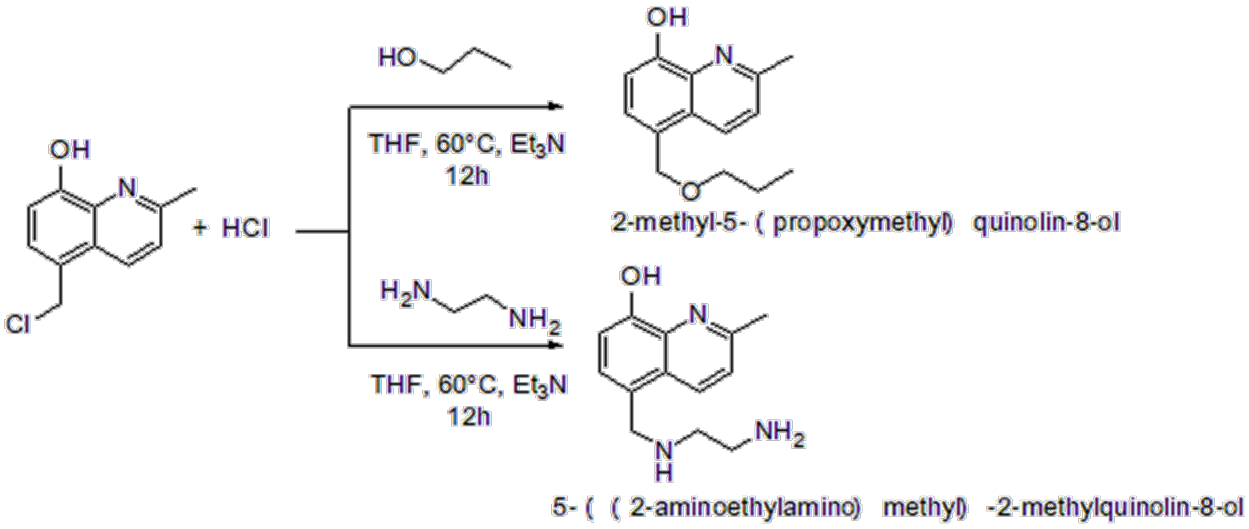

Figure 1.23: Synthesis of 2-(8-(benzyloxy)quinolin-2-yl)-1-phenyl-1H-phenanthro[9,10-d]imidazole

Chapter 2

Quantum computation methods

2.1 Introduction

The study of microscopic phenomena and systems such as atoms and molecules requires the use of the concepts of quantum mechanics, that is based on Schrödinger equation. This function allows access to the physical and chemical properties of the studied system. The resolution of this second-order differential equation gives us the energy values and the associated wave functions. Unfortunately, due to the electron-electron repulsion term presented in the Hamiltonian formalism of poly-electronic systems, this equation can not be solved analytically. Thus, several approximations have been proposed to resolve this equation numerically [54].

This chapter presents a description of the basic ideas of the main quantum methods used in theoretical chemistry to resolve the Schrödinger equation and to extract their properties together with their detailed equations.

2.2 The Schrödinger equation

The Schrödinger equation is the basis of quantum mechanics [55]. Thus, the non-relativistic, time-independent Schrödinger equation describing the electronic structure of atomic or molecular systems can be written as follows:

$$\widehat{H}\psi = E\psi \tag{2.1}$$

[56]

In which:

$$\widehat{H} = \sum_{i=1}^{Na} -\frac{1}{2M_a}\nabla^2 + \sum_{i=1}^{n}\frac{1}{2}\nabla^2 - \sum_{a=1}^{Na-1}\sum_{b>a}^{Na}\frac{Z_a Z_b}{r_{ab}} - \sum_{a=1}^{Na}\sum_{i=1}^{n}\frac{Za}{rai} + \sum_{i=1}^{n-1}\sum_{j>i}^{n}\frac{1}{r_{ij}} \tag{2.2}$$

With:

- $$\sum_{i=1}^{Na} -\frac{1}{2Ma}\nabla^2 \tag{2.3}$$

  and

  $$\sum_{i=1}^{n}\frac{1}{2}\nabla^2 \tag{2.4}$$

  are correspond to the kinetic energy operators associated with nuclei and electrons, respectively.

- $$\sum_{a=1}^{Na-1}\sum_{b>a}^{Na}\frac{Z_a Z_b}{r_{ab}} \tag{2.5}$$

  is correspond the interaction between nuclei.

$$\sum_{a=1}^{Na}\sum_{i=1}^{n}\frac{Z_a}{r_{ai}} \tag{2.6}$$

is correspond the nucleus-electron interaction.

- $$\sum_{i=1}^{n-1}\sum_{j>i}^{n}\frac{1}{r_{ij}} \tag{2.7}$$

  is correspond electron-electron interaction.

[57]

2.3 Approximation of Born-Oppenheimer

This approximation is considered the first approximation that proposed to simplify the resolution of the Schrödinger equation, which based on the fact that the mass of an electron is nearly two thousand times less than that of the nucleus, thereby, the movements of nuclei are very slow compared to the movements of electrons, which leading to consider the nuclei as fixed. Thus, within the framework of this approximation, the Hamiltonian formalism may be reduced to the following equation:

$$\widehat{H} = \sum_{i=1}^{n} -\frac{1}{2}\nabla_i^2 - \sum_{a=1}^{N_a-1}\sum_{b>a}^{Na}\frac{Z_a Z_b}{r_{ab}} - \sum_{a=1}^{N_a}\sum_{i=1}^{n}\frac{Z_a}{r_{ai}} + \sum_{i=1}^{n-1}\sum_{j>i}^{n}\frac{1}{r_{ij}} \tag{2.8}$$

The eigenvalue E of equation (2.8) corresponds to the total energy of the system and contains the kinetic energy (E_K) of the electrons, the interaction energy (E_{Ne}) between the nuclei and the electrons, the electronic and nuclear repulsion energies (E_{ee}) and (E_{NN}) [58].

2.4 *ab-initio* methods

Although the Born-Oppenheimer approximation simplify slightly the analytical resolution of the Schrödinger equation, but it remain incapable to resolving it in polyatomic systems, due to the electronic repulsion term in the Hamiltonian formalism. Thus, farther

approximations should be proposed to face this. [59].

2.4.1 Hartree method

In order to render the Schrödinger equation in the framwork of Born-Oppenheimer approximation possible for resolving, Hartree proposed an approximation which consists of reducing the problem to a single particle moving at its own average potential created by the presence of its supposedly fixed partners, this first simplification called the principle of the self-consistent field, the so-called Hartree method. [60]. The equations for this methodes are precursors to the "Self Consistent Field" SCF . Therefore, the total wavefunction ψ may be written as a product of one-electron wavefunctions.

$$\psi = \psi_1(1)\psi_2(2)\dots\psi_n(n) \tag{2.9}$$

[61]

2.4.2 Hartree-Fock method

The Hartree polyelectronic wave function does not satisfy either the electron indistinguishability principle or the Pauli exclusion principle. To take these two principles into account, Fock proposed writing the total wave function in the form of a determinant, called the Slater determinant. This determinant is made up of monoelectronic functions called spin-orbital and applies to closed-shell systems (comprising an even number of electrons). Each orbital spin is the product of a spatial function ϕ(orbital) depending on the spatial coordinates of the electron and a spin function that can take exclusively two opposite values denoted α and β. The spin density is zero for a closed-shell system. Therefore, the system is symmetrical with respect to these two values and it becomes possible to describe a pair of electrons in terms of the same orbital ϕ_i. In this way, the polyelectronic determinant associated with the system is made up of N/2 orbitals

$\phi_1, \phi_2, \ldots, \phi_n$ and the Pauli exclusion principle is verified because two orbital spins of the determinant comprising the same spatial function have different spin functions. The polyelectronic wave function is written in the summarized form as follows:

$$\psi(1, 2, \ldots, n) = \frac{1}{\sqrt{n!}} |\phi_1(1)\alpha\phi_1(2)\beta \ldots \phi_n/2(n/2-1)\alpha\phi_n/2(n/2)\beta| \tag{2.10}$$

With:

ϕ single-electron molecular orbital and α and β are the spin functions. This formalism allowing the obtention of such wave function ψ called restricted Hartree-Fock (RHF). The Hartree-Fock theory is based on the variational principle , the statement of which can take the following form: for any normalized, antisymmetric wave function ψ, the value of the expected energy will always be greater than the energy of the exact function ψ_0. Where E_0 is the lowest eigenvalue associated with the exact eigenfunction ψ_0. In this way, the optimal Slater determinant ψ_{HF} is obtained by minimizing the term $\langle\psi|H|\psi\rangle$. From the wave function defined in (2.5), we arrive, for the ϕ_i orbitals, at one-electronic equations of the form:

$$\widehat{H}^{eff}(1)\phi_i(1) = \varepsilon_i\phi_i(1) \tag{2.11}$$

$$\widehat{H}^{eff}(1) = h(1) + V_{eff}(1) = h(1) + \sum_{a}^{n/2}[2J_a(1) - K_a(1)] \tag{2.12}$$

$$h(1) = -\frac{1}{2}\nabla_i^2 - \sum_{N_a=1}^{N_a}\frac{Z_a}{r_{ia}} \tag{2.13}$$

The index 1 represents the position of an electron and the term V_{eff} represents the average potential in which each electron moves, it is made up of a sum of coulomb

operators $\widehat{J}_a$, and exchange $\widehat{K}_a$, defined as follows:

$$\widehat{J}_j(1) = \int \frac{1}{r_{12}} \phi_j(2)\phi_j(2) d\tau_2 \tag{2.14}$$

$$\widehat{K}_j(1) = \int \frac{1}{r_{12}} \phi_j^*(2)\phi_i(2) d\tau_2 \tag{2.15}$$

The factor of 2 means that there are two electrons in each orbital. Thus, the Hartree-Fock expression for the molecule's energy E^{RHF} can be written as follows:

$$E^{RHF} = \langle \psi_{HF} | H | \psi_{HF} \rangle = 2 \sum_{i}^{n/2} \varepsilon_i - \sum_{i}^{n/2} \sum_{j}^{n/2} (2J_{ij} - K_{ij}) \tag{2.16}$$

The first term is the sum of the energies of the occupied molecular orbitals, the terms $\widehat{J}_{ij}$ and $\widehat{K}_{ij}$ are determined by operation of the Coulomb operator and exchange on $\phi_i(1)$ and multiply the result by $\phi_i^*(1)$ and integrate over the whole space [62].

2.4.3 The Hartree-Fock-Roothaan method

The Hartree-Fock equations are too complex to be solved directly by numerical analysis techniques, thereby, it is necessary to perform an additional transformation more suitable for numerical treatment, to do this, a new approximation consists of expressing the molecular orbitals (MO) as linear combination of atomic orbitals φ_k (called LCAO) approximation). [63]. These basic functions are generally centered on the nucleus of the different atoms of the molecule. Thus, the orbitals can be written in the form:

$$\phi_i = \sum_{k=1}^{N'} C_{ik} \varphi_{ik} \tag{2.17}$$

The subscript k refers to the wave function of an atomic orbital, and the subscript i refers to a molecular orbital. The calculation of MO therefore boils down to determining the coefficients C_{ik}. The energy of an electron ε_i in a molecular orbital of the molecule

is calculated based on the coefficients C_{ik} for each molecular orbital. This results in the Roothaan and Hall equations [64], which are written as follows:

$$\sum_{k=1}^{N'} C_{ik}\widehat{H}^{eff}\varphi_k = \varepsilon_i \sum_{k=1}^{N'} C_{ik}\varphi_k \tag{2.18}$$

To calculate $\widehat{H}^{eff}$, an estimate of the coefficients of the other molecular orbital ϕ_j must be made. Multiplying equation (2.13) by φ_j^* (where j=1,2,3...,N') and integrating, we obtain the following expression:

$$\sum_{k=1}^{N'} C_{ik}(H_{jk}^{eff} - \varepsilon_i S_{jk}) = 0 \tag{2.19}$$

The terms H_{jk}^{eff} are called the Fock matrix.

$$H_{jk}^{eff} = \langle\varphi_j|\widehat{H}^{eff}|\varphi_i\rangle \tag{2.20}$$

The terms S_{jk} are called the covering matrix.

$$S_{jk} = \langle\varphi_j|\varphi_k\rangle \tag{2.21}$$

Using variation theory, the coefficients are optimized by taking the derivative of ε_i of each coefficient equal to zero.

2.4.4 Configuration interaction method (CI)

The CI is a post-Hartree-fock method used to improve the electronic structure calculations by consideirng electron correlation effects. Thus, this last is considered using a linear combination of the ground-state HF wave function with a large number of excited configurations. In practical CI methods, only electron transitions from the high-occupied (HO) to the low unoccupied (LU) molecular orbital are considered.

- (CIS): Configuration Interaction Single excitation.
- (CID): Configuration Interaction Double excitation.

The CI wavefunction is expressed as follow:

$$\psi_{CI} = C_0\phi_0 + \sum C_{ij}\phi_{ij} + ... \tag{2.22}$$

Where:

- ϕ_0 is the Hartree-Fock reference determinant.
- ϕ_{ij} is is the excited determinants generated by promotion of electrons from occupied to virtual orbitals.
- C_0 and C_{ij} are the CI coefficients which are optimized to minimize the energy.

[65]

2.4.5 Møller–Plesset perturbation theory

For the first forty years, Møller–Plesset perturbation theory was largely ignored, with quantum chemists concentrating on variabl methods. Theoretically physicists developed and computerized the 1950_s in the 1960_s MPn methods up to order n=6 .
Christian Møller and Milton Plesset wrote in the paper: "Perturbation theory was developed to deal with an n-electron system in which the Hartree-Fock solution appears as a zero-order approximation ". On the other hand, Møller and Plesset used the Hartree-Fock theory as a starting point while adding a small perturbation caused by the deviation of the Hartree-Fock Hamiltonian [66].
In the Moller-Plesset method, the zero-order Hamiltonian is defined as a sum of the mono-electronic Hamiltonians $\hat{H}_i^{HF}$:

$$\hat{H}^{(0)} = \sum_{i=1}^{N} \hat{H}_i^{HF} \tag{2.23}$$

and the disturbance of order 1 is:

$$\hat{H}^{(1)} = \hat{H}_i^{electronic} - \hat{H}^{(0)} \tag{2.24}$$

The HF energy associated with the HF wave function of the normalized ground state is given by the following relation:

$$E_{HF} =< \Psi^{HF}/\hat{H}^{electronic}/\psi^{HF} >$$

(2.25)

$$E_{HF} =< \Psi^{HF}/\hat{H}^{(0)}/\psi^{HF} > + < \Psi^{HF}/\hat{H}^{(0)}/\psi^{HF} > \tag{2.26}$$

$$= E^{(0)} + E^{(1)} \tag{2.27}$$

and order energy (2):

$$E_0^{(2)} = \sum_{j\neq 0} \frac{< \psi_j^{HF}/\hat{H}^{(1)}/\psi_0^{HF} >< \psi_0^{HF}/\hat{H}^{(1)}/\psi_j^{HF} >}{E_0^{(0)} - E_j} \tag{2.28}$$

This energy correction is called MP2 calculation .

2.5 Density functional theory (DFT)

The study of the properties of a molecular system often requires consideration of electronic correlation effects. In recent years, density functional theory (DFT) has shown significant potential for the study of molecular systems and chemical problems. There are several major reasons that make DFT an attractive theoretical method for chemistry.

- This theory includes most of the electronic correlation in its formalism.
- The method can be applied to covalent, ionic, or metallic systems.
- Study of larger molecular systems become accessible.

The DFT method was conceptualized in its initial version by Thomas and Fermi after the foundation of quantum mechanics in 1927. This method is used for calculating the quantum states of atoms, molecules, solids, experimental molecular dynamics [67]. It used also in biological systems, in which they have used it to validate the conclusions drawn from the analysis of experiments [68]. It is also used to calculate the structure and interaction of atoms in molecules and crystals. The basic idea for this method is that it is possible to replace the external potential V(r) by the density distribution n(r) [69]. In the DFT method, we assume that electrons do not interact with each other. The electron density is written as follows:

$$\rho(r) = \sum_i |\phi_i(r)|^2 = 2\sum_i^o {}^{cc}|\phi_i(r)|^2 \tag{2.29}$$

with:

ϕ : Non interacting orbitals

ψ : Wave functions

The sum of electron density in all space is written in terms of the total number of electrons n:

$$\int \rho(r)dr = n \tag{2.30}$$

[70].

In the DFT method, the energy of the system is written as follows:

$$E^{DFT} = E^{core} + E^{nuclear} + E^{coulomb} + Exc[\rho] \tag{2.31}$$

With:

- E^{core}: the energy of a single electron with the nuclei.

- $E^{nuclear}$: the energy of the repulsion between nuclei for a given nuclear configuration

- $E^{coulomb}$: the repulsion energy the electrons.

The exchange and correlation energies are written as follows:

$$E_{xc} : \int \rho(r)\epsilon_{xc}[\rho(r)]dr$$

$\rho(r)$ is the electron density is determined from the Khon-Sham orbital:

$$\rho(r) = \sum_{i=1}^{N} |\psi_i|^2 \tag{2.32}$$

[71].

2.5.1 The B3LYP functional

Several functionals, named as hybrid functionals, which including a Hartree-Fock part and a DFT part, have been developed to describe the exchange term. The most famous from them is the B3LYP hybrid functional [72], in which the formalism of the exchange and correlation energy is written as follows:

$$E_{XC}^{B3LYP} = a_0 E^{LDA}_{X} + (1 - a_0)E^{HF}_{XC} + a_1 \Delta E^{Becke}_{X} + E^{LDA}_{C} + a_2(E^{LYP}_{C} - E^{LDA}_{C}) \tag{2.33}$$

With: a_0=0,80, a_1=0,72 et a_2=0,81. This functional is famous, because it gives very good results and, therefore, is extremely popular.

2.5.2 The PBE functional

This functional was proposed by Perdew, Burke and Ernzerhof in 1996 [73], and is designed to improve upon the Local density Approximation (LDA) by incorporating gradient coorrections to the exchange-correlation energy. It is known for its general applicability and gives rather accurate results for a wide range of systems. It classified as a generalized gradient approximation (GGA) functionals for the exchange-correlation energy E_{xc}. It is widely used in materials science due to its good balance between accuracy and computational cost.

The exchange and correlation expression is written as follows:

$$E_{XC}^{PBE} = \int \rho(r)\epsilon_{PBE}^{XC}(\rho, \Delta\rho)dr \tag{2.34}$$

Where: $\rho(r)$ is the electron density and ϵ_{PBE}^{XC} is the exchange-correltaion energy per electron.

2.5.3 The B3PW91 functional

The B3PW91 functional is a hybrid functional used in DFT calculations, in which it combines the Becke's 3-parameters (B3) exchange functional with the Perdew-Wang 1991 (PW91) generalised gradient approximation exchange-correlation functional. The exchange and correlation expression is written as follows:

$$E_{B3PW91}^{XC} = (1-a)E_{LSDA}^{X} + aE_{HF}^{X} + b\Delta E_{GGA}^{X} + cE_{C}^{LSDA} + dE_{PW91}^{GGA_C} \tag{2.35}$$

Where: E_X^{LSDA}=Local Spin Density Approximation (LSDA) exchange energy.

ΔE_X^{GGA}=Gradient correction to exchange.

E_C^{LSDA}=LSDA correction energy.

$E_C^{GGA_{PW91}}$=generalized gradient approximation (GGA) correlation energy.

a, b, c and d are emerically determined parameters that define the weight of each contribution.

2.5.4 The CAM-B3LYP functional

The CAM-B3LYP is an hybrid exchange–correlation functional proposed by Yanai, Takeshi, David P. Tew, and Nicholas C. Handy. It combines the hybrid qualities of B3LYP and the long-range correction presented by Tawada *et al.* It is considered as a modified version of B3LYP functional which designed to correct its shortcomings in long-range electron interactions, particularity charge transfer excitations in Time-Dependent DFT (TD-DFT) calculations.

The exchange-correlation energy expression is given by the following equation:

$$E_{XC}^{CAM-B3LYP} = (\alpha+\beta)E_X^{SR-HF}+(1-\alpha-\beta)E_X^{SR-DFT}+(\alpha)E_X^{LR-HF}+(1-\alpha)E_X^{LR-DFT}+E_C^{B3LYP} \tag{2.36}$$

Where:

- SR (Short-Range) and LR (Long-Range) refer to different distance regions in electron interactions,
- E_X^{DFT} is the DFT exchange energy (from GGA functionals),
- E_C^{B3LYP} is the standard B3LYP correlation energy,
- α and β are parameters control the fraction of exact exchange at different distances.

2.6 The atomic orbital basis set

The LCAO method expresses molecular orbitals as a linear combination of atomic orbitals (AOs), called basis functions [63].

The molecular orbitals written in the LCAO method are a linear combination of atomic

orbitals (AO), called basis functions, written as follows:

$$\psi_{n,l,m} = NY_{lm}(\theta,\phi)P(r)^{n-1}exp(-\frac{2r}{na_0}) \tag{2.37}$$

With:

- P is a polynoial,
- r and Y_{lm} are the classic angular functions.

Slater [74] proposed a new type of functions named as STO which are the best defined analytical OA of the following form:

$$\psi_{n,l,m} = Nr^{n-1}exp(-\zeta r)Y_{lm}(\theta,\phi) \tag{2.38}$$

With:

- N is the normalization factor,
- ζ is the orbital expontial,
- $Y_{l,m}(\zeta,\phi)$ is the spherical harmonics.

In this type of function, the exponential poses great difficulty in calculating integrals in polyatomic systems. Thus, Boys replaced this exponential with Gaussian function type(αr^2).

$$g(\alpha,r) = CX^nY^lZ^mexp(-\alpha r^2) \tag{2.39}$$

α is a constant determining the size of the function.
The r^2 dependence of the exponential term makes the Gaussian functions less efficient than the Slater-type orbitals (STO) in two points. While this basis provides a fairly good description of the electron density at distances far from the nucleus, the description

of the behavior of the exact wave function near the nucleus is quite poor (See Figure 2.1).

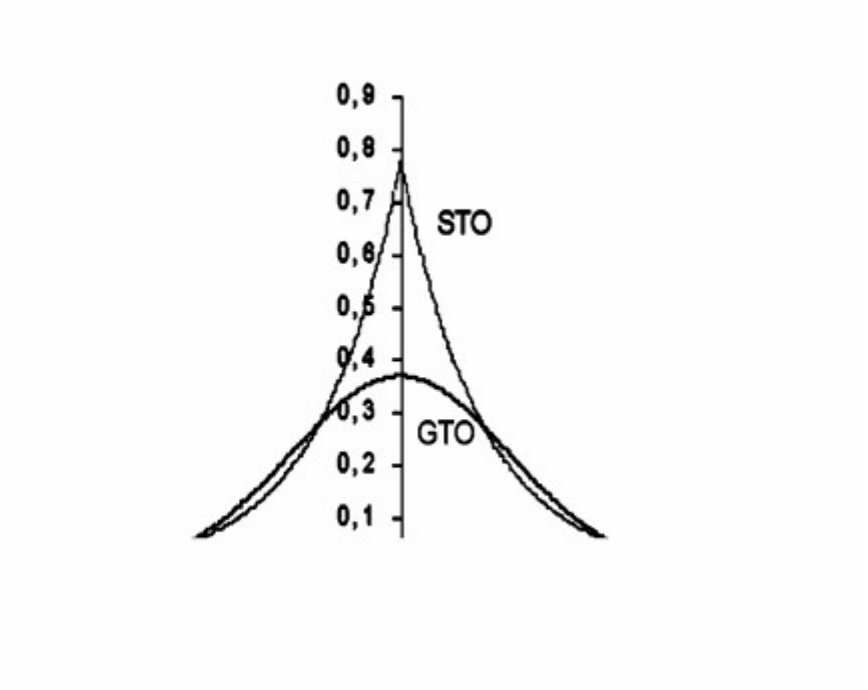

Figure 2.1: Comparison between STO and GTO

Therefore, it's replaced by a linear combination of several Gaussians. To understand the base improvement strategy, we divide the space into three regions.

2.6.1 The inner orbitals

The nuclear potential has spherical symmetry because the electrons are positioned close to the nucleus and the atomic orbitals fit perfectly, but since the energy is very sensitive to the position of the electron close to the nucleus, it is preferable to use a large number of Gaussian orbitals.

2.6.2 The valence zone

In this region, the electron density is de-localized between several atoms [71], in which it has not a spherical symmetry. Therefore, we should be use to describe them the following:

- The split valence zeta multiple For example, for carbon, a DZ base will use two valence s orbitals 2s (inner) and 2s' (outer) and six p orbitals; 2px , 2py , 2pz (inner) and 2px , 2py , z (outer). The usual good-quality bases are DZ and TZ [75].

- The addition of polarization orbitals; it must be taken into account that atoms in the molecule undergo deformation of the electron cloud due to the environment. This phenomenon can be taken into account by introducing additional functions into the atomic basis set, called polarization functions. The addition of these functions is very useful for obtaining a good description of quantities such as dissociation energy, dipole moments,... etc. These functions allow us to increase the flexibility of the basis set by taking into account the deformation of valence orbitals during the deformation of the molecule. These orbitals are of type p, d for hydrogen, d, f and g for atoms in the 2nd and 3rd periods, ..., etc. [76].

2.6.3 The diffuse zone

Beyond the valence shell, far from the nuclei, diffuse orbitals can be added. These AOs are not essential in usual systems, but become so when we are interested in long-range interactions (Van der Waals complex), species with lone pairs and charged species (anions). these type of orbitals are denote by the (+) sign. [77].

2.6.4 Common nomenclature of basis set

Except the minimal basis STO-3G, the widely used basis set is symbolized by n-n'n"... (++)(**).

- ++ designates sets of diffuses

- ** designates functions d on atoms of the second period, and functions p on hydrogen [71].

Chapter 3

Quantum models and descriptors for chemical reactivity

3.1 Introduction

The study of the stability of certain molecules and their resulting physical and chemical properties remains a challenge for researchers in various academic and industrial fields. Quantum chemistry offers the possibility of studying chemical reactivity and calculating and predicting some physicochemical properties of certain materials. Different quantum theories have been discovered for doing this. In this chapter we will present the most used quantum models and descriptors that used to study chemical structures and related properties, namely, the frontier molecular orbital method, the global reactivity indices derived from conceptual DFT, Quatum Theory of Atoms in Molecules (QTAIM),...etc.

3.2 Frontier molecular orbital method

The frontier molecular orbital (FMO) theory was developed in the 1950s by K. Fukui [78] to explain the regioselectivity observed during reactions involving aromatic compounds.

Fukui's original idea was to postulate that during a reaction between a nucleophile and an electrophile, the charge transfer that occurs near the transition state primarily involves the electrons in the nucleophile's highest occupied molecular orbital (HOMO). As a result, the electron density associated with these electrons, which he called frontier electrons, should explain the reactivity.

3.3 Global reactivity indices

In recent years, various approaches of great importance in quantum chemistry based on the theorems of Kohn and Hohenberg have emerged. Thus, the first theorem of Kohn and Hohenberg [79] shows that the electron density $\rho(r)$ determines the number of electrons N in the system as shown by the following relation:

$$N = \int \rho(r) dr \tag{3.1}$$

$\rho(r)$ determines v and the Hamiltonian of the N-electron system, and the energy E; thus E is a functional of $\rho(r)$ or of N and v(r).

$$E = E[\rho(r)] \tag{3.2}$$

$$E = E[N, V(r)] \tag{3.3}$$

The variation in the energy of the system is due to the perturbation of the number of electrons or external potential exerted when another reactant approaches. The energy of the molecule can therefore be expressed in the form of a Taylor development:

$$(\frac{\partial^m E}{\partial n \partial n'}), avec : m = n + n' \tag{3.4}$$

3.3.1 The electronegativity χ

According to the definition of Iczkowski and Margrave [80], electronegativity is defined as the derivative of energy with respect to N (N is the number of electrons), it is a global property that does not change from one point to another in space.

$$\chi = -(\frac{\partial E}{\partial N})_V \tag{3.5}$$

The electronegativity χ can be re-expressed according to the finite difference approximation by:

$$\chi = \frac{1}{2}(EI + EA) \tag{3.6}$$

Where EI and EA are the ionization energy and electron affinity respectively, which are given by:

$$EI = E(N_0 - 1) - E(N_0) \tag{3.7}$$

$$EI = E(N_0) - E(N_0 + 1) \tag{3.8}$$

3.3.2 The chemical potential μ

By analogy with the chemical potential $\mu_i = (\frac{\partial G}{\partial n_i})_{P,T,n_j}$ in thermodynamics, the partial derivative of energy with respect to the number of electrons has been called the electronic chemical potential μ [81].

$$\mu = (\frac{\partial E}{\partial N})_V \tag{3.9}$$

The chemical potential μ can be expressed according to the finite difference approximation by:

$$\mu = \frac{-(I + A)}{2} \tag{3.10}$$

3.3.3 The hardness η

Parr and Pearson [82] identified hardness as the second derivative of energy with respect to the number of electrons according to the following relation:

$$\eta = (\frac{\partial^2 E}{\partial N^2})_V = (\frac{\partial \mu}{\partial N})_V \tag{3.11}$$

The approximate expression of hardness is given by:

$$\eta = \frac{1}{EI - EA} \tag{3.12}$$

Chemical hardness η is a measure of the stability of the system; the system with the maximum hardness is the most stable.

3.3.4 The softness S

Softness [83] is defined as the inverse of hardness, it is the ability of an atom or molecule to retain an acquired charge, this property is given by the following relation:

$$S = \frac{1}{2\eta} = \frac{1}{2}(EI - EA) \tag{3.13}$$

3.3.5 The electrophilicity ω

The electrophilicity ω [84]is defined as the energetic stabilization due to charge transfer when the system acquires an electronic charge ΔN. The approximate expression of ω in the ground state is:

$$\omega = \mu^2/2\eta \tag{3.14}$$

Where μ is the electronic chemical potential and η is the chemical hardness.

3.4 Quantum theory of atoms in molecules

In 1985, Bader [85] was careful enough to write that the atom and its properties may be defined by quantum mechanics. Thus, the topology analysis proposed by Bader was firstly used for analyzing electron density in "atoms in molecules" (AIM) theory, which is also known as "the quantum theory of atoms in molecules" (QTAIM) (Figure 3.1).

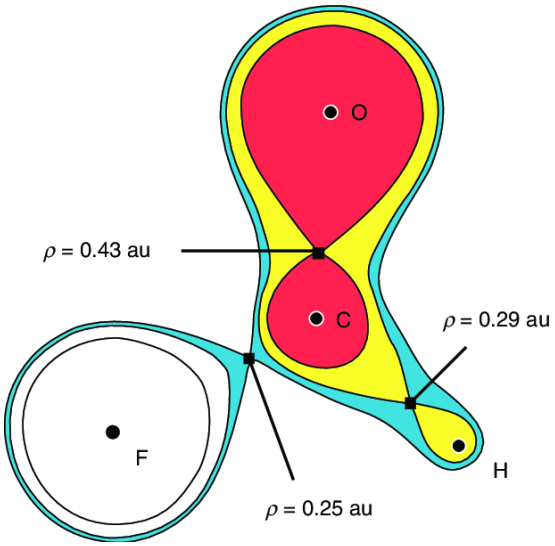

Figure 3.1: Electron density in HFC=O molecule

Basing on topological analysis of electronic density, QTAIM is a model of quantum chemistry used to distinguish chemical systems. Thus, this method was developed to study the properties of atoms, bonds and other interactions between atoms and molecules, and to determine the electronic density values, the Laplacian, and the potential energy values for critical points. In QTAIM analysis, most properties are derived from the electron density $\rho(r)$. Thereby, the electron density gradient is zero at critical points (cp). These latter can be divided into four types of critical points (Figure 3.2) based on the second derivative of the electron density (Hess matrix), that are as follow:

- (3,-3) critical points type or NCPs: these points are characterized by all second

derivatives in the three directions being negative, indicating the location of the nucleus.

- Type (3,-1) critical points, or BCPs. In these points, the second derivative in two directions is negative and the third direction is positive, indicating the presence of a chemical bond.
- Type (3,+1) critical points: or CCPs, here, the second derivative in two directions is positive and the third direction is negative, indicating the presence of a ring.
- Type (3,+3) critical points: or RCPs, where all second derivatives in the three directions are positive and indicate the presence of a cage

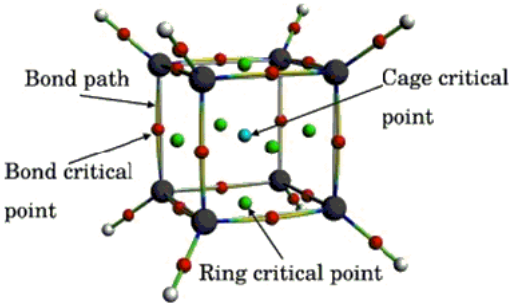

Figure 3.2: Types pf bond critical points

3.5 The molecular electrostatic potential (MEP)

Molecular electrostatic potential (ESP) has been widely used for prediction of nucleophilic and electrophilic sites for a long time. It is also valuable in studying hydrogen bonds, halogen bonds, molecular recognitions and the intermolecular interaction of aromatics (Figure 3.3). This function measures the electrostatic interaction between a unit point charge placed at r and the system of interest. A positive (negative) value implies that

current position is dominated by nuclear (electronic) charges.

$$V_{ESP}(r) = V_{nuc}(r) + V_{ele}(r) = \sum_A \frac{Z_A}{r - R_A} - \int \frac{\rho(r')}{r - r'} dr' \tag{3.15}$$

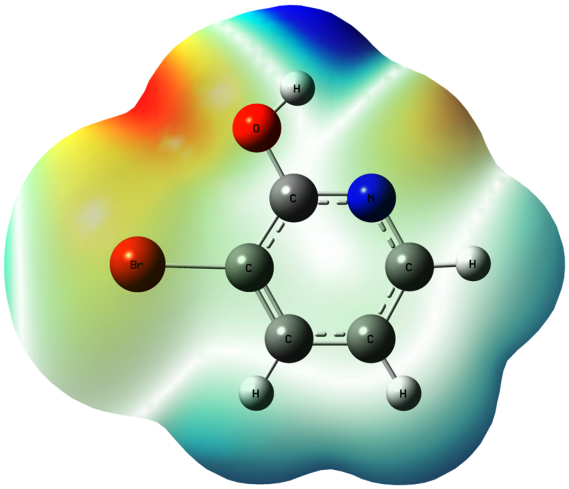

Figure 3.3: Map of molecular electrostatic potential of 3-bromopyridin-2-ol molecule

Chapter 4

General aspects and theoretical estimation of molecular optics

4.1 Optical field

Optics is an important field of physics [86], it is the science where we study the interaction between light and matter. It is divided into two types; linear optics (LO) and nonlinear optics (NLO). When the light waves are characterized by low intensity and do not interact with each other when they penetrate matter and propagate through a medium, this domain is called linear optics. contrariwise, when light becomes more intense and the optical properties begin to intensify, along with other properties of light; this is the domain of non-linear optics [87].

Optical properties are used in the development of optoelectronic devices for communications, optical switching, information, and information processing.

The nonlinear optics was first discovered by Franken and his co-workers in 1960, leading to the discovery of harmonic generation, shortly after Maiman demonstrated the first functional laser in 1960.

In recent years, organic materials have attracted scientific and economic interest due to

their properties, such as high photoelectric coefficients fast response times. They are also the most promising candidate materials for optoelectronic applications, encouraging the exploration of new colored materials with exceptional optical properties [88]. Thus, several electronic devices in many fields of application have been replaced by optical devices in recent years [89].

4.1.1 Linear optical OL

In the linear optics, the light waves are of low intensity and do not interact with each other as they enter and propagate through a medium. The interaction between light and matter does not depend on the intensity of illumination.
In 1988, Bishop showed that when a molecule undergoes of an external electric field, its energy changes according to the following equation:

$$\Delta E = -\mu_i E - \alpha_{ii} E^2 - \frac{1}{2!}\alpha_{ij} E_i E_j - \frac{1}{3!}\beta_{ijk} E_i E_j E_k - \frac{1}{4!}\gamma_{ijkl} E_i E_j E_k E_l \qquad (4.1)$$

With:

- μ_i represents the components of the total dipole moment,
- α_{ij}, α_{ii} represents the non diagonal and diagonal components of the polarizability tensor,
- β_{ijk} represents the components of the first hyperpolarizability tensor,
- γ_{ijkl} represents the components of the second hyperpolarizability tensor [86]

The dipole moment μ

In structural chemistry, the dipole moment of a molecule is an important factor [90], physically defined as a measure of the residual voltage that remains even if the total system load is zero [86]

The total dipole moment in the case of high-power light interacting with matter, which in turn leads to NLO effects, can be expressed by the following statement [91]:

$$\mu_i = \mu_i^0 + \sum_j^{x,y,z} \alpha_{ij} E_j + \frac{1}{2!} \sum_j^{x,y,z} \beta_{ijk} E_j E_k \tag{4.2}$$

Where, μ_i^0 is the permanent dipole moment given by:

$$\mu^0 = \sqrt{\mu_x^2 + \mu_y^2 + \mu_z^2} \tag{4.3}$$

The polarizability α

The polarizability represents the tendency of a system's electron cloud to be distorted within the limits of a zero applied field [92], it is the second derivative of the energy of the system, given the applied electric field, which gives an information about the distribution of electrons in the molecule [86].

The polarizability is given by the following expression [92]:

$$< \alpha >= \frac{1}{3}(\alpha_{xx} + \alpha_{yy} + \alpha_{zz}) \tag{4.4}$$

The anisotropy of polarizability $\Delta\alpha$

The anisotropy of polarizability shows subtle variations depending on the structure of the studied compound [93], and it is given as follow:

$$(\Delta\alpha) = \frac{1}{\sqrt{2}} \sqrt{(\alpha_{xx} - \alpha_{yy})^2 + (\alpha_{yy} - \alpha_{zz})^2 + (\alpha_{zz} - \alpha_{xx})^2 + 6(\alpha_{xy}^2 + \alpha_{yz}^2 + \alpha_{xz}^2)} \tag{4.5}$$

4.1.2 Non-linear optical NLO

The non-linear optics is a set of phenomena resulting from the nonlinearity of the response of a physical medium to the action of an electromagnetic wave in the optical field. It also describes the behavior of light in a non-linear material [94]. The non-linear optical processes have received considerable attention due to their importance for optical signal processing and computer science [95].

The non-linear optical properties of molecules are of particular interest in chemistry and materials science, where new molecules or materials are sought with properties for applications in dynamic holography and optical switching technologies. These NLO properties play an important role in the study of other physical and chemical properties of molecules [89].

The first hyperpolarizability β

The first hyperpolarizability can be defined by 3×3×3 matrix and may be be reduced to 10 numbers using kleinmans notations; β_{xxx}, β_{xxy},β_{xyy}, β_{yyy}, β_{xxz}, β_{xyz}, β_{yyz}, β_{xzz}, β_{yzz}, β_{zzz}. [96], β_{tot} are defined as follows :

$$\beta_{tot} = (\beta_x^2 + \beta_y^2 + \beta_z^2) \tag{4.6}$$

witch:

$$\beta_x = \beta_{xxx} + \beta_{xyy} + \beta_{xzz} \tag{4.7}$$

$$\beta_y = \beta_{yyy} + \beta_{yzz} + \beta_{yxx} \tag{4.8}$$

$$\beta_z = \beta_{zzz} + \beta_{zxx} + \beta_{zyy} \tag{4.9}$$

[97] The first hyperpolarisability (β) provides information about the ability of the material to generate second-ordre non linear effect [98].

4.2 Quantum mechanical estimation of μ, α, β tensors

Non linear optical phenomena in the sense that they occur when the response of physical system to a non-linearly applied optical field depends on the intensity of the optical field, where as in linear optics, the intensity of the incident light, as in the case of classical interactions : elastic sattering, refraction and reflection [87].

Linear and non-linear optical properties such as polarizability α and hyperpolarizability β are estimated in two steps. The first step is to optimize the geometry of the structure, using DFT density functional theory using the B3LYP functional with the 6-311++G(d,p) basis.
Once the optimum geometry had been obtained, the polarizability and hyperpolarizability were calculated using the PBE function with the finite field method (FF).

4.3 Matter polarization

The most fundamental manifestation of light's interaction with matter, which of great technological importance, is the separation of charges induced by the electric field (polarization) [99] .
The phenomen of polarization accurs when laser radiation interacts with a material and is expressed according to N.Bloembergen model, with the following relationship:

$$P_i = \sum_j \chi^{(1)}\zeta_j + \sum_{jk} \chi^{(2)}_{ijk}\zeta_j\zeta_k + \sum_{jkl} \chi^{(3)}_{ijk}\zeta_j\zeta_k\zeta_l + ... \tag{4.10}$$

With P is the polarization induced along axis i by the electric field ζ of components ζ_j, ζ_l and ζ_l [100].

4.4 Calculation methods of μ, α, β tensor elements

4.4.1 The Hellmann-Feyman theorem

According to Hellman-Feyman theory, the exact electronic energies and wave functions of a molecule, known as relation (4.2) , allow us to calculate polarizability and hyperpolarizability either by deriving the dipole moment, or by deriving the total energy of the perturbed system, with respect to the applied external electric field:

$$\frac{\delta E}{\delta \lambda_i} =< \phi | \frac{\delta H}{\delta \lambda_i} | \phi > \tag{4.11}$$

λ_i are parametrs [101]

This theory can also be demonstrated for approximate wave functions [102]. In this theorem the for concern the derivative of energy with respect to a parameter, the electric field. The derivative of E with respect to F is there fore writhen:

$$\frac{dE}{dF} =< \frac{\delta \phi}{\delta F} | H | \phi > + < \phi | \frac{\delta H}{\delta F} | \phi > + < \phi | H | \frac{\delta \phi}{\delta F} > \tag{4.12}$$

The theory is as follows :

$$\frac{\delta E}{\delta F} = \frac{\delta < H >}{\delta F} =< \phi | \frac{\delta H}{\delta F} | \phi >=< \frac{\delta H}{\delta F} > \tag{4.13}$$

[103]

4.4.2 The Hartree-Fock coupled perturbation theorem (CPHF)

The Hartree-Fock theorem(CPHF) is a fundamental step in the analytical calculation of the first derivatives of the configuration interaction (CI) wave function energy and the second derovatoves of the Haryree-Fock (HF) wave function energy [104]. For Hartree-Fock equations:

$$F\phi_k = e_k\phi_k \tag{4.14}$$

Where F is the operator, ϕ_k is the function and e_k is the function and e_k is the energy .

$$F = F^{(0)} + F^{(1)} + F^{(2)} + ...F^{(p)} = \sum_{p\geqslant 0} F^{(p)} \tag{4.15}$$

$$\phi_k = \phi^{(0)}_k + \phi^{(1)}_k + \phi^{(2)}_k + ...\phi^{(p)}_k = \sum_{p\geqslant 0} \phi^{(p)}_k \tag{4.16}$$

$$e_k = e^{(0)}_k + e^{(1)}_k + e^{(2)}_k + ...e^{(p)}_k = \sum_{p\geqslant 0} e^{(p)}_k \tag{4.17}$$

The total energy E(ψ_i) of the system perturbed by an electric field ψ_i, defined as:

$$E(\psi_i) = \sum_{p\geqslant 0} E^{(p)}(\psi_i) \tag{4.18}$$

From the first, second and third derivatives of the energy with respect to the ψ_i component of the external electric field applied with change of signe, we obtain the dipole moment, the polarizability and the hyperpolarizability of first order, respectively: [100]

- The dipole moment μ:

$$\mu_i = \frac{-\delta E(\phi_i)}{\delta\phi_i}|_{\phi_i=0} \tag{4.19}$$

- The polarizability α :

$$\alpha_{ii} = \frac{-\delta E^2(\phi_i)}{\delta\phi_i^2}|_{\phi_i=0} \tag{4.20}$$

- The hyperpolarizability β :

$$\beta_{ii} = \frac{-\delta E^3(\phi_i)}{\delta\phi_i^3}|_{\phi_i=0} \tag{4.21}$$

4.4.3 Finite perturbation theory FF

The method Finite Perturbation theory FF was first introduced by H.D.cohen, who developed it to calculate the polarization of atoms with closed layers and used to calculate of the polarizability and first hyperpolarizability [100]. One method for calculating optical properties is the Finite Field (FF) method, used because it is a fast and easy numerical technique. A well-known drawback of the FF method is the dependence of the calculated quantity on the initial field strength [105].

This method makes it possible to evaluate the first hyperpolarizability as energy derivatives of the electric field.

The first hyperpolarizability is defined in the method as the third-order derivative of the energy or the second-order derivative of the dipole moment with respect to the electric field according to equation:

$$\beta = (\frac{\delta^3 E}{\delta E^3})_{E=0} = (\frac{\delta^2 \mu}{\delta E^2})_{E=0} \tag{4.22}$$

[106]

In this method, the dipole moment μ of a molecule in the presence of homogeneous electric field E_i is represented by the following expression.

$$\mu_i = \mu_{0i} + \alpha_{ij} E_j + \beta_{ijk} E_j E_K + \gamma_{ijkl} E_j E_k E_l + ... \tag{4.23}$$

Where μ_0 is the dipole moment, $\alpha_{ij} E_j$ is the polarizability, $\beta_{ijk} E_j E_k$ is the first hyperpolarizability and γ_{ijkl} is the second hyperpolarizability. The polarizability and the first hyperpolarizability are obtained by numerically deriving the dipole moment of the electric field comonents in the zero-field limit, for the diagonal terms :

$$\alpha_{zz} = \frac{\mu_z(E_z) - \mu_z(-E_z)}{2E_z} \tag{4.24}$$

$$\beta_{zzz} = \frac{\mu_z(E_z) + \mu_z(-E_z) - 2\mu_{0z}}{2E_z^2} \tag{4.25}$$

[107]

4.4.4 Practical application of nonlinear optics

Materials with non-linear optical properties are used for development of optoelectronic devices, optical switching and electro-optical modulators, information processing, optical frequency conversion, optical signal processing, and image processing using ultrashort laser pulses [94]. Development of optoelectronic devices, optical switching and electro-optical modulators, information processing, optical frequency conversion, optical signal processing, and image processing using ultrashort laser pulses.

4.4.5 The optical properties of organic materials

The choice of aromatic organic molecules was based on the strong delocalization of the π electrons in their structure, which leads to the creation of a high molecular polarizability. On the other hand, the substituted organic materials are characterized by very good non linear optical properties due to their donor and acceptor arrangement π-conjugated bond [96]. Inorganic materials have excellent chemical properties but low non-linear efficiency. These limitations have led to the search for new materials with good NLO properties. Conjugated molecules that lead to charge transfer systems have been extensively studied for their NLO properties. These conjugated systems allow charge transfer within the molecule in response to the external electronic field.

There are three factors that contribute to the system's non-linear response:

- The electronic richness of the π-conjugate center
- Flatness of the molecule

- The molecular symmetry

Due to the unique properties of organic molecules, namely, for their rapid non-linear response, they have been the subject of a tremendous both experimental and computational studies [105].

4.5 UV-Vis spectroscopy

4.5.1 Generalities

Electronic spectroscopy refers to the study of how materials absorb light in the ultraviolet (UV) and visible (Vis) regions of the electromagnetic spectrum, as it involves the excitation of electrons from lower to higher energy atomic or molecular orbitals upon exposure to light.

Electron transfer processes can occur in transition metal ions through d-d transitions or charge transfer between ligands and metals (ligand-to-metal or metal-to-ligand transitions) as well as in organic and organometallic molecules, primarily via n-π^* and π-π^* transitions. Such transitions are the reason in which the materials appear colored. While isolated atoms undergo only electronic transitions can be observed. However, molecules usually involves a simultaneous electronic, vibrational, and rotational excitations when exposed to UV-vis radiation [108].

According to the Beer-Lambert law [109], the strength of these absorption bands depends on both the oncentration C of the substance and the path length l of the sample.

$$A = log_{10}(I_0/I) = \epsilon.C.L \tag{4.26}$$

Where:

A is the absorbance,

I_0 is the intensity of the monochromatic light before absorption by the sample, while I is

its intensity after passing through the sample,

and ϵ is the extinction coefficient.

The change in energy is usually described using the following equation:

$$\Delta E = h\nu = hc/\lambda = hc\overline{\nu} \tag{4.27}$$

Where:

-ν is the frequency of the electromagnetic radiation,

-c is the speed of light in the vacuum,

-λ is the vacuum wavelength.

The UV-Vis spectrum is split into the UV region (200–400 nm) and the visible region (400–800 nm), which includes light visible to the human eye.

The properties of materials can be determined, in particular, by means of:

- TThe band gap, which arises from electronic transitions between the top of the valence band and the bottom of the conduction band, as explained by the band theory of solids,
- Electronic transitions occurring within the d orbitals of transition metal ions,
- Charge transfer processes occur when electron density moves from a filled orbital to a partially occupied orbital, such as from non-liant oxygen orbitals towards Mn^{+} filled orbital.
- Transitions between electronic levels: $n \rightarrow \pi^{*}$ or $\pi \rightarrow \pi^{*}$.

From equation (4.27), electrons can be excited from the ground state, typically a singlet state, to higher electronic states. The return to the ground state usually occurs through fluorescence, involving the emission of radiation.

4.5.2 Types of electronic transitions

Transitions of σ, π and n electrons

In the UV-Vis range, absorption is often attributed to the excitation of specific electrons in a particular group of the system, known as a chromophore, which is responsible for the 'color' of the compound. The substituents that do not inherently impart color but enhance (hyperchromic effect) or reduce (hypochromic effect) the coloring power of a chromophore are called auxochromes or antiauxochromes. Groups that cause a shift in the absorption maximum to lower or higher wavenumbers are known as bathochromic or hypsochromic groups, respectively.

In polyatomic molecular systems, electrons can occupy bonding (σ or π), antibonding (σ or π), or nonbonding (n) molecular orbitals. The order of increasing electronic energy is generally as follows: σ<π<n<σ^*<π^*.

The lectrons are raised from bonding or nonbonding orbitals to empty antibonding orbitals, as follow: σ→σ^*, π →π^*, n→π^* and n→σ^* (Figure 4.1).

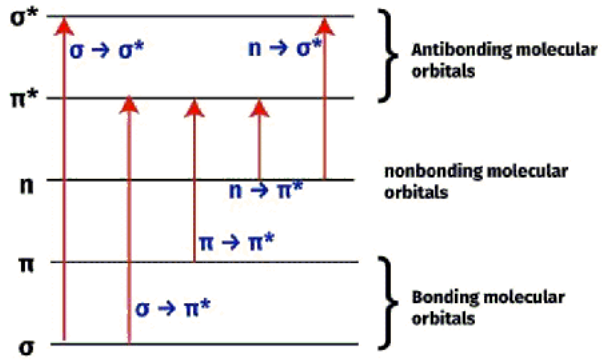

Figure 4.1: The possible electron transition in Uv-vis spectroscopy

d–d Transitions

The second type of electronic transition, characteristic of transition-metal compounds, involves the excitation of d-electrons or f-electrons in rare earth elements, particularly in the presence of a ligand or crystal field. In transition metals, the ligand field partially lifts the degeneracy of the d orbitals, enabling $d \rightarrow d$ transitions.

Charge-Transfer Transitions

Charge-transfer transitions arise in systems consisting of an electron donor and an acceptor, commonly known as donor–acceptor complexes. The interaction strength between the two species ranges from strong bonding, as observed in transition metal–ligand complexes, to the opposite extreme of transient contact CT complexes, which exist only momentarily during collisions between donor and acceptor molecules.

Electronic Transitions in Solids

The electronic structure of solids is governed by the widespread delocalization of valence electrons throughout the entire material. Extensive overlap of atomic orbitals results in the formation of closely spaced energy levels, known as bands. A gap is defined as an energy range with zero density of states can emerge depending on the distance between atomic orbitals and the extent of their interaction. This gap may disappear when the interaction between orbitals is strong enough to cause the bands to overlap. If the highest energy band is partially occupied, it is known as the conduction band; if it is fully occupied, it is referred to as the valence band. In this context, the conduction band refers to the empty band immediately above the valence band. The band structure model has been successfully used to explain the distinct properties of metals, semiconductors, and insulators.

4.5.3 Gap energy

Electronic gap energy

The band gap energy represents the energy difference between the energies of HOMO and the LUMO, which is analogous to the valence and conduction bands in inorganic materials. The conductive properties is influenced by the band gap energy, with insulators typically possessing a wide gap exceeding 4 eV, whereas semiconductors exhibit narrower gaps, usually below 3 eV. [110]. The electronic band structure of organic -conjugated semiconductors governs their band gap energy (Figure 4.2).

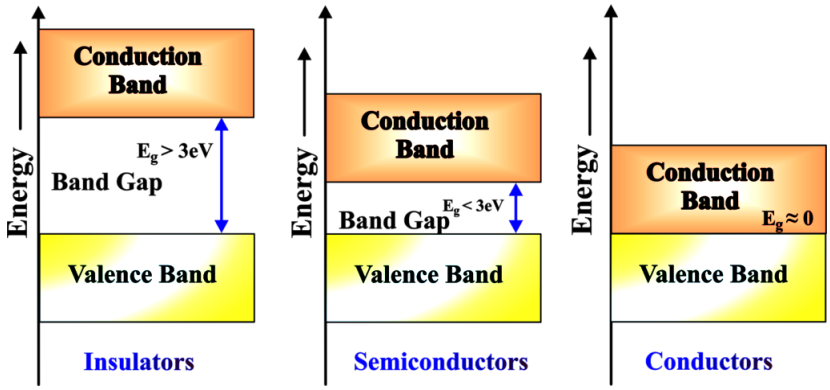

Figure 4.2: Classification of materials according to their band gap

The band gap energy (E_g) is a characteristic property of each semiconductor and significantly influences the performance of solar cells fabricated from it [111]. Semiconductors are essentially transparent to photons with energies below the band gap, as these photons lack sufficient energy to excite electrons from the valence band to the conduction band and are therefore not absorbed.

Optical gap energy

The band gap also known as the optical gap, energy gap, or mobility gap is a crucial property of materials that governs the optoelectronic performance of devices fabricated

from these materials. The band gap represents the minimum energy required for an electron to perform a transition from the valence band to the conduction band.

The optical band gap can be estimated from the UV-Vis spectrum using the following equation:

$$E_g = h.c/\lambda_{a.e} \approx 1240/\lambda_{a.e}(nm) \tag{4.28}$$

E_g denotes the optical band gap measured in electron volts (eV) and $\lambda_{a\cdot e}$ represents the absorption edge wavelength in nanometers (nm), determined from the onset of the low-energy absorption band, as shown schematically in Figure **??** [112]

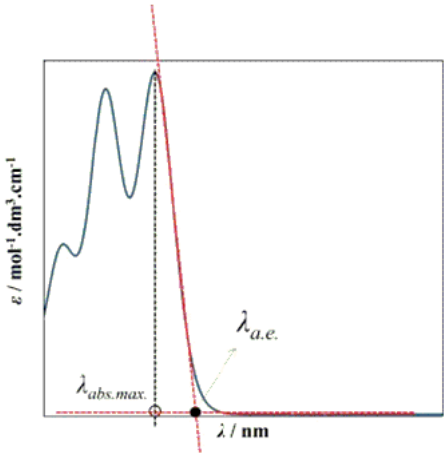

Figure 4.3: Determination of optical gap energy schematically

Part II

Results and discussion

Chapter 5

Results and discussion

5.1 Introduction

The development of abundant renewable energy resources is an opportunity to address both climate change and renewable energy includes energy from such sources as wind, biomass, geothermal, solar, hydropower, waste, and ocean energy. The demand for alternatives to fossil fuels has dramatically increased as a result of the shortage of traditional energy sources. The techniques that researchers are developing can draw energy from renewable resources. One of the primary sources of energy from renewable sources is the sun. Researchers can turn the heat and light energy from the sun into electrical energy using solar cells. [113] Solar energy is the most considerable alternative to fosil fuels because of its great potential and clean, but it has not yet achieved the promised efficiency and cost values. However, recent studies have shown that organic materials (OM) play a central role in the advancement of renewable energy, particularly in solar cell technology [114] The organic materials that possess non linear optical properties are of great interest for research because of their significant contribution to the advancement of photonic technologies gases [115]. Due to their physical and optical properties [105], these materials, called organic nonlinear optical materials are the objectof much attention because

they present high optical susceptibilities compared toinorganic materials [116]. Among the optical materials, OMs are characterized by availability, facile preparation and non expensive cost [1]. The quinoline compound is one of the most important OMs, that is an heterocyclic aromatic organic compound [92], formed by the fusion of benzene and pyridine molecules, its structural units are present in many pharmaceutical compounds and in aromatic N-based hetero-cycles that have been used since the 1960s for the development of antitumor drugs [117]. It is an important molecule in the pharmaco-medical field and is frequently used for the creation of materials in nonlinear optics [92]. In order to develop or to discover a new organic materials characterized by an optical properties, that may be used in solar cells or other industrial applications, we have decided to perform a computational study on the physical, optical and chemical properties of some series of quinoline derivatives (Figure 5.1) .The main goal is to predict the best position of the substituent that lead to a high nonlinear optical, physical and chemical properties.

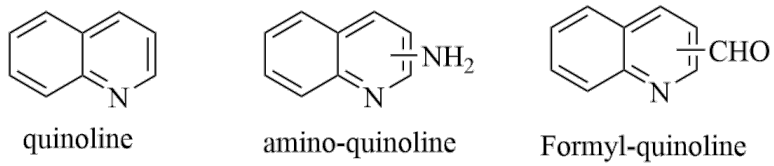

Figure 5.1: Structure of studied quinoline derivatives

5.2 Computational methods

In this study, the molecular structures of the quinoline derivatives were optimized through DFT calculations using the Lee-Yang Parr (B3LYP) hybrid functional in conjunction with the 6-311G++(d,p) basis set [118]. All calculations were performed using the Gaussian

[1] https://www.techno-science.net/glossaire-definition/Quinoleine.html

09 [119] software package and the Gaussview-5.0 molecular visualization program [120].

5.2.1 Optical Properties

The non-linear optical (NLO) properties of molecules are of particular interest in several fields; these properties play an important role in the determination of molecule's applications. Thus, electronic devices in several fields of application are replaced by optical devices [105]. The (LO) and (NLO) properties, namely the total static dipole moment (μ), mean polarizability (α), anisotropy of polarizability ($\Delta\alpha$), first hyperpolarizability (β) and Field-Induced Second-Harmonic Generation(EFISHG) ($\beta_{//}$), were calculated through the optimized structures utilizing the finite field method (FF) [115], used because it is a fast numerical technique [105].

- The dipole moment of a molecule is an important factor that has been obtained as follows:

$$\mu = \sqrt{\mu_x^2 + \mu_y^2 + \mu_z^2} \tag{5.1}$$

- The polarizability represents the tendency of the electronic system cloud of a system to be deformed in the limit of the applied field [92]. It is defined as:

$$< \alpha >= \frac{1}{3}(\alpha_{xx} + \alpha_{yy} + \alpha_{zz}) \tag{5.2}$$

- The anisotropy of polarizability ($\Delta\alpha$), is calculated using the following equation:

$$(\Delta\alpha) = \frac{1}{\sqrt{2}}\sqrt{(\alpha_{xx} - \alpha_{yy})^2 + (\alpha_{yy} - \alpha_{zz})^2 + (\alpha_{zz} - \alpha_{xx})^2 + 6(\alpha_{xy}^2 + \alpha_{yz}^2 + \alpha_{xz}^2)} \tag{5.3}$$

- The first hyperpolarizability (β) provides information about the ability of the material to generate second-order nonlinear effects [98] . In order to calculate this property, we predicted the molecule could also present good non-linear optical properties. [92] The calculated variation β confirms the nonlinear optical activity of the studied compounds. [93] Theoretical calculations of molecular first hyperpolarizability are widely used to understand the relationship between structure and nonlinear optical properties [121] calculated as follows:

$$\beta_{tot} = \sqrt{(\beta_x^2 + \beta_y^2 + \beta_z^2)} \tag{5.4}$$

With

$$\beta_x = (\beta_{xxx} + \beta_{xyy} + \beta_{xzz}) \tag{5.5}$$

$$\beta_y = (\beta_{yyy} + \beta_{yzz} + \beta_{yxx}) \tag{5.6}$$

$$\beta_z = (\beta zzz + \beta_{zyy} + \beta_{zxx}) \tag{5.7}$$

- The electric field-induced second harmonic generation (EFISHG) is defined as:

$$\beta_{//}(-2w, w, w) = \beta_{//} = \frac{3}{5} \sum_i \frac{u_i \beta_i}{\overrightarrow{u}} \tag{5.8}$$

were:

$\overrightarrow{u}$: the norm of the dipole moment

μ_i: the components of the vectors μ

β_i: the i components of the β vectors

The Global Chemical Reactivity Descriptors (GCRD), namely, the global hardness η, electronegativity χ, the electronic potential μ, the chemical softness S, and electrophilic-

ity, ω are calculated from the energy of HOMO and LUMO that are related to the ionization potential (I) and the electronic affinity (A).

$$I = -E_{HOMO} \tag{5.9}$$

$$A = -E_{LUMO} \tag{5.10}$$

Here, the μ, χ, η, ω, and S were calculated using the following equations [12–16].

$$\eta = I - A/2 \tag{5.11}$$

$$\chi = I + A/2 \tag{5.12}$$

$$\mu = -(I + A)/2 \tag{5.13}$$

$$\omega = \mu^2/2\eta \tag{5.14}$$

$$S = 1/2\eta \tag{5.15}$$

The Quantum Theory of Atoms In Molecules (QTAIM) [122], Natural Bond Orbitals (NBO) [**?**], Frontier Molecular Orbitals (FMOs) [123] and the IR, UV-VIS spectra and the optical properties were calculations using the functional PBE [73], with the 6-311G++ (d, p) basis set. The frequencies are calculated to determine the IR spectrum data revealing that the geometry is in equilibrium with the minimum energy, and no imaginary frequency was obtained.

5.2.2 Frontier Molecular Orbitals (FMO)

The molecular electronic properties and chemical reactivity of quinoline and its derivatives are determined by the energy electronic gap between the two molecular orbitals. [123] The most occupied molecular orbital (HOMO) and the least occupied molecular orbital

(LUMO) are called the frontier molecular orbitals because they are located at the outermost boundaries of the electrons of the molecule. [98].

The principle of these two molecular orbitals is practical for reactions with other molecular structures [124], the best responses of first hyperpolarizability are obtained by systems in the energy electronic gap $|HOMO - LUMO|$ is low.

In this work, the frontier molecular orbitals have been analyzed to confirm their optical properties (NLO).

Besodes the energy gap between the two HOMO and LUMO orbitals is an intramolecular charge transfer, so the smaller the energy gap, the stronger the first hyperpolarizability β, which makes the NLO material active [121]. This indicates that there is an inverse relationship between the energy gap $|HOMO-LUMO|$ and the first hyperpolarizability β

The GAUSSIAN 09 [117] package program at DFT /B3LYP level with 6-311G ++(d,p) basis set has also derived the HOMO, LUMO energy.

The $|HOMO - LUMO|$ energy electronic gap is achieved by the following expression:

$$GAP = E_{HOMO} - E_{LUMO} \tag{5.16}$$

5.2.3 Global Chemical Reactivity Descriptors (GCRD)

GCRD was estimated to understand the chemical reactivity of the quinoline derivative. The overall hardness η, electron potential μ, chemical softness S, electrophilicity ω. The global hardness η, electronegativity χ, the electronic potential μ, the chemical softness S, electrophilicity ω.

From the energy of HOMO and LUMO, we have determined this property. The energy levels of HOMO and LUMO are related to the ionization potential (I) and the electronic

affinity (A), as defined in equations 10 and 11:

$$I = -E_{HOMO} \tag{5.17}$$

$$A = -E_{LUMO} \tag{5.18}$$

Here, the μ, χ, η, ω, and S were calculated using the following equations [12- 16]: The results are listed in Table 11.

$$\eta = I - A/2 \tag{5.19}$$

$$\chi = I + A/2 \tag{5.20}$$

$$\mu = -(I + A)/2 \tag{5.21}$$

$$\omega = \mu^2/2\eta \tag{5.22}$$

$$S = 1/2\eta \tag{5.23}$$

5.2.4 MEP maps analysis

MEP analysis used to predict the electrophilic and nucleophilic attack site of the quinoline carboxaldehyde molecule was calculated at the optimized geometry B3LYP/6-311++G(d,p). Fig.8 represents the three-dimensional MEP of quinoline carboxaldehyde. On this surface, the negative areas (red, orange, and yellow) of the MEP are related to electrophilic reactivity, with the red color indicating that the region near the oxygen was electron-rich. The surface of the MEP represents the different values of the electrostatic potential by different colors. The code of these colors for the quinoline carboxaldehyde molecule is compared between -0.0669 a.u and 0.0669 a.u, red and blue are deeper. The blue color represents the areas with the highest positive electrostatic potential, which is the strongest attraction, and the red color represents the areas with the highest negative

electrostatic potential, which is the strongest repulsion.
For the quinolinecarboxaldehyde molecule, the negative regions are located on the nitrogen and oxygen atoms N13, and O18 respectively indicating the site for the electrophilic attack, and the positive region is located on the hydrogen atoms indicating the site for nucleophilic attack.

5.2.5 QTAIM analysis

The quantum theory of atoms in molecules (QTAIM), developed by Richard, F, W, Bader [122], based on the analysis of the electronic density ρ [125], theory has been widely used to analyze the nature of interactions in the molecular system, to classify and understand binding interactions in terms of quantum mechanics [126].
QTAIM is a theory that provides a tool for understanding atoms in molecules [127]. The concepts of this theory are based on the analysis of the electron density ρ which provides a series of critical points: (3,-1), (3,+1), (3,-3) and (3, +3). The critical point (3, -1) known as the critical binding point (BCP), means that the electron density decreases in two perpendicular directions of space, and increases in the third direction, which is important associated with the presence of a stabilizing interaction and hydrogen bonding (HA), this bonding is divided at three families:

- Strong hydrogen bond: $\nabla^2\rho(r) < 0$ and $H(r) < 0$

- Weak hydrogen bonding : $\nabla^2\rho(r) > 0$ and $H(r) > 0$

- Medium hydrogen bonding: $\nabla^2\rho(r) <0$ and $H(r) > 0$
  [128]

[127] and are located between two neighboring atoms, defining a bond between them. (3,-3) means that the electron density decreases in the three perpendicular directions of space, is called the nuclear critical point (NCP), and indicates the position of every atom except hydrogen. The (3,+1) called the critical point of the ring (RCP) means that the electron density decreases in one direction of space and increases in the other two perpendicular directions of space, is in the middle of several bonds forming a ring. The point (3,+3) known as the critical cage point (CCP) means that the electron density increases in all three directions in space, and is found when several rings form a cage.
The critical point (3,-1) plays an important role in describing molecular structure, the presence of this point is a necessary and sufficient condition for the existence of the bonding interaction, whatever the nature of the bond, and indicates that an electron charge density has accumulated between the nuclei thus bonded [128].
The type of interaction is classified with the signs of the electron density Laplacian $\nabla^2\rho(r)$ and electron energy density H(r).

- Non-polar covalent bond: $\nabla^2\rho(r)<0$ and H(r)<0

- Covalent polar bonds, strong hydrogen bonds: $\nabla^2\rho(r) > 0$ and $H(r) < 0$

- Closed shell interactions: $\nabla^2\rho(r) > 0$ and $H(r) > 0$
  [128]

[129] In the critical point (3,-1), if:

- $\nabla^2\rho(r) < 0$, the bonds is classified as shared
- $\nabla^2\rho(r) > 0$, the bonds is classified as closed-shell

[2] The electron density $\rho(r)$ gives the number of expected electrons that can be found at

[2] https://www.cryst.bbk.ac.uk/PPS2/projects/loesel/chap03c.htm

a particular location during the measurement [130]. Laplacian charge density $\nabla^2\rho(r)$, local potential energy density V(r), local gradient kinetic energy density G(r), and total energy density H (r) = (V (r) + G (r) [126] for quinoline and quinoline derivatives are grouped in the tables 12, 13, 14, 15, 16. If the system has large values of $\rho(r)$ and $v(r) < 0$, this indicates polar and nonpolar covalent bonding interactions, otherwise it indicates closed-shell interactions.

When $\nabla^2\rho(r) > 0$, the interactions are non-covalent, when $\nabla^2\rho(r) > 0$ and $0.5 < -G(r)/v(r) < 1$, the interactions are then partially covalent [131], if $\nabla^2\rho(r) < 0$ indicates the bond is covalent.

5.3 Optimized geometries and choice of the computational level

First, in order to validate the DFT functional to perform our study, we have decided to realize a comparative analysis of the geometric properties of the quinoline molecule between experimental data [117] and B3LYP/6-311++G(d, p) computational level. The values of these data are collected in Table 5.1, while the optimized structure of quinoline using B3LYP/6-311++G(d, p) theoretical level is given in (Figure 5.2)

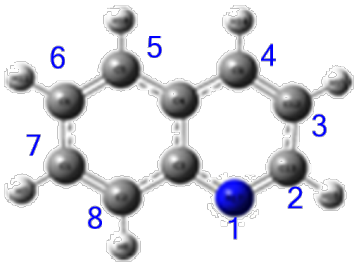

Figure 5.2: Structure of quinoline together with atoms labels

Table 5.1: Some selected theoretical and experimental values of geometrical parameters associated with quinoline structure

/	HF		DFT	EXP
/	3-21G**	6-31G**	B3LYP/6-311++G(d,p)	/
Bond lengths (Å)				/
C1-C2	1.358	1.358	1.374	1.381
C2-C3	1.414	1.418	1.418	/
C3-C4	1.403	1.406	1.429	/
C4-C5	1.416	1.419	1.418	/
C5-C6	1.358	1.357	1.374	1.365
C6-C1	1.412	1.417	1.416	1.424
C3-N17	1.363	1.365	1.364	/
C13-N17	1.300	1.291	1.314	1.316
C12-C9	1.357	1.355	1.372	1.357
C9-C4	1.418	1.471	1.416	/
Bond angle/degrees				
C2-C1-C6	120.44	120.61	120.60	120.17
C6-C5-C4	120.35	120.41	120.43	/
C3-C2-C1	120.30	120.32	120.42	/
C4-C3-N17	120.61	122.43	122.40	/
N17-C13-C12	122.96	124.08	124.16	/
C13-C12-C9	118.73	118.45	118.71	/
C12-C9-C4	119.59	119.27	119.32	/
C3-N17-C13	119.43	/	117.91	/
C1-C5-C6	120.35	120.20	120.32	/

By a comparison between these values of the experimental and theoretical geometrical parameters, we can notice clearly that the optimized quinoline geometry with the B3LYP/6-311++G(d,p) computational level is an appropriate method for calculating their properties because it gave the more closes values to the experimental data. Therefore, the B3LYP/6-311++G(d,p) theoretical level is the appropriate theoretical method for optimizing the structure of quinoline derivatives.

5.3.1 Choice of the best DFT functional and basis set

First, we have opted to select the appropriate DFT functional that gives the best optical properties. Thus, the calculated gas phase optical properties, namely, μ, α, $\Delta\alpha$, β and $\beta_{//}$ of quinoline using B3LYP [118], CAM-B3LYP [132], PBE [133] and B3PW91 [134] functionals are collected in Table 5.2, while these obtained in DMSO solvent using COSMO model are given in Table 5.3.

Table 5.2: Calculated values (in a.u) of μ, α, $\Delta\alpha$, β, $\beta_{//}$ of quinoline using B3LYP, CAM-B3LYP, PBE and B3PW91 functionals

	μ	α	$\Delta\alpha$	β_{tot}	$\beta_{//}$
B3LYP	2.282	45.503	92.931	14.721	8.326
CAM-B3LYP	2.332	44.658	89.907	15.366	8.659
PBE	2.227	115.847	95.852	14.383	8.242
B3PW91	2.271	112.444	92.673	14.783	8.391

Table 5.3: Calculated μ, α, $\Delta\alpha$, β, $\beta_{//}$ (in a.u) of quinoline using B3LYP, CAM-B3LYP, PBE and B3PW91 functionals of quinoline using COSMO model with DMSO solvent at DFT/6-311++G(d, p)

	μ	α	$\Delta\alpha$	β_{tot}	$\beta_{//}$
B3LYP	3.661	168.806	141.333	26.669	15.636
CAM-B3LYP	3.665	164.458	134.458	27.267	15.956
PBE	3.548	172.822	147.173	26.512	15.626
B3PW97	3.645	164.82	133.889	27.202	15.916

An analysis of the values in Table 5.2 and Table 5.3 indicates that the NLO properties obtained using the COSMO/DMSO solvent model are better than that in gas phase. On the other hand, a comparison between the LO and NLO obtained by different functionnals indicates that the values obtained by the use of PBE one are better than that obtained using B3LYP, CAM-B3LYP and B3PW91, in which we can notice that the value of α is 172.8 a.u for PBE functional, while for B3PW91, B3LYP and CAM-B3LYP is 164.8, 168.8 and 164.5 a.u, respectively. Thereby, for the PBE functional is the appropriate DFT functional for calculating the optical properties of the studied quinoline derivatives.

Table 5.4: PBE values of polarizability α (in a.u) for quinoline with different basis set in gas phase

Basis set	6-31G	6-311G	6-31+G(d,p)	6-311++G(d, p)
α	95.49	101.9	103.2	105.2

On the other hand, in order to select the appropriate basis set, a supplementary analysis was performed on different basis set using PBE functional, in which the obtained results were presented in Table 5.4. We can notice from 5.4 that with increasing of the basis set the value of the polarizability increase. Also, the addition of a diffuse function (+) increase the value of α that may be to the addition of the polarization functions (d, p) tends to increase the polarization capacity. In addition, PBE DFT functional with the p polarization function enhances the values of the polarizability. We notice clearly also that the calculations with 6-311G++(d,p) basis set gave the best values of the polarizability capacity α. Consequently, for realizing our study on the optical properties of quinoline derivatives, the best DFT method is that with PBE functional and the 6-311++G(d, p) basis set (PBE/6-311++G(d, p) in DMSO solvent, in which the obtained results are summarized in Table 5.5.

From the values of LO and NLO properties of quinoline (Table 5.5), and by a comparison with previous properties of some organic OMs [117] , we can conclude that

Table 5.5: Values of μ, α, $\Delta\alpha$, β and β_{tot} (in a.u) of quinoline with the COSMO model and in the DMSO solvent at PBE/6-311++G(d, p) theoretical level.

	μ	α	$\Delta\alpha$	β_{tot}	$\beta_{//}$
PBE/6-311++G(d, p)	3.31	168.5	147.2	380.0	15.92

quinoline has a good LO and NLO properties, the thing that encourage us to do a study on its derivatives with the aim to finding a new compounds with a best optical properties. Thereby, we calculate the optical properties of two quinoline derivatives with different electronic nature of the substituent that are amino-quinoline and formyl-quinoline. The obtained B3LYP/6-311++G(d,p) optimized structures of these derivatives are given in (Figure 5.3).

Table 5.6: Values of μ, α, $\Delta\alpha$, β and $\beta_{//}$ in (a.u.) of quinoline with the COSMO model and in the DMSO solvent at the PBE/6-311++G(d, p) theoretical level

	μ	α	$\Delta\alpha$	β_{tot}	$\beta_{//}$
PBE/6-311++G(d, p)	3.548	172.822	147.173	26.512	15.916

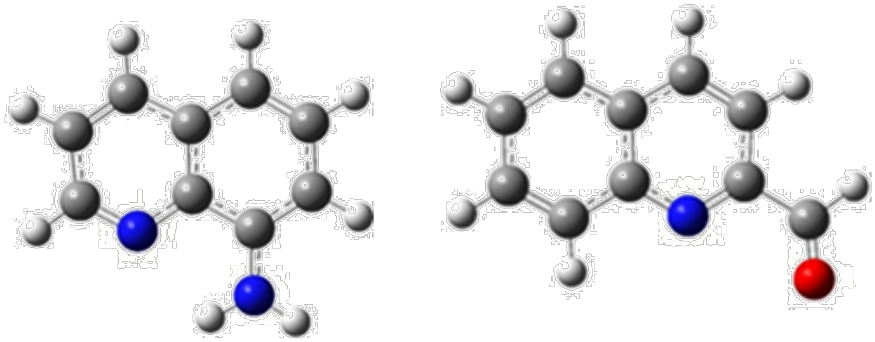

Figure 5.3: Structure of 7-amino-quinoline (a) and 2-formyl-quinoline (b)

For each quinoline derivative, we will study the optical properties of its position iso-

mers. Thus, the values of LO and NLO properties associated with the amino-quinoline molecule are calculated according to the equations mentioned above and collected in (Table 5.7). We can notice from 5.7 that the presence of an electron realising group such as amino group on the quinoline moiety increases the NLO properties, namely the first hyperpolarizability. Additionally, we notice that position 7 (7-amino-quinoline derivative) has the high value of the first hyperpolarizability (β=3866 a.u), in comparison with the other position isomers. Thus, the electron releasing group in position 7 of quinoline widely enhance the NLO property of quinoline, in which the difference between the value of the first hyperpolarizability in quinoline and in 7-aminoquinoline is in order of 3486 a.u. In order to perform a complete study on the effect of electronic nature of the substituent on the quinoline moiety, we have also studied the optical properties of the quinoline system with a withdrawing group, in which the obtained results are collected in Table 5.7.

Table 5.7: PBE/6-311++G(d, p) in DMSO solvent LO and NLO properties (in a.u) of amino-quinoline position isomers

	Aminoquinoline						
Property/position	2	3	4	5	6	7	8
μ	0.33	4.59	5.83	6.32	6.59	5.30	3.48
α	148.80	192.49	118.53	95.94	134.19	188.69	177.39
β	807.77	3847.96	1091.30	213.80	151.93	3866.22	2502.763
$\beta_{//}$	272.90	-414.45	-110.73	21.62	-2.90	523.07	515.50

From the results of Table 5.8 and by a comparison between the optical properties of all formyl-quinoline isomers, we can observe that the best properties are associated to the isomer in position 2, namely the first hyperpolarizability (μ= 3869 a.u). On the other hand, the electron withdrawing group (formyl group) increase slightly the first

Table 5.8: PBE/6-311++G(d, p) in DMSO solvent LO and NLO properties (in a.u) of formyl-quinoline

Formyl-quinoline							
Property/position	2	3	4	5	6	7	8
μ	7.71	3.54	3.54	3.00	6.31	5.87	7.61
α	203.55	203.467	197.61	196.794	203.17	203.32	196.13
β	3869.57	3604.17	2118.08	1016.53	2070.55	2403.23	1021.92
$\beta_{//}$	-1398.37	-2154.17	-1269.32	-211.02	-1118.64	-1441.69	-483.425

hyperpolarizability in compared to the electron-releasing group (amino group) by about 3.35 a.u. Also, the formyl group increase dramatically the first hyperpolarizability with compared to the quinoline moiety by 3843 a.u.

In a continuation to our study, we have also performed a study of quinoline derivative system having both electron-releasing and electron withdrawing groups. Thus, we have selected the best position obtained previously from the formyl-quinoline (position 2) and we have try several possibilities by changing the position of the amino group. Thereby, the studied quinoline derivatives are n-amino-2-formylquinoline, in which n varies from 3 to 8. The obtained optical properties for these molecular systems are summarized in Table 5.9.

Table 5.9: PBE/6-311++G(d, p) in DMSO solvent LO and NLO properties (in a.u) of n-amino-6-formylquinoline derivatives

Position of NH_2	3	4	5	6	7	8
μ	8.73	11.00	10.79	12.32	9.31	5.09
α	234.7	225.8	228.8	263.9	239.8	235.8
β	2621	3946	3507	19728	9849	8536

Table 5.10: PBE/6-311++G(d, p) in DMSO solvent LO and NLO optical properties of quinoline, 6-amino-quinoline, formyl-quinoline, 6-amino-1-formyl-quinoline and formyl-quinoline dimer

	Quinoline	7-amino-Q	2-formyl-Q	2-formyl-Q dimer	6-amino-2-formyl-Q
μ	168.514	197.575	203.558	394.082	263.981
α	168.514	197.757	203.558	394.082	263.981
β	380.029	3866.221	3869.57	6369.421	19728.32

The results of Table 5.9 show clearly that the isomer of quinoline derivative having the NH_2 in position 6 and COH in position 2 gave the good optical properties in terms of first hyperpolarizability (β=19728.32 a.u.). This result may be explained by the high possible larger distance between the two electron-releasing and electron-withdrawing groups, in which they cannot influence each other.

Because the materials do not exist in separate molecules, in which one molecule may influence on the other, we have calculated the optical properties of the dimer for the quinoline derivative that have the better optical properties that is the formyl-quinoline. For simplify the comparison analysis between the optical properties of this latter and other quinoline derivatives, we have collected the obtained values of μ, α and β of quinoline, 7-amino-quinoline, 2-formyl-quinoline, 6-amino-2-formyl-quinoline, and 2-formyl-quinoline dimers in Table 5.10.[3]

From Table 5.10 and by comparison between the hyperpolarizability of second-order β values of different structures, we can notice clearly that the value β associated to the 2-formyl-quinoline dimer (β=6369.421 a.u) is twice higher than that of 2-formyl-quinoline (β=3869.57 a.u.). On the other hand, the value of the first hyperpolarizability corresponding to the 6-amino-2-formyl-quinoline, is always remaining the best results, in which β= 19728.32. This fact suggests that the long distance between electron-releasing

[3] Q:Quinoline

and electron withdrawing groups gave the best optical properties in one monomer better than that in dimer with one substituent.

FMO analysis

The molecular electronic properties and physico-chemical reactivity of quinoline and its derivatives are determined by the electronic gap energy between the two molecular orbitals [123]; the highest occupied molecular orbital (HOMO) and the lowest unoccupied molecular orbital (LUMO) [98].

The principle of these two molecular orbitals is practical for reactions with other molecular structures [124].

In this work, the frontier molecular orbitals have been analyzed to confirm their NLO optical properties. Besides the gap energy between the two HOMO and LUMO orbitals is an intramolecular charge transfer, so the smaller the energy gap, the stronger the first hyperpolarizability β, which makes the NLO material active [121].

The HOMO and LUMO energies have been calculated in B3LYP/6-311G++(d, p) theoretical level using GAUSSIAN 09 [117] program, in which the $|HOMO - LUMO|$ gap electronic energy is achieved by the following expression:

$$E_{GAP} = E_{HOMO} - E_{LUMO} \tag{5.24}$$

Table 5.11 collects the values of the optical properties of the studied quinoline derivatives together with their gap electronic energies.

We notice from Table 5.11 that the 6-amino-2-formyl-quinoline is characterized by higher values of β and a small value of gap electronic energy. Thus, in this molecule, electron transition from HOMO to LUMO is easy by small activation energy and thus the charge transfer is large, making this molecule active in conducting electricity, together with the best NLO properties. Therefore, this molecule may be used in the development

Table 5.11: B3LYP/6-311G++(d, p) values (in a.u) of optical properties and electronic gap energy (in eV) of quinoline, 7-amino-quinoline, 2-formyl-quinoline, 6-amino-2-formyl-quinoline and 2-formyl-quinoline dimer

	Quinoline	7-amino-quinoline	2-formyl-quinoline	2-formyl-quinoline dimer	6-amino-2-formyl-quinoline
μ	3.311	5.307	9.680	15.071	12.32
α	168.514	197.757	203.558	394.082	263.981
β	380.029	3866.221	3863.57	6369.421	19728.32
E_{gap}	4.73	4.35	4.35	3.67	2.72

of NLO materials to apply in photovoltaic cells or other industrial applications.

5.3.2 Global Chemical Reactivity Descriptors (GCRD)

GCRD was estimated to understand the chemical reactivity of the studied quinolines derivatives. Here, we try to find a relation between the GCRD descriptors and the NLO optical properties, or, by another term, the relation between chemical and physical properties. The GCRD's descriptors values were calculated using the above equations and are summarized in Table 5.12.

The analysis of the GCRD of quinolines and their different derivatives indicates that the 6-amino-2-formyl-quinoline has the smallest LUMO and gap energies. We know that this derivative has the best NLO properties, thereby, the quinolines with the best NLO properties has also the smallest gap energy. On the other hand, this derivative has the highest index of affinity (A=0.102 eV) and ionization (I=0.251 eV), accounting for their dual reactivity as electron acceptor and donor. In addition, the analysis of chemical hardness (η) indices shows that the 6-amino-2-formyl-quinoline has the smallest index (0.074 eV), which indicates that it is the more reactive molecule among the studied quinoline derivatives. For the electronegativity (χ) and chemical potential (μ) indices, we can notice that the 6-amino-2-formyl-quinoline is characterized by the highest value of

electronegativity (χ=0.176 eV) and the smallest values of chemical potential (μ=-0.176 eV), indicating that this molecule has the behavior of accepting electrons .

Table 5.12: GCRD values (in eV) for quinoline and some its derivatives at B3LYP/6-311++G(d, p) theoretical level

	Quinoline	7-amino-quinoline	2-formyl-quinoline	6-amino-2-formyl-quinoline
HOMO	-6.64	-7.07	-6.26	-6.15
LUMO	-1.90	-2.72	-1.90	-3.43
gap	4.73	4.35	4.35	2.72
I	6.64	7.07	6.26	6.15
A	1.90	2.72	1.90	3.43
η	4.73	4.35	4.35	2.72
χ	4.27	4.90	4.08	4.79
μ	-4.27	-4.90	-4.08	-4.79
S	0.21	0.23	0.23	0.37
ω	1.93	2.76	1.91	4.21

5.3.3 MEP analysis

Molecular Electrostatic Potential (MEP) analysis was used to predict the electronic density distribution at the structure of the formyl-quinoline molecule through the B3LYP/6-311++G(d, p) optimized geometry. The main goal is to find a relationship between the MEP and the optical properties of the studied quinolines derivatives. Thus, Figure 5.20 presents the three-dimensional MEP maps of the 2-formyl-quinoline and . On this surface, the negative areas (red, orange, and yellow) of the MEP are related to the positive charged region, while the red color indicating that the region nears the oxygen was electron-rich. The blue color represents the areas with the highest positive electrostatic potential, which is the strongest attraction, and the red color resents the areas with the highest negative electrostatic potential, which is the strongest repulsion. The surface of

the MEP represents the different values of the electrostatic potential by different colors. Thus, the code of these colors for the 2-formyl-quinoline molecule is compared between -0.0669 a.u (red) and 0.0669 a.u (blue).

We can notice from Figure 5.20 that is associated with the MEP of the formyl-quinoline molecule; the negative regions are located on the nitrogen and oxygen atoms N_{13} and O_{18}, respectively, indicating that region is characterized by high electron density. On the other hand, the positive region is located on the hydrogen atoms accounting for a deficient electron density region. This distribution of electron density along the formyl-quinoline structure, make it have a high polar dipole, which may explain the best NLO properties of this quinoline derivative.

5.3.4 QTAIM analysis

Figure 5.23 presents an analysis of the quinoline geometry using QTAIM theory critical points together with analysis of the electron density at the critical point (3,-1), while Table 5.13) collects the QTAIM (3,-1) bond parameters of quinoline.

Table 5.13: QTAIM (3,-1) bond critical point parameters in (a.u.) of quinoline

Interaction	Bcp_{label}		ρ	$\nabla^2\rho(r)$	H(r)
C1-C2	20	0.320	-0.915	-0.339	
C2-C3	21	0.299	-0.827	-0.294	
C3-C4	27	0.293	-0.784	-0.282	
C4-C5	32	0.295	-0.799	-0.287	
C5-C6	31	0.319	-0.914	-0.339	
C6-C1	35	0.281	-0.968	-0.280	
C3-N17	22	0.324	-0.969	-0.430	
C13-N17	24	0.354	-0.952	-0.528	
C13-H16	23	0.354	-0.952	-0.528	
C12-H15	35	0.281	-0.968	-0.280	
C2-H8	18	0.282	-0.977	-0.280	

From Figure 5.23 and Table 5.13, we note that all cbp values for quinoline are negative. We can see also that all the cps are characterized by a negative sign of the Laplacian $\nabla^2\rho(r) < 0$ and $H(r) < 0$ of (3,-1) indicates electron density in the region between the two bonded atoms, accounts that the bond is classified as shared (the shared bond is between covalent bonded atoms). Additionally, the values of $\nabla^2\rho(r) < 0$, indicate that these interactions are very strong and the associated bonds are covalent. Also, we notice that the C_{13}-H_{16} bond has the highest negative value, indicating its purely covalent nature.

The molecular graphs of the 7-amino-quinoline together with analysis of the associated electron density with (3,-1) critical points obtained by QTAIM are depicted in (Figure 5.26), while their QTAIM (3,-1) bond critical points parameters are collected in (Table 5.14).

Figure 5.26 presents an analysis of the 7-amino-quinoline geometry using QTAIM theory, and shows an analysis of the electron density at the critical point (3,-1).

Table 5.14: QTAIM (3,-1) bond critical point parameters in (a.u.) of 7-amino-quinoline

Interaction	Bcp_{label}	ρ	$\nabla^2\rho(r)$	H(r)
C2-C3	38	0.300	-0.828	-0.295
C4-C7	26	0.297	-0.803	-0.291
C8-C9	34	0.293	-0.786	-0.281
C9-H10	40	0.280	-0.963	-0.277
C9-N11	39	0.357	-0.930	-0.531
C3-N11	36	0.321	-0.934	-0.434
C7-H16	221	0.277	-0.939	-0.275
C8-N17	28	0.302	-0.839	-0.406
N17-H18	29	0.341	-0.163	-0.464
N17-H19	22	0.340	-0.163	-0.463

From (Figure 5.26) and (Table 5.14), we note that all BCPs values for 7-amino-quinoline are negative, also, we can see that all the BCPs are characterized by a negative sign of the Laplacian $\nabla^2\rho(r) < 0$ and $H(r) < 0$ of (3,-1) indicates electron density in the region between the two bonded atoms, the bond is classified as shared (the shared bond is between covalent bonded atoms), that all these interactions are also very strong bonds. The C_9H_{10} bond has the highest negative value, indicating its purely covalent nature.
In order to find the interaction type in dimer system and to understand its enhancement on the NLO properties of the dimer in comparison with the monomer one, we have undertaken a QTAIM analysis of 2-formyl-quinoline dimer.
The B3LYP-6-311G++(d,p) optimized structure of 2-formyl-quinoline dimer is given in Figure(Figure 5.27) together with the distances of the most important intramolecular interactions.

From (Figure 5.30), we can notice that the shorter distance between the 2-formyl-quinoline monomer in dimer system is 4.24 Å which associated with C...H interaction that may be a favorable NCI. On the other hand, the highest distance at the optimized

structure of this molecular system is attributed to the O...O interaction, that be explained by the non stabilized interaction (repulsion) between two atoms with the same electronic character.

The molecular graphs of 2-formyl-quinoline dimer together with QTAIM analysis of electron density with (3,-1) critical points are illustrated in (Figure 5.30), while QTAIM (3,-1) bond critical point are given in Table 5.15.

Table 5.15: QTAIM (3,-1) bond critical point parameters in (in a.u) of 2-formyl-quinoline dimer.

Interaction	BCP_{label}	ρ	$\nabla^2\rho(r)$	H
O37-C35...O18-C16	32-79	0.119	-0.544	-0.136
C35-H36...C16-H17	81-78	0.277	-0.943	-0.268
C35-C29...C16-C10	30-76	0.440	-0.261	-0.655
C29-N32...C10-N13	77-72	0.347	-0.964	-0.507
H7...C25	47	0.431	-0.1511	0.123

According to the results in Table 5.15, we can notice that except BCP number 47, the $\nabla^2\rho(r) < 0$, H(r) and H of all other BCPs are less then 0, indicating that these bonds are classified as shared. For the $C_{25}...H_7$ bond, we observed that the $\nabla^2\rho(r) < 0$ and $H(r) > 0$ is not a covalent bond, as shown in (Figure 5.30). This electrostatic interaction (C...H) may be classified as non conventional weak hydrogen bond. This last is considered as link between the two separated molecules of the 2-formyl-quinoline monomer may be the origin of the enhancement of the NLO properties in this dimer molecular system.

5.3.5 UV-Vis Spectral analysis

In this work the excitation energies were calculated using the time-dependent DFT method (TD-DFT), in which the results of the calculations are summarized in Table 5.16

and the spectra are shown in Figure 9. In this work, we have traced the tangent of the curve that is the intersection with the energy axis (h) to determine the band gap energies (Table 15, column 1 (nm) and column 2 (eV)). According to the results of the calculations presented in the (Table 5.16), we can notice that except 6-amino-2-formylquinoline, that has a gap energy (E_{gap}=2.72 eV) lower than 3 eV, unlike all other derivatives that have a gap value higher than 4 eV. Thereby, the 6-amino-2-formylquinoline is the alone studied quinoline derivative that may be considered as a semiconducter organic material [135].

Additionally, it has the highest optical gap (Eg=1.50 eV) and the quinoline has the smallest optical gap (Eg= 1.15 eV) and the highest electronic gap energy (Eg= 4.73 eV). Therefore, we conclude that there is an inverse relationship between the optical and the electronic gap energy in the studied series of quinoline derivative. On the other side, the 6-amino-2-formyl–quinoline derivative give good NLO properties that it related with the smallest electronic gap energy and the highest optical gap energy. [4]

Table 5.16: Values of electronic gap (in eV), optical gap (in nm and eV) and optical properties (in a.u) for quinoline and its derivatives

/	Quinoline	7-amino-Q	2-formyl-Q	6-amino-2-formyl-Q	2-formyl-Q dimer
Gap_{optc}(nm)	372	410	480	485	420
Gap_{optc}(eV)	1.15	1.27	1.49	1.50	1.30
$Gap_{electronic}$(eV)	4.73	4.35	4.35	2.72	3.67
β	380	3866	3869	19728	6369
α	168.5	197.8	203.6	264	394.1
μ	3.311	5.307	9.68	12.32	15.071

[4] Q=Quinoline

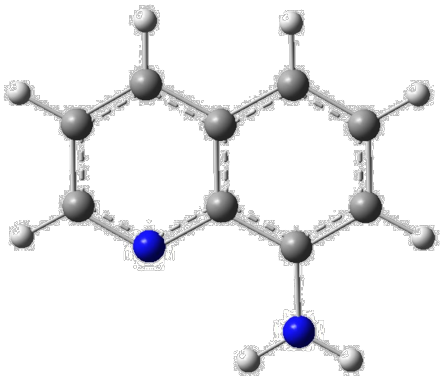

Figure 5.4: 8-amino-quinoline

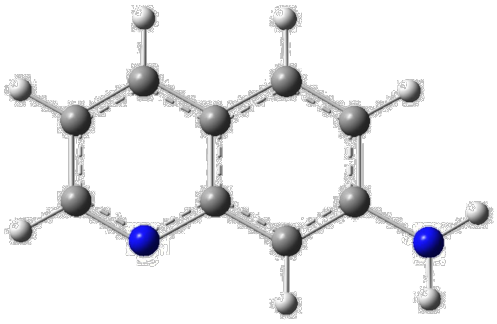

Figure 5.5: 7-amino-quinoline

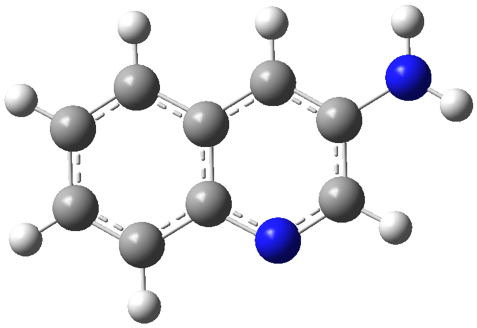

Figure 5.6: 6-amino-quinoline

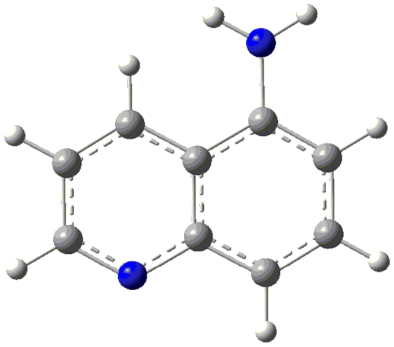

Figure 5.7: 5-amino-quinoline

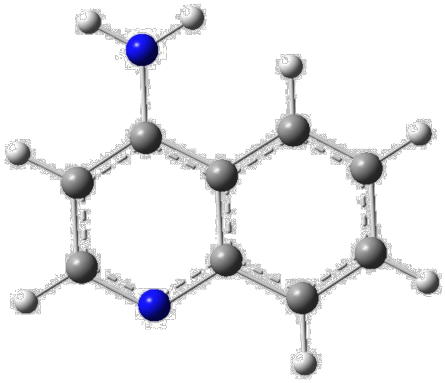

Figure 5.8: 4-amino-quinoline

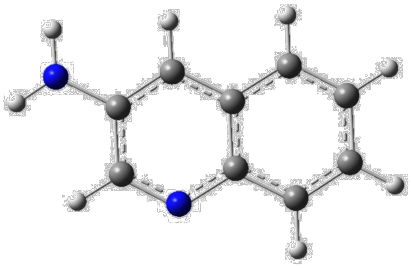

Figure 5.9: 3-amino-quinoline

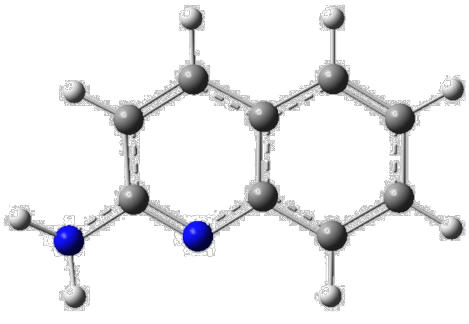

Figure 5.10: 2-amino-quinoline

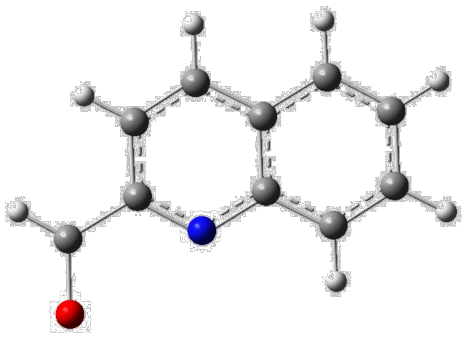

Figure 5.12: 2-formyl-quinoline

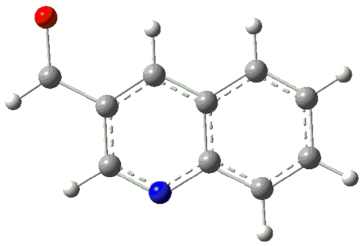

Figure 5.13: 3-formyl-quinoline

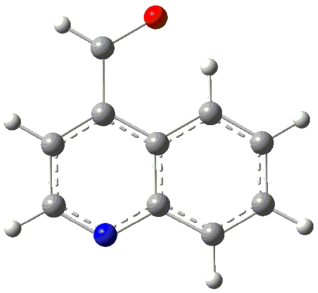

Figure 5.14: 4-formyl-quinoline

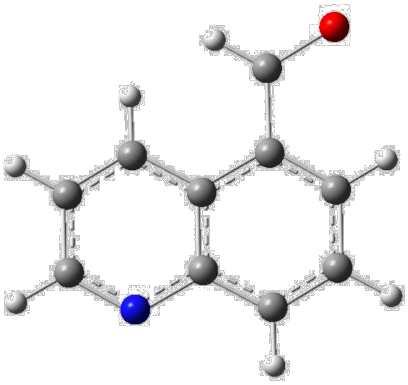

Figure 5.15: 5-formyl-quinoline

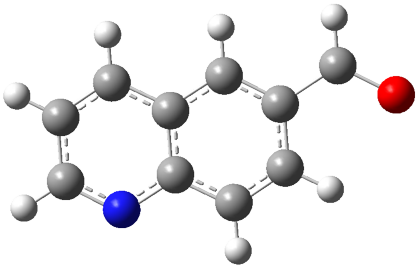

Figure 5.16: 6-formyl-quinoline

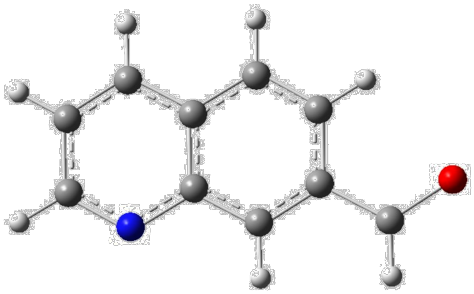

Figure 5.17: 7-formyl-quinoline

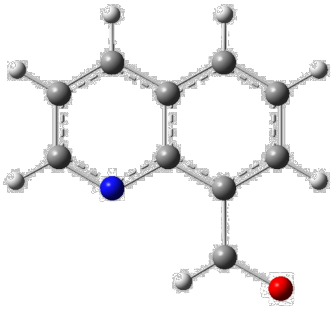

Figure 5.18: 8-formyl-quinoline

Figure 5.19: formyl-quinoline position isomers

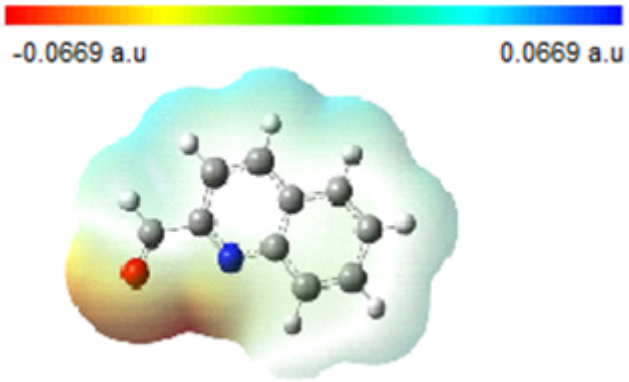

Figure 5.20: Molecular electrostatic potential map of formyl-quinoline molecule

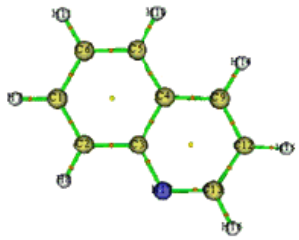

Figure 5.21: Molecular graphs of quinoline

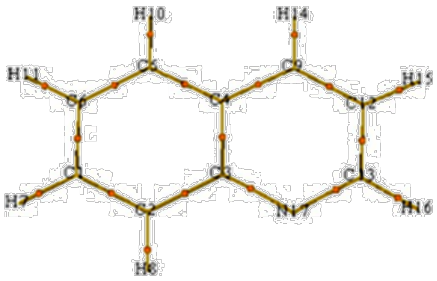

Figure 5.22: Analysis of electron density with (3,-1) critical point of quinoline

Figure 5.23: QTAIM molecular graphs of quinoline and analysis of electron density with (3,-1) critical points

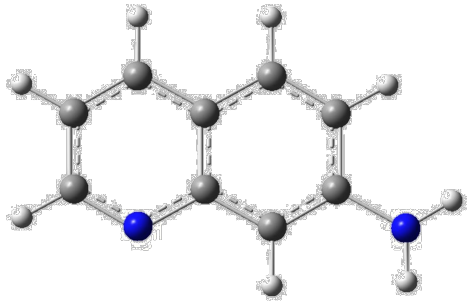

Figure 5.24: Molecular graphs of 7-amino-quinoline

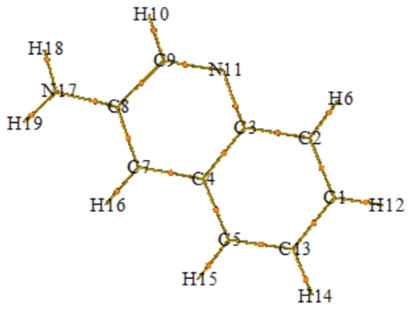

Figure 5.25: analysis of electron density with (3,-1) critical point of 7-amino-quinoline

Figure 5.26: QTAIM molecular graph of 7-amino-quinoline together with analysis of electron density with (3,-1) critical points

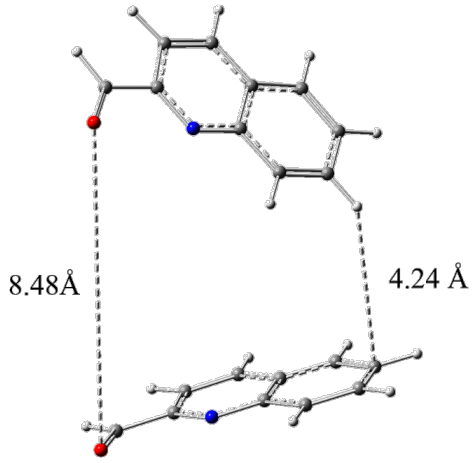

Figure 5.27: B3LYP-6-311G++(d,p) optimized structure of 2-formyl-quinoline dimer together with the distances of the pertinent intramolecular interactions

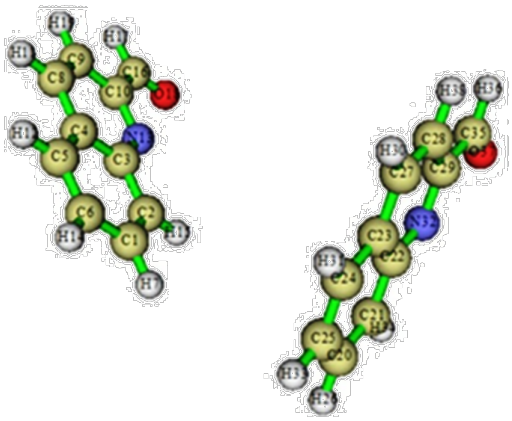

Figure 5.28: Molecular graphs of 7-amino-quinoline

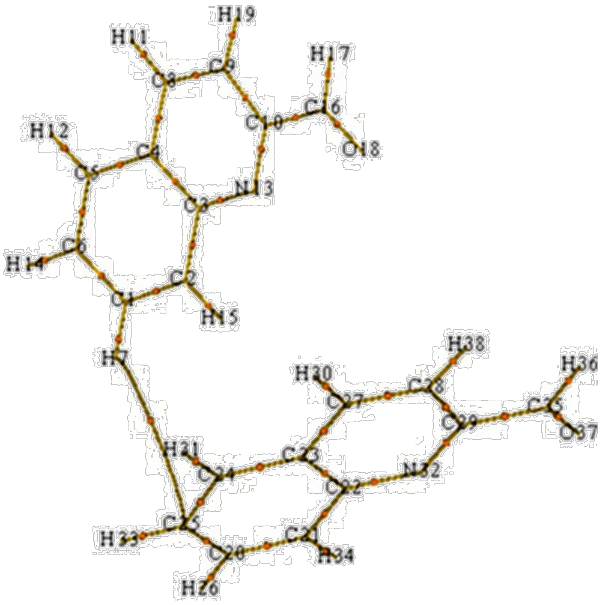

Figure 5.29: analysis of electron density with (3,-1) critical point of 7-amino-quinoline

Figure 5.30: QTAIM molecular graph of 2-formyl-quinoline dimer together with analysis of electron density with (3,-1) critical points

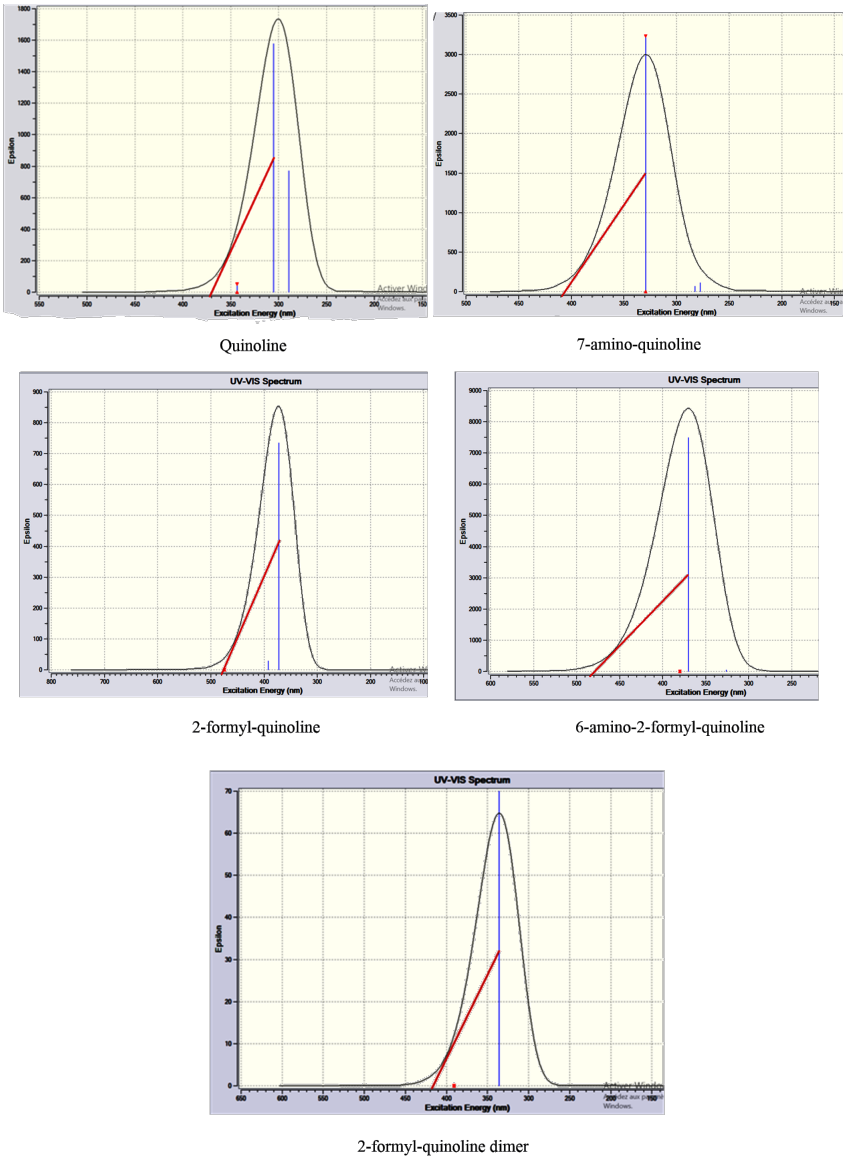

Figure 5.31: Theoretical Uv-vis spectrum of quinoline, 7-amino-quinoline, 2-formyl-quinoline, 6-amino-2-formyl-quinoline and 2-formyl-quinoline dimer

Conclusion

In this work, we have studied computationally using different DFT methods the LO and the NLO properties of some quinoline derivatives for the goal of possible use as organic, non-expensive materials in photovoltaic uses in solar cells and other NLO applications such as optical communications.
The main outcomes of this study is the followings:

- For the choice of the best DFT functional, our results indicate that B3LYP functional with the 6-311++G(d,p) basis set is the best method for the geometry optimization.
- For the optical properties, we have found that the best functional is PBE with the COSMO/DMSO solvent model.
- The presence of an electron-releasing group on the quinoline, namely in position 7, increases its NLO properties, while the electron-withdrawing group, especially in position 2, increases the NLO properties.
- The interaction between different molecules of quinoline derivatives in dimer systems also increases the NLO properties of these organic material systems.
- The analysis of electronic gap energy indicates that there is an inverse relationship between Egap and the first hyperpolarizability β, which makes the 6-amino-2-formyl-quinoline an electricity conductor with better NLO properties.

- Analysis of GCRD descriptors shows that the 6-amino-2-formyl-quinoline derivative has dual electronic behaviors, which can act as an electron donor or acceptor.

- MEP analysis of the 2-formyl quinoline derivative indicates that the electron density distribution along its structure makes it have a polar character that leads to good NLO properties.

- QTAIM analysis demonstrates that all bond critical points on the quinoline and 7-aminoquinoline are related to a covalent bond, while the 2-formyl quinoline dimer shows the presence of conventional weak interaction that may be the origin of the increases of NLO properties regarded to the separated molecule.

- The IR spectrum of quinoline, 7-aminoquinoline, and 2-formylquinoline analyses shows the presence of the characterized picks that are related to the pertinent bonds of each structure, namely, C=N in quinoline, N-H in 7-aminoquinoline, and C=O and CH (aldehyde) in 2-formylquinoline.

- - UV-Vis spectrum analysis indicates that 6-amino-2-formylquinoline may be considered as a semiconductor organic material, in which it has the smallest electronic gap and the highest optical gap, accounting for an inverse relationship between the optical and the electronic gap energy.

- The 6-amino-2-formyl-quinoline derivative is the most most promising organic material for possible future use as an alternative organic photovoltaic material in solar cells due to its good NLO properties, as well as chemical and physical properties that relate to the smallest electronic gap energy and the highest optical gap energy.

In perspective, we will study the influence of other geometrical parameters and the environment, such as the inclusion on supramolecular systems of the selected quinoline derivative on their physical, chemical and optical properties.

Bibliography

[1] Berthold Anft. Friedlieb ferdinand runge: A forgotten chemist of the nineteenth century. *Journal of Chemical Education*, 32(11):566, 1955.

[2] Richard Anschütz. *Der Chemiker August Kekule-Band 2: Abhandlungen, Berichte, Kritiken, Artikel, Reden*, volume 2. SEVERUS Verlag, 2012.

[3] IA Bessonova and S Yu Yunusov. Quinoline alkaloids of haplophyllum. 1977.

[4] Basavarajaiah Suliphuldevara Matada, Raviraj Pattanashettar, and Nagesh Gunavanthrao Yernale. A comprehensive review on the biological interest of quinoline and its derivatives. *Bioorganic & Medicinal Chemistry*, 32:115973, 2021.

[5] Shweta Jain, Vikash Chandra, Pankaj Kumar Jain, Kamla Pathak, Devendra Pathak, and Ankur Vaidya. Comprehensive review on current developments of quinoline-based anticancer agents. *Arabian Journal of Chemistry*, 12(8):4920–4946, 2019.

[6] Sunayana Tyagi, Milind Sharad Pande, and Mojahidul Islam. Recent insights and clinical status on novel mefenamic acid nanocarriers for the treatment of rheumatoid arthritis. *Current Nanomaterials*, 2024.

[7] Basavarajaiah Suliphuldevara Matada, Raviraj Pattanashettar, and Nagesh Gunavanthrao Yernale. Corrigendum to" a comprehensive review on the biological

interest of quinoline and its derivatives"[bioorg. med. chem. 32 (2021) 115973]. *Bioorganic & Medicinal Chemistry*, 37:116098–116098, 2021.

[8] Raj K Bansal. *Heterocyclic chemistry*. New Age International, 2020.

[9] Peter G Dormer, Kan K Eng, Roger N Farr, Guy R Humphrey, J Christopher McWilliams, PJ Reider, Jess W Sager, and RP Volante. Highly regioselective friedländer annulations with unmodified ketones employing novel amine catalysts: Syntheses of 2-substituted quinolines, 1, 8-naphthyridines, and related heterocycles. *The Journal of Organic Chemistry*, 68(2):467–477, 2003.

[10] M Conrad and L Limpach. synthesen von chinolinderivaten mittelst acetessigester. *Berichte der deutschen chemischen Gesellschaft*, 20(1):944–948, 1887.

[11] Jean-Cristophe Brouet, Shen Gu, Norton P Peet, and John D Williams. Survey of solvents for the conrad–limpach synthesis of 4-hydroxyquinolones. *Synthetic Communications®*, 39(9):1563–1569, 2009.

[12] Raimo Saari, Jonna-Carita Törmä, and Tapio Nevalainen. Microwave-assisted synthesis of quinoline, isoquinoline, quinoxaline and quinazoline derivatives as cb2 receptor agonists. *Bioorganic & medicinal chemistry*, 19(2):939–950, 2011.

[13] Yan-Chao Wu, Li Liu, Hui-Jing Li, Dong Wang, and Yong-Jun Chen. Skraup-doebner- von miller quinoline synthesis revisited: Reversal of the regiochemistry for γ-aryl-β, γ-unsaturated α-ketoesters. *The Journal of Organic Chemistry*, 71(17):6592–6595, 2006.

[14] Bakr F Abdel-Wahab, Rizk E Khidre, Abdelbasset A Farahat, and Abdel-Aziz Sayed El-Ahl. 2-chloroquinoline-3-carbaldehydes: synthesis, reactions and applications. *Arkivoc*, 1:211–276, 2012.

[15] Sudharshan Madapa, Zehra Tusi, and Sanjay Batra. Advances in the syntheses of quinoline and quinoline-annulated ring systems. *Current Organic Chemistry*, 12(13):1116–1183, 2008.

[16] Leonard Sergeyevich Povarov. $\alpha\beta$-unsaturated ethers and their analogues in reactions of diene synthesis. *Russian Chemical Reviews*, 36(9):656, 1967.

[17] Rajeev Kharb and Hardeep Kaur. Therapeutic significance of quinoline derivatives as antimicrobial agents. *Int. Res. J. Pharm*, 4(3):63–69, 2013.

[18] Ashagrachew Tewabe Yayehrad, Gebremariam Birhanu Wondie, and Tesfa Marew. Different nanotechnology approaches for ciprofloxacin delivery against multidrug-resistant microbes. *Infection and drug resistance*, pages 413–426, 2022.

[19] Giorgia Sulis, Richeek Pradhan, Anita Kotwani, and Sumanth Gandra. India's ban on antimicrobial fixed-dose combinations: winning the battle, losing the war? *Journal of Pharmaceutical Policy and Practice*, 15(1):33, 2022.

[20] Sandeep K Singh and Shaija Singh. A brief history of quinoline as antimalarial agents. *Int. J. Pharm. Sci. Rev. Res*, 25(1):295–302, 2014.

[21] Linghang Zhuang, John S Wai, Mark W Embrey, Thorsten E Fisher, Melissa S Egbertson, Linda S Payne, James P Guare, Joseph P Vacca, Daria J Hazuda, Peter J Felock, et al. Design and synthesis of 8-hydroxy-[1, 6] naphthyridines as novel inhibitors of hiv-1 integrase in vitro and in infected cells. *Journal of medicinal chemistry*, 46(4):453–456, 2003.

[22] SHARMA Poonam, KAUR Kamaldeep, CHAWLA Amit, S RranJdh, and R Dhawan. A review on biological activities of quinoline derivatives. *Journal of Management, Information Technology and Engineering*, 2(1):1–14, 2016.

[23] Patricia A Carneiro, Raquel F Pupo Nogueira, and Maria Valnice B Zanoni. Homogeneous photodegradation of ci reactive blue 4 using a photo-fenton process under artificial and solar irradiation. *Dyes and Pigments*, 74(1):127–132, 2007.

[24] Farah Maria Drumond Chequer, Vinícius de Paula Venâncio, Maíra Rocha de Souza Prado, Thiago Mescoloto Lizier, Maria Valnice Boldrin Zanoni, Rommel Rodríguez Burbano, Maria Lourdes Pires Bianchi, Lusânia Maria Greggi Antunes, et al. The cosmetic dye quinoline yellow causes dna damage in vitro. *Mutation Research/Genetic Toxicology and Environmental Mutagenesis*, 777:54–61, 2015.

[25] Ibtisam Alali, Magdy A Ibrahim, N Roushdy, Al-Shimaa Badran, Alaa Muqbil Alsirhani, and AAM Farag. Synthesis, spectral analysis, and dft studies of the novel pyrano [3, 2-c] quinoline-based 1, 3, 4-thiadiazole for enhanced solar cell performance. *Heliyon*, 10(20), 2024.

[26] Yung-Sheng Yen, Jen-Shyang Ni, Wei-I Hung, Chih-Yu Hsu, Hsien-Hsin Chou, and Jiann-T suen Lin. Naphtho [2, 3-c][1, 2, 5] thiadiazole and 2 h-naphtho [2, 3-d][1, 2, 3] triazole-containing d–a- π–a conjugated organic dyes for dye-sensitized solar cells. *ACS Applied Materials & Interfaces*, 8(9):6117–6126, 2016.

[27] Audun Formo Buene, Nora Uggerud, Solon P Economopoulos, Odd R Gautun, and Bård Helge Hoff. Effect of π-linkers on phenothiazine sensitizers for dye-sensitized solar cells. *Dyes and pigments*, 151:263–271, 2018.

[28] Chao Teng, Xichuan Yang, Chao Yang, Shifeng Li, Ming Cheng, Anders Hagfeldt, and Licheng Sun. Molecular design of anthracene-bridged metal-free organic dyes for efficient dye-sensitized solar cells. *The Journal of Physical Chemistry C*, 114(19):9101–9110, 2010.

[29] Liu Yang, Zhiwei Zheng, Yan Li, Wenjun Wu, He Tian, and Zhaohui Wang. N-annulated perylene-based metal-free organic sensitizers for dye-sensitized solar cells. *Chemical communications*, 51(23):4842–4845, 2015.

[30] Zhaoyang Yao, Heng Wu, Yang Li, Junting Wang, Jing Zhang, Min Zhang, Yanchun Guo, and Peng Wang. Dithienopicenocarbazole as the kernel module of low-energy-gap organic dyes for efficient conversion of sunlight to electricity. *Energy & Environmental Science*, 8(11):3192–3197, 2015.

[31] Haining Tian, Xichuan Yang, Ruikui Chen, Rong Zhang, Anders Hagfeldt, and Licheng Sun. Effect of different dye baths and dye-structures on the performance of dye-sensitized solar cells based on triphenylamine dyes. *The Journal of Physical Chemistry C*, 112(29):11023–11033, 2008.

[32] Jagadeeswari Sivanadanam, Paramaguru Ganesan, Rajakumar Madhumitha, Md Khaja Nazeeruddin, and Renganathan Rajalingam. Effect of π-spacers on the photovoltaic properties of d–π–a based organic dyes. *Journal of Photochemistry and Photobiology A: Chemistry*, 299:194–202, 2015.

[33] Markus KR Fischer, Sophie Wenger, Mingkui Wang, Amaresh Mishra, Shaik M Zakeeruddin, Michael Gratzel, and Peter Bauerle. D-π-a sensitizers for dye-sensitized solar cells: linear vs branched oligothiophenes. *Chemistry of Materials*, 22(5):1836–1845, 2010.

[34] Barış Seçkin Arslan, Seda Nur Ülüş, Merve Gezgin, Burcu Arkan, Emre Güzel, Davut Avcı, Mehmet Nebioğlu, and İlkay Şişman. Insight into the effects of the donors and pi-spacers on the photovoltaic performance of quinoline and pyridocarbazole based dsscs. *Optical Materials*, 106:109974, 2020.

[35] Giovanny Carvalho Dos Santos, Eliezer Fernando Oliveira, Francisco Carlos Lavarda, and Luiz Carlos da Silva-Filho. Designing new quinoline-based organic

photosensitizers for dye-sensitized solar cells (dssc): a theoretical investigation. *Journal of molecular modeling*, 25:1–13, 2019.

[36] Barış Seçkin Arslan, Burcu Arkan, Merve Gezgin, Yavuz Derin, Davut Avcı, Ahmet Tutar, Mehmet Nebioğlu, and İlkay Şişman. The improvement of photovoltaic performance of quinoline-based dye-sensitized solar cells by modification of the auxiliary acceptors. *Journal of Photochemistry and Photobiology A: Chemistry*, 404:112936, 2021.

[37] W Helfrich and WG Schneider. Recombination radiation in anthracene crystals. *Physical Review Letters*, 14(7):229, 1965.

[38] Jeremy H Burroughes, Donal DC Bradley, AR Brown, RN Marks, K Mackay, Richard H Friend, Paul L Burns, and Andrew B Holmes. Light-emitting diodes based on conjugated polymers. *nature*, 347(6293):539–541, 1990.

[39] HM Zeyada, MM El-Nahass, and MM El-Shabaan. Photovoltaic properties of the 4h-pyrano [3, 2-c] quinoline derivatives and their applications in organic–inorganic photodiode fabrication. *Synthetic Metals*, 220:102–113, 2016.

[40] HM Zeyada, MM El-Nahass, and MM El-Shabaan. Comparable structural and optical properties of 4h-pyrano [3, 2-c] quinoline derivatives thin films. *Philosophical Magazine*, 96(12):1150–1170, 2016.

[41] Jieyun Wu, Jingdong Luo, Alex K-Y Jen, et al. High-performance organic second- and third-order nonlinear optical materials for ultrafast information processing. *Journal of Materials Chemistry C*, 8(43):15009–15026, 2020.

[42] Jieyun Wu, Wen Wang, Kaixin Chen, and Jingdong Luo. The synthesis of second-order nonlinear optical chromophores with conjugated steric hindrance for electro-optics at 850 nm. *Journal of Materials Chemistry C*, 8(16):5494–5500, 2020.

[43] Kai Fan, Xiangdong Xu, Yu Gu, Zelin Dai, Xiaomeng Cheng, Jun Zhou, Yadong Jiang, Ting Fan, and Jimmy Xu. Organic dast single crystal meta-cavity resonances at terahertz frequencies. *ACS Photonics*, 6(7):1674–1680, 2019.

[44] Galyna Sych, Dmytro Volyniuk, Oleksandr Bezvikonnyi, Roman Lytvyn, and Juozas V Grazulevicius. Dual interface exciplex emission of quinoline and carbazole derivatives for simplified nondoped white oleds. *The Journal of Physical Chemistry C*, 123(4):2386–2397, 2019.

[45] Mao Mao, Xiaolin Zhang, Bin Zhu, Jianbo Wang, Guohua Wu, Yan Yin, and Qinhua Song. Comparative studies of organic dyes with a quinazoline or quinoline chromophore as π-conjugated bridges for dye-sensitized solar cells. *Dyes and Pigments*, 124:72–81, 2016.

[46] Muhammad Khalid, Riaz Hussain, Ajaz Hussain, Bakhat Ali, Farrukh Jaleel, Muhammad Imran, Mohammed Ali Assiri, Muhammad Usman Khan, Saeed Ahmed, Saba Abid, et al. Electron donor and acceptor influence on the nonlinear optical response of diacetylene-functionalized organic materials (dfoms): density functional theory calculations. *Molecules*, 24(11):2096, 2019.

[47] Muhammad Usman Khan, Muhammad Ibrahim, Muhammad Khalid, Munawar Saeed Qureshi, Tahsin Gulzar, Khalid Mahmood Zia, Abdulaziz A Al-Saadi, and Muhammad Ramzan Saeed Ashraf Janjua. First theoretical probe for efficient enhancement of nonlinear optical properties of quinacridone based compounds through various modifications. *Chemical Physics Letters*, 715:222–230, 2019.

[48] Ria Sinha Roy and Prasanta K Nandi. Exploring bridging effect on first hyperpolarizability. *RSC advances*, 5(125):103729–103738, 2015.

[49] G Sathya Priyadarshini, Vidya Edathil, and Gopal Selvi. Non linear optical properties of potent quinoline based schiff bases. *Materials Today: Proceedings*, 51:1746–1750, 2022.

[50] Bakhat Ali, Muhammad Khalid, Sumreen Asim, Muhammad Usman Khan, Zahid Iqbal, Ajaz Hussain, Riaz Hussain, Sarfraz Ahmed, Akbar Ali, Amjad Hussain, et al. Key electronic, linear and nonlinear optical properties of designed disubstituted quinoline with carbazole compounds. *Molecules*, 26(9):2760, 2021.

[51] Azzeddine Belkheiri, Khadija Dahmani, Khaoula Mzioud, Mohamed Rbaa, Mouhsine Galai, Abdelfettah Hmada, Şaban Erdoğan, Burak Tüzün, Mohamed Ebn Touhami, Hamed A El-Serehy, et al. Advanced evaluation of novel quinoline derivatives for corrosion inhibition of mild steel in acidic environments: A comprehensive electrochemical, computational, and surface study. *International Journal of Electrochemical Science*, 19(10):100772, 2024.

[52] Khaoula Mzioud, Amar Habsaoui, Sara Rached, Redouane Lachhab, Nadia Dkhireche, Moussa Ouakki, Mouhssine Galai, Souad El Fartah, and Mohamed Ebn Touhami. Synergistic effect from allium sativum essential oil and diethylthiourea for corrosion inhibition of carbon steel in 0.5 m h2so4 medium. In *Proceedings of the Sixth International Symposium on Dielectric Materials and Applications (ISyDMA'6)*, pages 251–266. Springer, 2022.

[53] Haiqin Ren, Yan Liu, Zhili Gong, Bochuan Tan, Hongda Deng, Junle Xiong, Peng Shao, Qingwei Dai, Jiangtao Cao, and Riadh Marzouki. Pumpkin leaf extract crop waste as a new degradable and environmentally friendly corrosion inhibitor. *Langmuir*, 40(11):5738–5752, 2024.

[54] SM Blinder. Introduction to the hartree-fock method. In *Mathematical Physics in Theoretical Chemistry*, pages 1–30. Elsevier, 2019.

[55] Erwin Schrödinger and Collected Works. Schrödinger 1926c. *Annalen der Physik*, 79:734, 1926.

[56] Paul Arthur Hanle. *Erwin Schrödinger's statistical mechanics, 1912-1925*. Yale University, 1975.

[57] Max Born and W Heisenberg. Zur quantentheorie der molekeln. *Original Scientific Papers Wissenschaftliche Originalarbeiten*, pages 216–246, 1985.

[58] Lorenz S Cederbaum. Born–oppenheimer approximation and beyond. *Conical Intersections: Electronic Structure, Dynamics and Spectroscopy*, pages 3–40, 2004.

[59] Richard A Friesner. Ab initio quantum chemistry: Methodology and applications. *Proceedings of the National Academy of Sciences*, 102(19):6648–6653, 2005.

[60] Douglas R Hartree. The wave mechanics of an atom with a non-coulomb central field. part i. theory and methods. In *Mathematical Proceedings of the Cambridge Philosophical Society*, volume 24, pages 89–110. Cambridge university press, 1928.

[61] Hervé TOULHOAT. Modélisation moléculaire-bases théoriques (partie 2). 2007.

[62] Attila Szabo and Neil S Ostlund. *Modern quantum chemistry: introduction to advanced electronic structure theory*. Courier Corporation, 2012.

[63] Howard D Cohen and CCJ Roothaan. Electric dipole polarizability of atoms by the hartree—fock method. i. theory for closed-shell systems. *The Journal of chemical physics*, 43(10):S34–S39, 1965.

[64] George G Hall. The molecular orbital theory of chemical valency viii. a method of calculating ionization potentials. *Proceedings of the Royal Society of London. Series A. Mathematical and Physical Sciences*, 205(1083):541–552, 1951.

[65] Isaiah Shavitt. The method of configuration interaction. In *Methods of electronic structure theory*, pages 189–275. Springer, 1977.

[66] Chr Møller and Milton S Plesset. Note on an approximation treatment for many-electron systems. *Physical review*, 46(7):618, 1934.

[67] Samuel Francis Boys. Electronic wave functions ii. a calculation for the ground state of the beryllium atom. *Proceedings of the Royal Society of London. Series A. Mathematical and Physical Sciences*, 201(1064):125–137, 1950.

[68] Maylis Orio, Dimitrios A Pantazis, and Frank Neese. Density functional theory. *Photosynthesis research*, 102:443–453, 2009.

[69] Nathan Argaman and Guy Makov. Density functional theory: An introduction. *American Journal of Physics*, 68(1):69–79, 2000.

[70] Walter Kohn and L Sham. Density functional theory. In *Conference Proceedings-Italian Physical Society*, volume 49, pages 561–572. Editrice Compositori, 1996.

[71] NACEREDDINE Abdelmalek KHORIEF. Etude expérimentale et théorique des réactions de cycloaddition. 2011.

[72] Joachim Paier, Martijn Marsman, and Georg Kresse. Why does the b3lyp hybrid functional fail for metals? *The Journal of chemical physics*, 127(2), 2007.

[73] Carlo Adamo, Maurizio Cossi, Giovanni Scalmani, and Vincenzo Barone. Accurate static polarizabilities by density functional theory: assessment of the pbe0 model. *Chemical physics letters*, 307(3-4):265–271, 1999.

[74] John C Slater. The history of the xα method. In *The World of Quantum Chemistry: Proceedings of the First International Congress of Quantum Chemistry held at Menton, France, July 4–10, 1973*, pages 3–15. Springer, 1974.

[75] Fouad CHAFAA. Etude théorique des additions nucléophiles sure less dipôles-1,3. 2017.

[76] Fadila BOUHADJAR. *Etude quantique et classique des propriétés des satellites dans l'aile bleue du spectre d'absorption et d'émission des atomes alcalins perturbés par des gaz rares.* PhD thesis, BADJI MOKHTAR UNIVERSITY, 2018.

[77] Mouna CHERIET. *Etude par la méthode DFT des complexes d'inclusion de deux médicaments antituberculose Pyrazinamide et Isoniazide avec la Cucurbit [7] uril.* PhD thesis, 2019.

[78] Jeffrey I Seeman. Kenichi fukui, frontier molecular orbital theory, and the woodward-hoffmann rules. part iii. fukui's science and technology, 1918–1965. *The Chemical Record*, 22(4):e202100302, 2022.

[79] Andreas Görling. Density-functional theory beyond the hohenberg-kohn theorem. *Physical Review A*, 59(5):3359, 1999.

[80] Raymond P Iczkowski and John L Margrave. Electronegativity. *Journal of the American Chemical Society*, 83(17):3547–3551, 1961.

[81] TA Kaplan. The chemical potential. *Journal of Statistical Physics*, 122:1237–1260, 2006.

[82] Ralph G Pearson. Principle of maximum physical hardness. *The Journal of Physical Chemistry*, 98(7):1989–1992, 1994.

[83] Max Berkowitz and Robert G Parr. Molecular hardness and softness, local hardness and softness, hardness and softness kernels, and relations among these quantities. *The Journal of chemical physics*, 88(4):2554–2557, 1988.

[84] Pratim Kumar Chattaraj and Debesh Ranjan Roy. Update 1 of: electrophilicity index. *Chemical reviews*, 107(9):PR46–PR74, 2007.

[85] Richard FW Bader and TT Nguyen-Dang. Quantum theory of atoms in molecules–dalton revisited. In *Advances in quantum chemistry*, volume 14, pages 63–124. Elsevier, 1981.

[86] NOUDEM Patrick. *Etude Hartree-Fock et DFT des propriétés électroniques et d'optique non-linéaire de la 2-styrylquinoléine fonctionnalisée au Méthacrylate de Méthyle*. PhD thesis, 2023.

[87] Hasnaa El Ouazzani. *Propriétés optiques non linéaires du deuxième et troisième ordre de nouveaux systèmes organiques conjugués de type push-pull*. PhD thesis, Université d'Angers, 2012.

[88] Dominique Guichaoua. *Modulation des propriétés optiques non linéaires de polymères photoactifs conjugués et de complexes de coordination à base de ligand «iminopyridine azobenzène»*. PhD thesis, Université d'Angers, 2018.

[89] Anand HG Patel, Ahmed AK Mohammed, Peter A Limacher, and Paul W Ayers. Finite field method for nonlinear optical property prediction using rational function approximants. *The Journal of Physical Chemistry A*, 121(28):5313–5323, 2017.

[90] Imane Khelladi, Michael Springborg, Ali Rahmouni, Redouane Chadli, and Majda Sekkal-Rahal. Theoretical study on non-linear optics properties of polycyclic aromatic hydrocarbons and the effect of their intercalation with carbon nanotubes. *Molecules*, 28(1):110, 2022.

[91] Vinícius Manzoni, Rogerio Gester, Antonio R da Cunha, Tarciso Andrade-Filho, and Rodrigo Gester. Solvent effects on stokes shifts, and nlo response of thieno [3, 4-b] pyrazine: A comprehensive qm/mm investigation. *Journal of Molecular Liquids*, 335:115996, 2021.

[92] Mausumi Chattopadhyaya and Md Mehboob Alam. Effect of relative position of donor and acceptor groups on linear and non-linear optical properties of quinoline system. *Chemical Physics Letters*, 754:137582, 2020.

[93] Yahia Cherif Fatima, Djebar Hadji, and Benhalima Nadia. Molecular structure, linear, and nonlinear optical properties of piperazine-1, 4-diium bis 2, 4, 6-trinitrophenolate: a theoretical investigation. *Physical Chemistry Research*, 11(1):33–48, 2023.

[94] Jean Baptiste FANKAM FANKAM. *Simulations ab initio et DFT des propriétés électroniques et thermodynamiques de deux isoméres du dibromodinitrofluorescéine*. PhD thesis, UNIVERSITE DE YAOUNDE, 2021.

[95] Paras N Prasad. Nonlinear optical effects in organic molecules and polymers-theory, measurements and devices. In *Nonlinear Optical Materials*, volume 1017, pages 2–11. SPIE, 1989.

[96] Nouar Sofiane Labidi. Semi empirical and ab initio methods for calculation of polarizability (α) and the hyperpolarizability (β) of substituted polyacetylene chain. *Arabian Journal of Chemistry*, 9:S1252–S1259, 2016.

[97] Poornima S Liyanage, Rohini M de Silva, and KM Nalin de Silva. Nonlinear optical (nlo) properties of novel organometallic complexes: high accuracy density functional theory (dft) calculations. *Journal of Molecular Structure: THEOCHEM*, 639(1-3):195–201, 2003.

[98] ASLI Eşme and SEDA Güneşdoğdu Sağdınç. The linear, nonlinear optical properties and quantum chemical parameters of some sudan dyes. 2014.

[99] Annkatrin Sommer, EM Bothschafter, SA Sato, Clemens Jakubeit, Tobias Latka, Olga Razskazovskaya, Hanieh Fattahi, Michael Jobst, W Schweinberger, Vage Shir-

vanyan, et al. Attosecond nonlinear polarization and light–matter energy transfer in solids. *Nature*, 534(7605):86–90, 2016.

[100] Djebar HADJI et al. *Étude théorique et modélisation des propriétés optique non-linéaire des molécules organophosphoriques*. PhD thesis, 2017.

[101] Hadji Djebar et al. *Étude théorique et modélisation des propriétés optique non-linéaire des molécules organophosphoriques*. PhD thesis, 2017.

[102] Benoît Champagne. Thesis/thèse.

[103] Antoine Bodart. Thesis/thèse.

[104] Toshikazu Takada, Michel Dupuis, and Harry F King. Molecular symmetry. iv. the coupled perturbed hartree–fock method. *Journal of computational chemistry*, 4(2):234–240, 1983.

[105] Ahmed AK Mohammed. *Accurate Calculations of Nonlinear Optical Properties Using Finite Field Methods*. PhD thesis, 2017.

[106] Aurélie Plaquet. *Design of molecular switches exhibiting second-order nonlinear optical responses: ab initio investigations and hyper Rayleigh scattering characterizations*. PhD thesis, UNamur-Université de Namur, 2011.

[107] Guus JM Velders, Jean Michel Gillet, Pierre J Becker, and Dirk Feil. Electron density analysis of nonlinear optical materials: an ab initio study of different conformations of benzene derivatives. *The Journal of Physical Chemistry*, 95(22):8601–8608, 1991.

[108] H Förster. Uv/vis spectroscopy. *Characterization I: -/-*, pages 337–426, 2004.

[109] Donald F Swinehart. The beer-lambert law. *Journal of chemical education*, 39(7):333, 1962.

[110] Yuki Noguchi, Akinori Saeki, Takenori Fujiwara, Sho Yamanaka, Masataka Kumano, Tsuneaki Sakurai, Naoto Matsuyama, Motohiro Nakano, Naohisa Hirao, Yasuo Ohishi, et al. Pressure modulation of backbone conformation and intermolecular distance of conjugated polymers toward understanding the dynamism of π-figuration of their conjugated system. *The Journal of Physical Chemistry B*, 119(24):7219–7230, 2015.

[111] Tom Markvart and Luis Castañer. *Practical handbook of photovoltaics: fundamentals and applications*. Elsevier, 2003.

[112] Akhshay Singh Bhadwal, RM Tripathi, Rohit Kumar Gupta, Nishant Kumar, RP Singh, and Archana Shrivastav. Biogenic synthesis and photocatalytic activity of cds nanoparticles. *Rsc Advances*, 4(19):9484–9490, 2014.

[113] Jianqing Chen, Xin Cai, Donghui Yang, Dan Song, Jiajia Wang, Jinghua Jiang, Aibin Ma, Shiquan Lv, Michael Z Hu, and Chaoying Ni. Recent progress in stabilizing hybrid perovskites for solar cell applications. *Journal of Power Sources*, 355:98–133, 2017.

[114] Nafees Ahmad, Huiqiong Zhou, Ping Fan, and Guangxing Liang. Recent progress in cathode interlayer materials for non-fullerene organic solar cells. *EcoMat*, 4(1):e12156, 2022.

[115] Shawn B Allin, Thomas M Leslie, and Richard S Lumpkin. Solvent effects in molecular hyperpolarizability calculations. *Chemistry of materials*, 8(2):428–432, 1996.

[116] Jose P Abraham, D Sajan, I Hubert Joe, and VS Jayakumar. Molecular structure, spectroscopic studies and first-order molecular hyperpolarizabilities of p-amino acetanilide. *Spectrochimica Acta Part A: Molecular and Biomolecular Spectroscopy*, 71(2):355–367, 2008.

[117] Alan Hinchliffe and Humberto J Soscún Machado. Ab initio studies of the dipole polarizabilities of conjugated molecules: Part 3. one electron properties, dipole polarizability and first hyperpolarizability of quinoline and isoquinoline. *Journal of Molecular Structure: THEOCHEM*, 312(1):57–67, 1994.

[118] C Lee, W Yang, and RG Parr. Phys. rev. b: Condens. matter mater. phys. 1988.

[119] M Jea Frisch. Gaussian 09 revision a. 02. *(No Title)*, 2009.

[120] A Frisch, AB Nielson, AJ Holder, et al. Gaussview user manual. *Gaussian Inc., Pittsburgh, PA*, 556, 2000.

[121] Sibel Demir Kanmazalp. Investigation of theoretical calculations of 2-(1-phenylethylideneamino) guanidine compound: Nbo, nlo, homo-lumo and mep analysis by dft method. *Karaelmas Science & Engineering Journal*, 7(2), 2017.

[122] Chérif F Matta and Russell J Boyd. An introduction to the quantum theory of atoms in molecules. *The quantum theory of atoms in molecules: from solid state to DNA and drug design*, 2007.

[123] Evgeniy Kvasyuk, Aliaksei Sysa, Sultan Al Saud, Siyamak Shahab, Masoome Sheikhi, Sadegh Kaviani, and Anatoliy Zinchenko. Quantum chemical modeling, synthesis, spectroscopic (ft-ir, excited states, uv/vis) studies, fmo, qtaim, elf, lol, nbo, nlo and qsar analyses of nelarabine. 2022.

[124] Bhaskaran Sureshkumar, Yohannan Sheena Mary, Chacko Yohannan Panicker, Somasekharan Suma, Stevan Armaković, Sanja J Armaković, Christian Van Alsenoy, and Badiadka Narayana. Quinoline derivatives as possible lead compounds for anti-malarial drugs: Spectroscopic, dft and md study. *Arabian Journal of Chemistry*, 13(1):632–648, 2020.

[125] Abdelmalek Khorief Nacereddine, Lynda Merzoud, Christophe Morell, and Henry Chermette. A computational investigation of the selectivity and mechanism of the lewis acid catalyzed oxa-diels–alder cycloaddition of substituted diene with benzaldehyde. *Journal of computational chemistry*, 42(18):1296–1311, 2021.

[126] Chafika BENAISSA. *Etude Physico-chimique d'une série de Conducteurs Organiques à transfert de charge.* PhD thesis, Université de Biskra-Mohamed Khider.

[127] Abdelmalek Khorief Nacereddine. A medt computational study of the mechanism, reactivity and selectivity of non-polar [3+ 2] cycloaddition between quinazoline-3-oxide and methyl 3-methoxyacrylate. *Journal of Molecular Modeling*, 26:1–12, 2020.

[128] Yasmine MEZARI. *Étude théorique du complexe d'inclusion de 2-méthyl mercapto phénothiazine avec l'hydroxy propyl β-cyclodextrine par la méthode DFT.* PhD thesis, 2022.

[129] Tian Lu and Feiwu Chen. Multiwfn: A multifunctional wavefunction analyzer. *Journal of computational chemistry*, 33(5):580–592, 2012.

[130] Stephen Esser. Qtaim and the interactive conception of chemical bonding. 2018.

[131] Nyiang Kennet Nkungli and Julius Numbonui Ghogomu. Theoretical analysis of the binding of iron (iii) protoporphyrin ix to 4-methoxyacetophenone thiosemicarbazone via dft-d3, mep, qtaim, nci, elf, and lol studies. *Journal of Molecular Modeling*, 23:1–20, 2017.

[132] Takeshi Yanai, David P Tew, and Nicholas C Handy. A new hybrid exchange–correlation functional using the coulomb-attenuating method (cam-b3lyp). *Chemical physics letters*, 393(1-3):51–57, 2004.

[133] John P Perdew, Matthias Ernzerhof, Aleš Zupan, and Kieron Burke. Nonlocality of the density functional for exchange and correlation: Physical origins and chemical consequences. *The Journal of chemical physics*, 108(4):1522–1531, 1998.

[134] Stefan Grimme, Stephan Ehrlich, and Lars Goerigk. Effect of the damping function in dispersion corrected density functional theory. *Journal of computational chemistry*, 32(7):1456–1465, 2011.

[135] Gülşen Akın Evingür and Önder Pekcan. Optical energy band gap of paam-go composites. *Composite Structures*, 183:212–215, 2018.